Investigating the Effects of Extended Wake: the Role of Neuronal Firing and Long Term Consequences of Sleep Restriction in Adolescence

By

Alexander Vidal Rodriguez

A dissertation submitted in partial fulfillment of

the requirements for the degree of

Doctor of Philosophy

(Neuroscience)

at the

UNIVERSITY OF WISCONSIN – MADISON

2016

Date of final oral examination: 12/6/2016

The dissertation is approved by the following members of the Final Oral Committee:

Chiara Cirelli, Professor, Psychiatry
Giulio Tononi, Professor, Psychiatry
Matthew I. Banks, Associate Professor, Anesthesiology
Craig W. Berridge, Professor, Psychology
Peter Lipton, Professor, Neuroscience

Thanks and Acknowledgements

I would never have made it to where I am without the support of those around me, and I owe thanks to many people. My parents, Mario and Eva Rodriguez, formed the basis of my success and ensured that I practiced reading and math at a young age. I must thank them for providing so much, most of all an environment where I was able to prosper. I also have to thank Danny Rodriguez for being a good big brother and an example of aptitude and success from which I could draw inspiration.

As an undergraduate, I was fortunate to work in the lab of Edward Boyden, who provided my first real experience in a neuroscience lab. There, I experienced the benefits of working in a truly collaborative environment and also saw firsthand how much neuroscience relies upon engineering. I am thankful for the training and education I received there.

Five years ago, Chiara Cirelli and Giulio Tononi gave a hopeful rotating student a chance at researching sleep in a highly productive lab, and I have been very grateful for this opportunity. Dr. Cirelli has never ceased to amaze me with not only her encyclopedic knowledge of scientific literature, but also her high standards for data collection and analysis. When it comes to learning how to be a good scientist, I could think of no better example to follow. Vlad Vyazovskiy and Yuval Nir built a framework of tools and equipment that is still used in the lab, and I have directly benefited from their efforts. My fellow lab team members have been a constant source of ideas and encouragement through unsuccessful experiments, and I am grateful for all their help.

My friends and fellow students in Madison have also played a large role, and none more than Kendra Taylor, who has stuck with me through good times and bad. I am incredibly grateful to have found her, and for her constant support and companionship. And finally, thanks to Blue, the biggest dog in the world.

Table of Contents

Abstract

Sleep is a highly conserved behavioral state in which we spend roughly one third of our lives. We know that sleep is necessary due to the problems that extended wake brings. If wake continues without sleep, then severe deficits in attention, working memory, decision making, cognitive control, and even humor appreciation can result. Though the consequences of wake on behavior are well documented, there is still debate as to exactly how wake drives our need to sleep. In this thesis, I performed experiments to test the synaptic homeostasis hypothesis (SHY), which claims that wake leads to an overall increase in synaptic strength associated with learning, and that sleep is required to renormalize synaptic weights, with beneficial effects both at the cellular level (energy, supplies) and at the systems level (memory). In wake, neurons fire tonically, while during NREM sleep they alternate more or less synchronously between periods of tonic activity (ON periods) and periods of silence (OFF periods). This bistable firing pattern is reflected at the EEG level as slow-wave activity (SWA), which is the most reliable measure of sleep need available, being high at sleep onset, decreasing with sleep time, and increasing with wake duration. Because energy use in wake is higher than in NREM sleep, some have proposed that sleep is a time for neurons 'fatigued' from tonic firing to rest by entering OFF periods. In this view therefore, SWA would increase mainly because of longer OFF periods. According to SHY instead, the increase in SWA is mainly driven by the increase in synaptic strength, which leads to stronger coupling and higher synchrony among neurons.

In a first series of experiments, I tested the role of neuronal activity (firing rate) per se in driving the need for sleep. Mean firing rates increase together with synaptic strength across wake, and thus it is not easy to tease them apart. As a result, it was first necessary to find a way to increase firing independent of synaptic strength. I used optogenetic stimulation in mice

implanted with microwire electrode arrays to locally increase firing rates in NREM sleep to levels seen when the mice were kept awake by exploring novel objects, and then analyzed measures of sleep need following laser stimulation or sleep deprivation. After sleep deprivation by exploration of novel objects, I found that SWA, OFF period measures, and neuronal synchrony were all increased, as expected. After optogenetic stimulation in NREM sleep instead, SWA and OFF period measures showed no change, and synchrony was decreased. Because firing rates were similar between both conditions, these data suggest that firing rate alone is not sufficient to increase measures of sleep pressure, and thus it is unlikely that firing alone is a major determinant of sleep need.

Since SHY strongly links sleep need with synaptic plasticity, it also predicts that sleep should play a critical role in development, when learning and brain plasticity are at their highest and synapses undergo massive remodeling. Previous experiments have shown that sleep deprivation and restriction in adolescents can affect brain plasticity and structure in the short term, but despite the high prevalence of sleep restriction in human adolescents, few studies have investigated its long term effects. In a second series of experiments, I performed a five-day chronic sleep restriction (CSR) in adolescent mice, injected a viral tracer into secondary motor cortex (MOs), and then imaged projections from MOs throughout the brain when the mice reached adulthood. I found that, while there were no specific anatomical regions that showed significant changes, machine learning classification was able to reliably identify mice as belonging to control or CSR groups, indicating that there are subtle effects caused by sleep restriction. Within the same brains, I used excitatory and inhibitory presynaptic markers to measure the density and size of synaptic puncta in a number of brain regions, but was unable to

detect any consistent differences between control and CSR mice. These findings may be a true biological result, and/or they may reflect the technical limitations of the methods I used.

Altogether, this thesis demonstrates that cortical activity alone is unlikely to explain why sustained wake leads to an increased need for sleep. Additionally, chronic sleep disruption in early adolescence may affect adult brain connectivity, but further experiments at different ages are required to learn more.

Chapter I:

Introduction

General outline:

Sleep is a highly conserved behavioral state in which we spend roughly one third of our lives. The consequences of the sleep/wake cycle are broad. Industries have been built around sleep/wake aids and human cultures have been shaped by legends of sleep and dreams, yet the underlying purpose of sleep is still poorly understood. We appreciate the importance of sleep mostly due to the deficits that result from sleep deprivation. When lacking sleep, humans show significant deficits in attention, working memory, humor appreciation, decision making, and cognitive control (Dawson and Reid, 1997; Drummond et al., 2006; Killgore, 2010; Killgore et al., 2006a; Lim and Dinges, 2008). As time spent awake increases, these deficits build in severity, and sleep becomes harder to resist. Once allowed to sleep after extended wake, humans and other animals show an increase in sleep intensity and duration, and recover from cognitive deficits caused by sleep deprivation upon waking after this more intense sleep (Borbély et al., 1981). The increase in sleep intensity following sleep deprivation suggests an accumulation of sleep "pressure" in wake that is relieved only by sleep. However, it is still unclear exactly what the physiological substrates are that drive the accumulation of this pressure, and there are a number of hypotheses that attempt to explain wake's relation to sleep, and they are not mutually exclusive. Wake, as compared to NREM sleep, is associated with higher neuronal firing (Steriade and Hobson, 1976; Vyazovskiy et al., 2009), increased synaptic growth (de Vivo et al., 2016a) and overall increased energy usage (Harris et al., 2012). Sleep has been proposed to act as a time for cellular rest and replenishment of neuronal energy stores, and/or as a time for network-level adjustments of plasticity (Tononi and Cirelli, 2014; Vyazovskiy and Harris, 2013). In this thesis, I performed experiments to test the synaptic homeostasis hypothesis (SHY), which claims that wake leads to an overall increase in synaptic strength associated with learning, and

that sleep is required to renormalize synaptic weights, with beneficial effects both at the cellular level (energy, supplies) and at the systems level (memory) (Tononi and Cirelli, 2006, 2012, 2014). As further discussed below, there is a variety of electrophysiological, molecular, and structural evidence to support the claim of a net increase in synaptic strength after wake and a net decrease after sleep.

One of the key tenets of SHY is that synaptic strength, and often as a consequence the mean firing rate, will slowly increase with waking experience. Due to the energy demands of neural firing, it is advantageous for the brain to encode information as sparsely as possible (Attwell and Gibb, 2005). However, as some stimuli or patterns become more salient, for example as we gain new experiences in wake, the brain must then strengthen synapses and increase firing in order to communicate those new patterns (Tononi and Cirelli, 2014). This increasing strength cannot continue forever, as energy demands of the brain would quickly become overwhelming. Sleep provides an ideal environment for the brain to recover from the threat of runaway potentiation, as in the absence of outside stimuli, the brain can downscale synaptic strength without favoring any particular synapses. Indeed, there is quite extensive evidence showing that mean firing rates of populations of cortical and hippocampal neurons increase with wake and decrease with sleep (Miyawaki and Diba, 2016; Vyazovskiy et al., 2009; Watson et al., 2016). Moreover, when adolescent mice are subjected to sustained monocular deprivation, firing in the affected primary visual cortex first declines and then slowly recovers over days, and the recovery is state-dependent, with firing increasing only in wake but not in sleep (Hengen et al., 2016). Crucially, however, the rationale underlying SHY is that it is synaptic strength, not firing per se, that needs to be regulated across the sleep/wake cycle. This is because neuronal firing rate may or may not strictly follow changes in synaptic strength, because

it is affected at any given moment by many factors, including the levels of neuromodulators that modulate neuronal excitability and the balance between excitation and inhibition. Thus, according to SHY it is the increase in synaptic strength during wake, and not the increase in firing per se, that drives the need for sleep and is the real cause of increased sleep intensity (Tononi and Cirelli, 2014). Sleep intensity is best measured using slow wave activity (SWA), an index of the number and amplitude of slow waves during sleep (Halász et al., 2014). SWA is high at the beginning of sleep and declines as sleep progresses (Borbély et al., 2016). SWA at the beginning of sleep increases further if wake is extended (Borbély et al., 1981), and decreases with naps (Dijk et al., 1987a). According to SHY, the slow waves of sleep become bigger after sustained wake because synapses between neurons are more strongly coupled to each other, and sleep decreases SWA due to reduced synchrony following net synaptic depression. In a first series of experiments in mice, I tested the idea that increased firing per se is not a major driver of sleep pressure by using optogenetic stimulation to increase neuronal firing to wake-like levels during sleep, a time when synaptic potentiation is not favored (**Chapter II**).

Because SHY strongly links sleep need with synaptic plasticity, it also predicts that sleep should play a critical role in development, when learning and brain plasticity are at their highest. Indeed, children sleep longer than adults, which is observable in both rodents (Frank and Heller, 1997) and humans (Leger et al., 2012; Ohayon et al., 2004), and a hallmark of development in the brain is an initial surge in neural connectivity followed by an eventual pruning of those connections to establish the adult brain connectome (Innocenti and Price, 2005). If sleep is important to help regulate plasticity, it is possible that long term sleep restriction during development, as is often observed in human adolescents (Carskadon et al., 1998), could have permanent deleterious effects on the brain. In a second series of experiments in mice, I examined

measures of connectivity and synaptic density in adulthood following chronic sleep restriction in adolescence to determine if sleep disruptions early during development can have long lasting effects on brain structure (**Chapters III and IV**).

Electrophysiological correlates of sleep and wake:

To understand the role that sleep plays as a restorative force from wake, it is first necessary to understand the electrophysiological measures that are used to measure and study sleep. Sleep is defined as a period of rest in which animals have a higher threshold to respond to external stimuli as well as a stereotypical sleeping posture, often with circadian entrainment. Sleep in mammals and birds is further divided into rapid eye movement (REM) sleep and non-rapid-eye-movement (NREM) sleep. NREM sleep represents the bulk of sleep (70-80%), and is most concentrated towards the beginning of sleep, early in the night in diurnal animals or early in the day in nocturnal animals like the mice studied here. Sleep is typically not measured only by observing behavior, but also with electrophysiological tools including electroencephalography (EEG) with scalp electrodes and intracortical extracellular recording electrodes that yield local field potentials (LFPs) and multi-unit activity (MUA). Electromyography (EMG) is also an important tool and measures muscle activity with electrodes usually placed on the chin or legs in humans, or implanted into the neck muscle in rodents. EMG is high in wake, low in NREM sleep, and nearly undetectable in REM sleep. EEG detects fluctuations in the electrical field measured at the skull that are mostly caused by the changes in the postsynaptic potentials of large groups of cortical neurons, and can measure across 10 cm^2 of cortex or more depending on the type of electrode (Buzsáki et al., 2012). LFP is a measure similar to EEG, but comes from intracortical probes, generally reflects collective postsynaptic potentials of dendrites, and measures activity on the scale of hundreds of microns. MUA is a fast-sampled signal from

intracortical electrodes which is able to detect the rapid depolarization of individual or small populations of neurons firing action potentials (Buzsáki et al., 2012; Vyazovskiy and Harris, 2013). In wake, EEG and LFP signals are characterized by a shift toward higher frequencies when compared to NREM sleep, and are referred to as "activated". MUA in wake is characterized by tonic firing, and EMG shows sporadic muscle activity. In NREM sleep, EEG and LFP signals show greatly increased power in the lower frequencies, causing the signal to become "synchronized". These low frequency oscillations are particularly enriched within the 0.5-4 Hz range, and are referred to as slow waves. Slow wave activity (SWA) is defined as the spectral power of EEG or LFP within this range, and is widely accepted as a marker for NREM sleep intensity as it is high at sleep onset and decreases as sleep progresses (Borbély et al., 2016). In rats, MUA during NREM sleep shows patterns of tonic firing (ON periods) lasting 800 ms on average that alternate with periods of silence (OFF periods) with an 85ms average duration, resulting in an overall lower firing rate in NREM sleep than in wake, while EMG shows little or no activity (Brown et al., 2012; Vyazovskiy et al., 2009). The cycling of ON and OFF periods at the extracellular level reflects an intracellular phenomenon known as the slow oscillation, a <1 Hz rhythm that causes the membrane potential of cortical neurons to cycle between up states of relative depolarization (seen extracellularly as ON periods) and down states of relative hyperpolarization that span between 8-20 mV on average (extracellularly OFF periods) (Steriade et al., 2001). It was generally believed that the initiation of the down state is due to an absence of excitatory input to cortical neurons, also known as disfacilitation, more so than active inhibition by chloride currents (Timofeev et al., 2001). However, more recent evidence in vivo demonstrates that activating somatostatin-positive interneurons in the cortex is sufficient to reliably induce OFF periods and slow waves similar to those seen in NREM sleep, while

inhibiting these same cells reduces SWA. Unlike disfacilitation, this mechanism of SWA via somatostatin-positive cells could explain the rapid, synchronous onset of OFF periods and slow waves (Funk et al., Submitted).

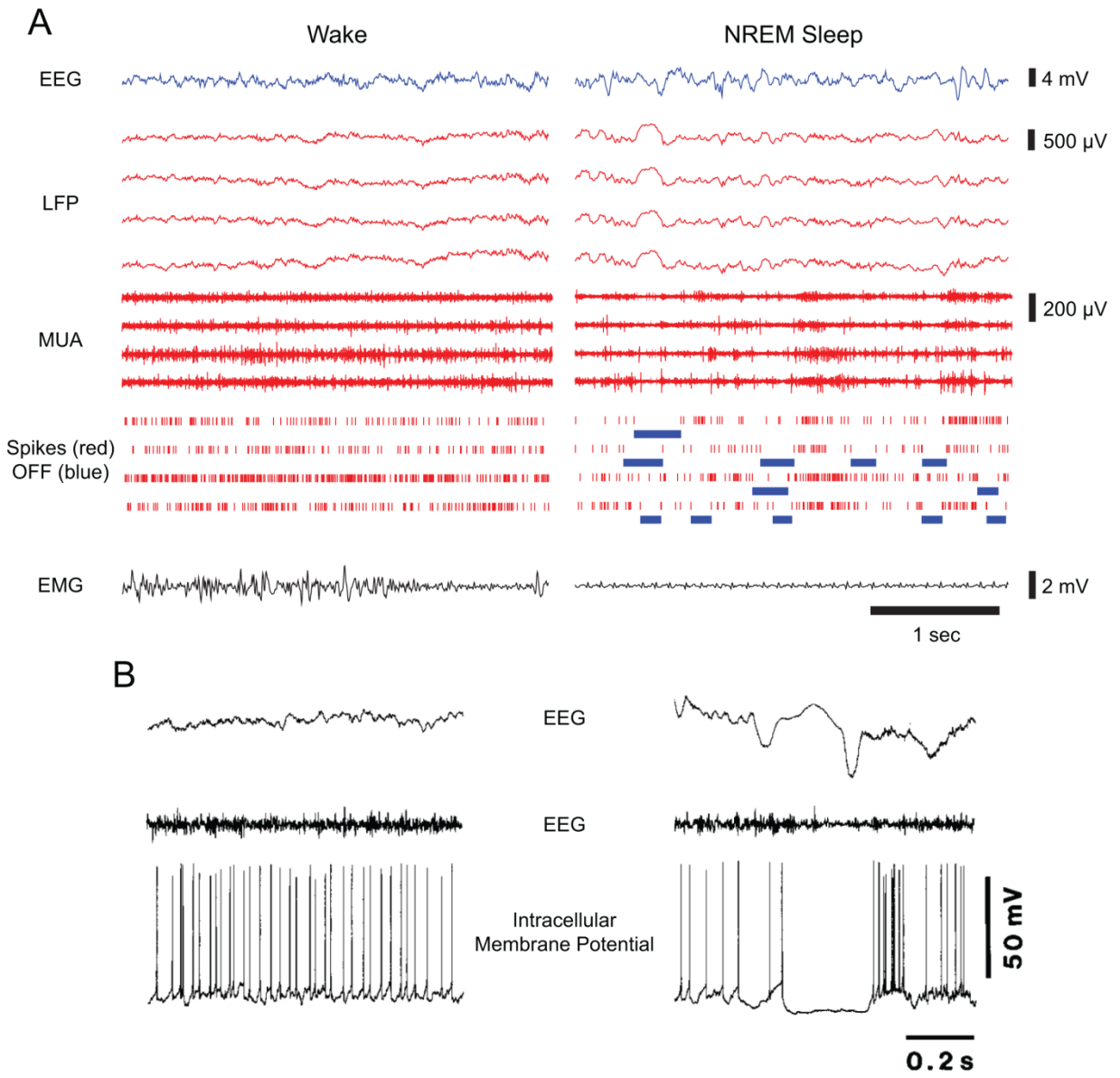

Figure 1. Electrophysiological correlates of sleep and wake. **A)** Representative traces of electroencephalogram (EEG), local field potential (LFP), extracellular multi-unit activity (MUA), and electromyogram (EMG) in wake and sleep in a mouse. MUA spikes that are above threshold are recorded as red lines, and OFF periods for each spike train are indicated in blue. Note the loss of muscle tone in the EMG, along with the appearance of slow waves in the EEG and LFP in NREM sleep, which often correspond with coordinated OFF periods in the MUA. **B)** Example of LFP, EMG and intracellular membrane potential taken from wake (left) and NREM sleep (right) in regular-spiking (putative excitatory) cortical neurons, so called because they fire regular spikes in response to a depolarizing current. Modified from (Steriade et al., 2001).

Wake-promoting and sleep-promoting systems

Sleep is a carefully coordinated state, and the tonic activity of wake or bistable firing of sleep depends upon a number of important brain regions. Almost a century ago, a Viennese scientist named Baron Constantin von Economo noticed that patients afflicted with a particular form of encephalitis suffered from either intense lethargy or intractable insomnia. Upon investigation, he found that the lethargic patients had suffered lesions to the posterior hypothalamus and rostral midbrain, while insomniacs had damage in the basal forebrain and preoptic area. Given these observations, he concluded that distinct sleep and wake promoting areas were separated by location in the hindbrain (Saper et al., 2001; Von Economo, 1930). Though it took some time for a causal link between the brainstem and forebrain activity to be found, Italian and American scientists Moruzzi and Magoun were the first to discover that electrical stimulation of the central paramedial brainstem between the superior and inferior colliculi was sufficient to cause EEG waveforms in anesthetized cats to change from sleep-like high amplitude low frequency to wake-like low amplitude high frequency patterns (Moruzzi and Magoun, 1949). In what is now known as the ascending reticular activating system (ARAS), a number of nuclei in the brainstem and hypothalamus are responsible for releasing wake-promoting neuromodulators, including serotonin, orexin, histamine, acetylcholine, noradrenaline, dopamine, and glutamate.

Serotonin is primarily produced in the brainstem in the dorsal raphe nucleus (DRN). Firing of the DRN is highest during wake, and diminishes in NREM and REM sleep. Systemic injection of serotonin agonists is sufficient to increase waking and reduce sleep (Monti and Jantos, 2008). The actions of serotonin are complex, and may promote quiet wake more so than

active wake. Despite this caveat, serotonin is generally regarded as a wake-promoting neuromodulator (Brown et al., 2012).

Orexin (also known as hypocretin) neurons are found in the perifornical area of the lateral hypothalamus (LH). Like the DRN, orexinergic cells in the LH are most active during wake when compared to sleep (Lee et al., 2005a; Mileykovskiy et al., 2005). Intracerebroventricular injections of orexin are also sufficient to induce increased waking (Piper et al., 2000). The absence of orexinergic neurons causes narcolepsy in dogs (Sakurai, 2013), and orexin levels are reduced in living narcoleptic humans (Nishino et al., 2000), with postmortem studies in humans showing that narcoleptic patients have a loss of orexinergic cells (Thannickal et al., 2000). Following a knockout of orexin or antagonism of orexin receptors, rodents will also show narcoleptic symptoms (Chemelli et al., 1999), further suggesting that orexin is important for the maintenance of wake (Brown et al., 2012). Pharmacogenetic excitation and inhibition of orexinergic neurons causes an increase and decrease in wake, respectively (Sasaki et al., 2011), suggesting that orexin assists in maintaining the wake state. It is thought that the inhibition of orexinergic neruons by median pre-optic (MnPO) and ventrolateral pre-optic (VLPO) cells plays a large role in the transition into sleep (Saper et al., 2005).

Histamine also originates in the hypothalamus from a region known as the tuberomammilary nucleus (TMN). Cells in the TMN fire mostly during wake, with reduced firing rates in NREM and REM sleep (John et al., 2004). Activation of histamine receptors has a variety of effects, all of which contribute to increased wakefulness (Lin, 2000). In mice, a complete knockout or acute antagonism of the H_1 histamine receptor do not significantly alter the amount of time spent in each sleep stage compared to wild type mice, but the number of short wake bouts during the light cycle is significantly reduced (Huang et al., 2006). Moreover,

contrary to cholinergic, orexinergic, and noradrenergic neurons, histamine neurons start firing only after behavioral arousal and EEG activation (Takahashi et al., 2006). Overall, these findings indicate that histamine action on H_1 receptors is important to maintain, rather than to initiate, wakefulness.

Cholinergic neurons, found in both the basal forebrain and the pedunculopontine and laterodorsal tegmental nuclei (PPT/LDT) within the brainstem, are also wake promoting cells. In contrast to many of the other wake-promoting systems, cholinergic cells fire just prior to behavioral arousal (Boucetta et al., 2014) in addition to having high firing during wake and REM sleep (Lee et al., 2005b). Activating cholinergic cells within the PPT depolarizes cortical cells (Steriade, 2004), and direct application of acetylcholine to the cortex causes a marked increase in firing rate (Castro-Alamancos and Gulati, 2014). Lesioning the basal forebrain cholinergic cells is not sufficient to change the total amount of time spent in NREM or REM sleep from baseline (Blanco-Centurion et al., 2006), but recent optogenetic studies have demonstrated that specific stimulation of basal forebrain cholinergic neurons is sufficient to induce EEG activation and transitions into wake (Irmak and de Lecea, 2014), suggesting that previous lesions were simply not complete. Additionally, it is probable that these cells are necessary for the adenosine-dependent expression of sleep homeostasis (Kalinchuk et al., 2008). Other recent optogenetic studies show that cholinergic neurons in the PPT/LDT are instead more important for REM sleep rather than for wake, as stimulation of these neurons in NREM sleep causes transitions into REM sleep (Van Dort et al., 2015).

Cells that release noradrenaline (NA) can be found within the locus coeruleus (LC). Firing in the LC is high during wake, low during NREM sleep, and lowest in REM sleep. Though the LC is small, consisting of only 1500 cells per hemisphere in the rat (Berridge, 2008;

Sara, 2009), chemical stimulation of the region is sufficient to induce wake-like EEG throughout the cortex (Berridge and Foote, 1991), and optogenetic stimulation is sufficient to trigger transitions from sleep to wake, as measured by both behavior and electrophysiology (Carter et al., 2010). Conversely, inactivating the LC bilaterally in wake causes a shift in cortical EEG towards lower, sleep-like frequencies (Berridge et al., 1993). The LC acts through the neuromodulator noradrenaline (NA), which has excitatory G-coupled protein receptors on neurons throughout the cortex (Berridge and Abercrombie, 1999; Hein, 2006). NA, combined with the LC's broad network of connections that reaches throughout the brain, allows the LC to modulate neural firing in a number of ways in wake. LC firing increases a few hundred milliseconds or even a few seconds before EEG transitions to an activated state (Takahashi et al., 2010). Further, LC firing is observed to increase depending upon the salience of both stressful or rewarding stimuli, but decreases with adaptation to a stimulus (Abercrombie and Jacobs, 1987a, 1987b; Berridge, 2008).

The dopaminergic system, consisting primarily of the substantia nigra and ventral tegmental area (VTA), is more complex when it comes to the regulation of sleep and wake. Unlike many other wake-promoting regions, mean firing rates of dopaminergic neurons within the substantia nigra and VTA do not change across wake and sleep (Miller et al., 1983), which has prompted many to believe that dopamine (DA) is not crucially involved in the regulation of sleep and wake. However, the pattern of VTA firing does change from slow steady firing in NREM sleep to burst firing in wake and REM sleep (Dahan et al., 2006). Moreover, DA itself is known to be wake-promoting, partly because drugs such as amphetamines and modafinil which act via DA greatly increase behavioral arousal (Boutrel and Koob, 2004). This may be in part due to DA's connections to other wake-promoting centers such as the DRN and LC, or via direct

connections to the cortex (Monti and Jantos, 2008). DA is also implicated in attention, as injection of a dopamine receptor antagonist within the frontal eye field was sufficient to alter the responses of V4 neurons, leading to greater response magnitudes and selectivity (Noudoost and Moore, 2011). Recently, direct stimulation of the VTA has been shown to induce waking from general anesthesia (Taylor et al., 2016), and optogenetic stimulation of tyrosine-hydroxylase-containing VTA neurons in mice is sufficient to induce transitions into wake and maintain wakefulness, while chemogenetic inactivation of these same neurons promotes nest-building behavior, decreases sleep latency, and increases NREM sleep duration (Eban-Rothschild et al., 2016).

Glutamate is the most prevalent excitatory neurotransmitter in the brain and is found in many areas where it can help to further modulate brain state. For example, there is a subpopulation of glutamatergic neurons in the hypothalamus that is activated by orexin and acts as a positive feedback mechanism to further promote the activity of orexinergic neurons (Li et al., 2002). Activation of the cortex relies in part on signals from the thalamus, and the relay of signals to the cortex from the thalamus is achieved by glutamatergic neurons projecting throughout cortex (Hur and Zaborszky, 2005).

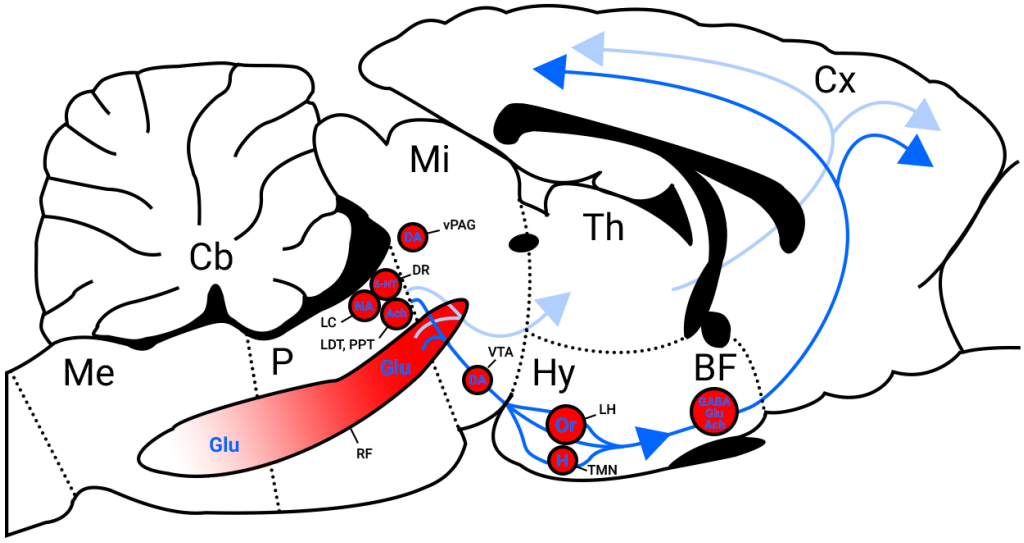

Figure 2. A schematic of the ascending reticular activating system (ARAS) and its projections in the mouse brain. Nuclei are shown as labeled red circles with their primary neurotransmitter shown in blue inside the circle and names in black outside the circle. Anatomical regions: Me = medulla; Cb = cerebellum; P = pons; Mi = midbrain; Th = thalamus; Hy = hypothalamus; BF = basal forebrain; Cx = cortex. Nuclei: RF = reticular formation; LC = locus coeruleus; LDT = laterodorsal tegmental nucleus; PPT = pedunculopontine tegmental nucleus; DR = dorsal raphe nucleus; vPAG = ventral periaqueductal gray; VTA = ventral tegmental area; LH = lateral hypothalamus; TMN = tuberomammillary nucleus; Neurotransmitters: Glu = glutamate; NA = noradrenaline; 5-HT = serotonin; Ach = acetylcholine; DA = dopamine; Or = orexin; H = histamine.

In contrast to the ARAS, GABAergic cells within the MnPO and VLPO of the anterior hypothalamus, as well as other glutamatergic and GABAergic cells in the basal forebrain, are among the few sleep-active cells in the brain and send inhibitory efferents to many of the wake-promoting nuclei. Additionally, stimulation of a newly discovered GABAergic medullary nucleus, the parafacial zone, is sufficient to induce a transition into NREM sleep (Anaclet et al., 2014). It is thought that a balance between wake-active and sleep-active areas constitutes a “flip-flop” switch which controls the shifts between behavioral states and prevents rapid switching of

states or prolonged periods of mixed-state activity (Jones, 2005; McGinty and Szymusiak, 2000; Saper et al., 2005).

Regulatory processes of sleep:

According to an influential model of sleep regulation called the two-process model of sleep regulation, the need for sleep can be modeled by two separate drives, referred to as Process C and Process S (Borbély and Achermann, 1999; Borbély et al., 2016). Process C is the circadian component, which fluctuates depending upon the time of day and entrains human sleep towards the night and sleep in nocturnal rodents towards the day. Thus, Process C controls the timing, rather than the duration and intensity, of sleep. Process C is primarily controlled by the suprachiasmatic nucleus (SCN), a group of cells that sits just dorsal to the optic chiasm (Saper, 2013). Clock genes with a transcription cycle of roughly 24 hours are known to regulate timing and cellular rhythms and are present within most cells (King and Takahashi, 2000), but the SCN plays a central role in their coordination. Following a knockout of the clock gene Bmal1, circadian rhythms are lost entirely. A partial restoration of this gene to only the SCN is sufficient to restore global rhythms, underscoring the importance of the SCN in particular. The SCN, primarily via connections to the hypothalamus and thalamus, is able to exert its control over behavioral rhythms like sleep and wake as well as body temperature, which also displays a circadian rhythm (Frank et al., 2013).

The second component of the two-process model is Process S. Process S represents the homeostatic component, which steadily increases with time spent awake, and is only decreased by sleep (Borbély and Achermann, 1999). Process S predicts that extended wake will result in greater pressure to sleep. Indeed, the more time spent awake, the more urgent the need to sleep

becomes. If wake continues without sleep, then cognitive deficits begin to build resulting in slower reaction times, lapses in memory and altered cognitive processing (Brown et al., 2012; Killgore, 2010). These and other effects will be discussed in more detail below.

In recovery sleep that follows periods of extended wake, sleep duration is usually higher than in baseline sleep, though total duration is ultimately constrained by circadian pressure. More consistently, extended wake is followed by an increase in the intensity of NREM SWA (from now on called SWA). SWA intensity refers specifically to the spectral power of EEG or LFP between 0.5 and 4 Hz. In line with the predictions of Process S, increased SWA scales with the duration of wake preceding sleep, at least for up to 24 hours of wake (Borbély and Achermann, 1999). Reciprocally, sleep that follows wake interrupted by naps shows lower SWA than baseline sleep (Werth et al., 1996). Regardless of its starting value, SWA declines across sleep. Early SWA reflects large, steep slow waves that eventually become smaller over the course of sleep (Vyazovskiy et al., 2007). SWA not only tracks sleep pressure, but is also somehow causally related to its decline across sleep, as suppression of SWA in the first few hours of sleep delays the natural decrease of SWA across sleep (Dijk et al., 1987b). Additionally, the more intense SWA is, the higher the arousal threshold required for wake (Neckelmann and Ursin, 1993). For these reasons, SWA is widely accepted as the most reliable measure of sleep pressure.

Though first believed to be mostly independent, more recent studies have pointed to evidence that Process S and C are able to modulate each other (Borbély et al., 2016). For example, the slope of slow waves is at its highest in the middle of the day, when circadian pressure is low (Lazar et al., 2015). REM duration, which already increases with total sleep time, peaks when the end of sleep coincides with normal circadian wake time (Dijk and Czeisler, 1995). Following knockout of certain clock genes, not only is the circadian clock altered, but the

SWA response to sleep deprivation is altered as well (Franken, 2013). Sleep pressure also has some effects on circadian functioning. When sleep pressure is high, neuronal firing in the SCN in reduced (Deboer et al., 2007), as well as SCN firing in response to light (van Diepen et al., 2014). Ultimately, this translates to a lower suprachiasmatic area fMRI BOLD signal (Schmidt et al., 2009) and blunted circadian phase shifts in response to light (Mistlberger et al., 1997).

SWA intensity, being derived from EEG or LFP, is a spatial sum of neuronal activity and a reflection of both the amplitude and synchrony of activity in the summed area (Musall et al., 2014). Because changes in either of these could modulate SWA, increasing sleep pressure may be the result of a combination of several different mechanisms. By investigating the different consequences of prolonged wake, we can better understand the forces behind SWA intensity as a measure of Process S.

The behavioral consequences of prolonged wake

If wake is maintained for extended periods of time, negative cognitive, behavioral, and physiological changes will accumulate. One of the first observations of the devastating effects of prolonged wake was made by the Russian scientist Marie de Manacéine, who found that several days of total sleep deprivation in puppies proved fatal. Upon anatomical investigation, she discovered that the brain was the most severely impacted organ (de Manacéine, 1894).

Since Marie's initial experiments, the effects of sleep deprivation and sleep restriction have been well described in humans and other species with a variety of tests. Sleep deprivation specifically refers to maintaining constant wake for hours or days, while sleep restriction refers to reducing the daily amount of sleep, usually over several days or weeks. Both chronic sleep restriction and acute deprivation have been shown to have similar effects over time (Van Dongen

et al., 2003). In humans, the task that most reliably tracks deficits with increasing wake time is arguably the psychomotor vigilance test (PVT), which challenges sustained attention by requiring subjects to respond to a cue with a button press as quickly as possible (Dinges and Powell, 1985). After sleep deprivation, response times are generally slower, and subjects are more prone to long (>500 ms) lapses before responding. The increasing response times tracked over several days overlap incredibly well with a line drawn to match the superposition of Processes S and C, providing extra support for the two-process model (Lim and Dinges, 2008). These lapses in attention can have severe consequences on everyday function, especially when it comes to tasks such as driving. A classic study has estimated that the driving impairment caused by 23 hours of sleep deprivation is equivalent to a blood alcohol level of 0.08% (Dawson and Reid, 1997). Verbal learning is also affected by sleep deprivation, as subjects who have been deprived have difficulty remembering lists of memorized words (Drummond et al., 2000). More complex behaviors are also adversely affected by prolonged wake. The Iowa Gambling Task (IGT) is a card selection task used to test a subject's ability to avoid high-risk decks of cards in favor of decks which give modest, but reliable, rewards. Over time, sleep deprived subjects stop choosing the reliable decks and shift to choosing cards from the risky deck (Killgore et al., 2006a). Further experiments have suggested that this riskier behavior is driven by a decreasing emphasis on long term information, with sleepy subjects instead overemphasizing short term information (Olson et al., 2014). Additionally, sleepy human subjects are unable to appreciate humor in the same way as rested subjects (Killgore et al., 2006b). However, not all performance is adversely affected. Sleep deprivation does not appear to degrade performance on a cognitive interference task known as the Stroop test, though it is unclear if this is could be due to a practice effect. Alternatively, it is possible that the self-paced nature of the test is less affected by sleep

deprivation than task-paced tests such as a PVT or driving simulator (Sagaspe et al., 2006). It is possible to recover some performance in certain tasks with the use of stimulants. Caffeine causes sleep deprived subjects to perform better at the PVT (Lim and Dinges, 2008), but not at the gambling task (Killgore et al., 2007) or humor appreciation (Killgore et al., 2006b), indicating that the cognitive deficits caused by loss of sleep are not all due to impaired attention alone. In short, sleep deprivation causes a myriad of cognitive deficits, and the accumulation of sleep pressure can affect high-level as well as low-level processing. Thus, any hypothesis attempting to explain why extended wake causes cognitive deficits should consider a mechanism that is not specific to any one brain region or local circuit.

As many molecular or genetic assays of sleep deprivation require brain tissue and thus cannot be performed on humans, the high conservation of sleep among animals means that rodents and flies can provide natural model systems. Rodents respond similarly to humans on a PVT-style test after sleep deprivation (Christie et al., 2008). On a test of higher-order function requiring delayed pressing of a lever, rats following sleep restriction performed worse than their rested counterparts and displayed less controlled behavior (Kamphuis et al., 2016). Fruit flies have also demonstrated many of the hallmarks of sleep homeostasis, including a rebound in sleep time and intensity after extended wake. Like more complex animals, flies' performance in a vigilance task is also lower after sleep deprivation compared to rested flies (Huber et al., 2004). Using model systems, we are able to learn far more about electrophysiological, molecular, and metabolic changes in sleep deprivation than we can in humans, and can investigate different causes as to what drives Process S.

Increasing synaptic plasticity in wake as a motivation for sleep

A major prediction of SHY is that an increase in overall cortical plasticity is instrumental for the increase in SWA after extended wake (Tononi and Cirelli, 2014), and computational studies confirm that an increase in synaptic plasticity would result in a greater recruitment of neurons, thus leading to higher synchrony and SWA (Esser et al., 2007). As we spend time awake, we navigate the world and learn new things. This learning leads overall to potentiation of synapses within the cortex, and wake is indeed a state conducive to such potentiation, one reason being that cortical concentrations of NA are higher in wake than sleep. NA has been shown to be permissive of plasticity, and successful long term potentiation (LTP) within hippocampus as well as visual and somatosensory cortex requires the activation of adrenergic β receptors (Connor et al., 2011; Gu, 2002). Further, in line with the idea that wake promotes synaptic potentiation, converging evidence shows that genes coding for important plasticity proteins such as Arc, brain-derived neurotrophic factor (BDNF), Homer, and NGFI-A are all upregulated after wake when compared to sleep (Cirelli, 2006; Vyazovskiy et al., 2008) and without NA, there is a blunted rebound in SWA intensity following sleep deprivation (Cirelli et al., 2005).

Electrophysiological experiments also confirm the presence of a net increase in synaptic strength following wake. After prolonged wake, rats showed an increase in the slope and amplitude of cortical evoked potentials, consistent with synaptic potentiation. Attempts to induce further LTP were less successful following wake than sleep, suggesting that wake had already somewhat saturated LTP (Vyazovskiy et al., 2011). Similar conclusions have been reached in humans, with learning leading to larger changes in cortical excitability after sleep compared to wake (de Beukelaar et al., 2016), and LTP becoming harder to induce after extended wake (Kuhn et al., 2016).

In sleep deprived rats, those who spent more time exploring had higher levels of BDNF expression and SWA intensity than controls (Huber et al., 2007). Additionally, microinjections of BDNF into the cortex during wake are sufficient to cause in increase in SWA in sleep, while injecting BDNF blockers instead decreases SWA (Faraguna et al., 2008). Quantification of the expression and phosphorylation levels of the excitatory AMPA receptors (AMPARs), established markers of synaptic strength (Malenka and Bear, 2004), also support these findings. After wake, AMPARs that contain the GluR1 subunit show increased expression specifically within synaptoneurosomes, while there is no difference in total expression of these receptors between wake and sleep, and greater AMPAR phosphorylation is observed in animals following wake than after sleep (Vyazovskiy et al., 2008). Spines harboring synapses also become larger as wake progresses. In flies, the number of synapses increases over just a few hours of wake, providing structural evidence of plastic changes even over short time scales (Bushey et al., 2011). In adolescent mice, there is a net gain in the number of spines after wake and a net decrease after sleep, consistent with predictions of SHY (Maret et al., 2011). Recently, electron microscope imaging in mouse cortex has revealed that the sizes of the axon/spine interface, an ultrastructural measure of synaptic strength, increase after wake and decreases after sleep (de Vivo et al., 2016a).

Neuronal firing and energy demands in wake as drivers for sleep

The brain is one of the largest users of energy within the body. In humans, the brain accounts for ~20% of total oxygen consumption, while being only 2% of total body mass (Harris et al., 2012). Among all of the energy demands of neurons, those surrounding neuronal signaling are the largest, accounting for roughly 65% of adenosine triphosphate (ATP) use in rodent gray matter (Attwell and Gibb, 2005). Glucose is the primary source of ATP for the brain. ATP is

mainly produced via oxidative phosphorylation, which takes place in mitochondria. Another pathway is via glycolysis, which is less efficient but does not require mitochondria to produce ATP. Glycolysis often occurs in astrocytes, and the resulting products are shuttled to neurons (Gjedde et al., 2002). The concentration of lactate, one product of glycolysis, has been shown to steadily increase over the course of wake (Dash et al., 2012). The concentration of glucose itself seems mostly unaffected by sleep/wake history, though glucose concentration does steadily increase across NREM sleep, suggesting that it might provide a time for the brain to recover glucose stores in easily depleted areas (Dash et al., 2013). SWA in sleep is tied to reduced cerebral blood flow in humans, providing further evidence that metabolic demands are lower during sleep (Hofle et al., 1997) Mitochondrial proteins are known to be upregulated as a result of extended wake (Cirelli et al., 2004), and it has been confirmed that mitochondria also grow in size with extended wake compared to sleep. Perhaps most important, the changes in mitochondria size following sleep restriction lasted at least 36 hours following recovery sleep, meaning that sleep restriction can have long lasting structural effects on cells (de Vivo et al., 2016b). Another consequence of increased energy production would be an increase in reactive oxygen species (ROS), a common byproduct of cellular metabolism that in high concentrations can result in cellular damage or death (Martindale and Holbrook, 2002). Thus, there is no doubt that wake represents a higher metabolic burden for the brain than sleep.

Not only are there significant changes in brain metabolism across the sleep/wake cycle, but the metabolic pathway of ATP itself also plays some role in regulating sleep. Through enzymatic activity, ATP is metabolized into adenosine, a protein which is known to act as a sleep-promoting factor strong enough such that injections of adenosine into the ventricles of the cat are sufficient to trigger a transition into sleep (Feldberg and Sherwood, 1954; Porkka-

Heiskanen and Kalinchuk, 2011). Glutamatergic activity increases adenosine levels, and cortical adenosine concentration tracks Process S fairly well in that it increases as time awake increases, and declines as sleep progresses. Wake-dependent adenosine levels are highest within the basal forebrain, where adenosine can inhibit the activity of wake-promoting neurons via adenosine receptors (Porkka-Heiskanen et al., 2000). These same receptors are antagonized by the popular stimulant caffeine (Huang et al., 2005). Adenosine also has a direct role in mediating SWA response after extended wake. In mice lacking the adenosine receptor A_1, sleep deprivation does not result in a corresponding SWA increase in recovery sleep (Bjorness et al., 2009).

In wake, cortical firing rates are higher than those of NREM, and they further increase with time spent awake (Vyazovskiy et al., 2009). Therefore, as neuronal firing increases, so too should the energy demands of the brain and cortical adenosine concentration. Some have hypothesized that the most important function of sleep is to give neurons an opportunity to rest, therefore decreasing overall energy demand as compared to wake (Vyazovskiy and Harris, 2013). An issue with this idea, however, is that it cannot account for REM sleep, where firing rates are often just as high as in wake for extended periods of time (Vyazovskiy et al., 2009). Moreover, neuronal plasticity is fundamentally linked to neural activity and the use of energy within the brain. For instance, NA-permitted plasticity in wake is energy demanding in part because it requires protein synthesis (Gu, 2002). Thus, is neural firing alone the primary reason why extended wake increases sleep pressure, or is it because it is linked to neuronal plasticity and synaptic potentiation? If neuronal activity is the primary driver of sleep, then the ultimate purpose of sleep, or at least of NREM sleep, would be to allow neurons to rest by entering periods of non-firing (OFF periods) more frequently than in wake. Although popular, this idea

until recently had not been tested directly, most likely because of a previous inability to separate firing rates from plasticity.

Since plasticity, neural firing, and energy demands are so well correlated, it is difficult to assess the role of plasticity separate from firing alone. In this thesis, I attempt to dissociate the two by comparing sleep deprivation using novel objects to optogenetically enhanced neuronal firing in NREM sleep, a time with relatively low NA tone and plasticity. The underlying assumption is that firing rates will be similar in these two conditions, but only firing in wake will be associated with increasing synaptic strength.

The effects of development on sleep and plasticity

SHY links sleep need to the regulation of plasticity, and it predicts that sleep should be especially important in development, a time when the brain is most plastic. Indeed, sleep duration shows changes in line with brain development. In humans, as with rodents, total sleep duration in children declines with increasing age, along with the proportion of sleep that is REM sleep (Basner et al., 2007; Frank and Heller, 1997; Ohayon et al., 2004). This trend continues through adulthood, though at a much slower rate, until it finally reaches a stable level at about age 60 (Ohayon et al., 2004). These changes are not limited to sleep duration, as SWA increases with age and reaches a peak at about the age of 11. Through the ages of 11 to 17, SWA decreases by about 65%, a magnitude of decline that well exceeds any other change throughout a human's lifespan (Feinberg and Campbell, 2010). These same trends are not restricted to humans, as rodents also show high initial SWA that decreases over time (Nelson et al., 2013). An interesting fact about adolescent sleep demonstrated in both humans and rodents is that despite high total SWA in early adolescents, late adolescents show a much larger SWA rebound after sleep

deprivation when compared to early adolescents (Jenni et al., 2005; Nelson et al., 2013). These rapid changes in SWA dynamics suggest that changes in underlying brain plasticity or connectivity in adolescence are a likely cause.

The developing brain rapidly grows and overdevelops connections, leading to a much higher interconnectivity in the developing brain compared to the adult brain (Innocenti and Price, 2005). In humans, though gray matter density and glucose metabolism both peak around age 6, synaptic density reaches a much earlier peak at around age 2-3, after which it steadily falls with increasing age, leveling off after adolescence (Huttenlocher, 1979; Paus et al., 2008). This timeline of decreasing synaptic density is in line with decreasing total SWA (Feinberg and Campbell, 2010). This observation is consistent with the claims of SHY, as it predicts that SWA reflects synaptic strength. The previously mentioned lack of SWA rebound in young adolescents (Jenni et al., 2005; Nelson et al., 2013) is then likely due to an already saturated network not being able to increase in strength any more until the extra connections are pruned away with development, thus decreasing the 'floor' of SWA. As SHY predicts that the primary role of sleep is the downscaling of synapses, it is possible that disrupting sleep during development while synapses are still being pruned could permanently impact brain structure.

Such permanent disruptions are not without precedent, as developing animals go through several 'critical periods', times during which certain neural circuit growth or structuring must take place, or they will never form correctly (Hensch, 2005). In some cases, the critical period requires sensory input. One common example is ocular dominance plasticity in the visual cortex. If one eye is deprived of stimulation during the critical period, then that eye will never provide meaningful sensory input, regardless of later visual stimuli (Berardi et al., 2000). Sleep disruption can affect this plasticity, as kittens sleep deprived after monocular deprivation do not

show the same loss of cortical responses to the deprived eye or the same enhancement of the responses to the non-deprived eye that is seen in kittens allowed to sleep afterwards (Frank et al., 2001). Molecular differences between wake and sleep may also contribute, as nitrous oxide (NO) and BDNF, both partially regulated by wake duration, have been shown to have opposite effects on axon growth cone stability, with NO leading to growth cone collapse and BDNF to stabilization (Ernst et al., 2000). NA, which is higher in wake, has also been shown to be necessary for proper formation of ocular dominance plasticity (Gu, 2002). Outside of the critical period, extended wake can still have long term effects, such as a persistent increase in the size of mitochondria even 36 hours after the end of a chronic sleep restriction (de Vivo et al., 2016b).

A growing literature suggests that human adolescents are often chronically sleep restricted, in part due to early school times mixed with a shift towards later sleep preference (Carskadon et al., 1993, 1998; Minges and Redeker, 2016). Despite this research, few studies have looked at the long term effects of chronic sleep restriction in adolescence. To search for such effects, I subjected adolescent mice to a five-day chronic sleep restriction and then examined their brains in adulthood, looking at measures of brain connectivity as well as synaptic size and density.

Summary

The behavioral cost of wake is well understood, but there is still controversy over whether increasing plasticity or neuronal firing per se contributes most to the accumulation of sleep pressure across wake. I will be performing experiments to test SHY, which claims that sleep need is driven by increasing synaptic strength in wake, and sleep primarily acts to renormalize synaptic weights. In **Chapter II**, I attempt to disentangle neuronal activity from

synaptic potentiation by optogenetically forcing neural activity during NREM sleep to mimic the activity observed during sleep deprivation with novel objects. I show in mice, as in rats, that SWA, OFF measures and neural synchrony increase after sleep deprivation, but after optogenetic stimulation in NREM sleep, SWA and OFF measures do not change, and synchrony decreases, suggesting that neural activity alone is not sufficient to increase sleep need.

Because SHY links sleep need and plasticity, it predicts that sleep should be especially important in development, when brain plasticity is at its highest. Indeed, sleep shows changes across development, and sleep disruptions at a young age have been shown to have short term negative impacts on plasticity. However, despite sleep restriction being a pervasive problem among human adolescents, few studies have looked at the long term consequences of sleep restriction in adolescence. In **Chapter III**, I perform a five-day chronic sleep restriction in adolescent mice, inject a viral tracer into secondary motor cortex, and then examine the brains of the same mice in adulthood. I find that while no specific regions show marked differences in connectivity from secondary motor cortex, machine learning classification is able to reliably identify sleep restricted mice, indicating that there are subtle, heterogeneous differences in the adult brain caused by sleep restriction. In **Chapter IV**, I take a closer look at the presynaptic structure of these same mice by labeling brain sections for excitatory and inhibitory presynaptic markers. I show that the density and size of presynaptic puncta in adult brains do not change in predictable ways due to sleep restriction in adolescence, though it is unclear whether this is due to a true biological result or a methodological limitation.

References

Abercrombie, E.D., and Jacobs, B.L. (1987a). Single-unit response of noradrenergic neurons in the locus coeruleus of freely moving cats. I. Acutely presented stressful and nonstressful stimuli. J. Neurosci. *7*, 2837–2843.

Abercrombie, E.D., and Jacobs, B.L. (1987b). Single-unit response of noradrenergic neurons in the locus coeruleus of freely moving cats. II. Adaptation to chronically presented stressful stimuli. J. Neurosci. *7*, 2844–2848.

Anaclet, C., Ferrari, L., Arrigoni, E., Bass, C.E., Saper, C.B., Lu, J., and Fuller, P.M. (2014). The GABAergic parafacial zone is a medullary slow wave sleep-promoting center. Nat. Neurosci. *17*, 1217–1224.

Attwell, D., and Gibb, A. (2005). Neuroenergetics and the kinetic design of excitatory synapses. Nat. Rev. Neurosci. *6*, 841–849.

Basner, M., Fomberstein, K.M., Razavi, F.M., Banks, S., William, J.H., Rosa, R.R., and Dinges, D.F. (2007). American Time Use Survey: Sleep Time and Its Relationship to Waking Activities. Sleep *30*, 1085–1095.

Berardi, N., Pizzorusso, T., and Maffei, L. (2000). Critical periods during sensory development. Curr. Opin. Neurobiol. *10*, 138–145.

Berridge, C.W. (2008). Noradrenergic modulation of arousal. Brain Res. Rev. *58*, 1–17.

Berridge, C.W., and Abercrombie, E.D. (1999). Relationship between locus coeruleus discharge rates and rates of norepinephrine release within neocortex as assessed by in vivo microdialysis. Neuroscience *93*, 1263–1270.

Berridge, C.W., and Foote, S.L. (1991). Effects of locus coeruleus activation on electroencephalographic activity in neocortex and hippocampus. J. Neurosci. *11*, 3135–3145.

Berridge, C.W., Page, M.E., Valentino, R.J., and Foote, S.L. (1993). Effects of locus coeruleus inactivation on electroencephalographic activity in neocortex and hippocampus. Neuroscience *55*, 381–393.

de Beukelaar, T.T., Van Soom, J., Huber, R., and Wenderoth, N. (2016). A Day Awake Attenuates Motor Learning-Induced Increases in Corticomotor Excitability. Front. Hum. Neurosci. *10*.

Bjorness, T.E., Kelly, C.L., Gao, T., Poffenberger, V., and Greene, R.W. (2009). Control and Function of the Homeostatic Sleep Response by Adenosine A1 Receptors. J. Neurosci. *29*, 1267–1276.

Blanco-Centurion, C., Xu, M., Murillo-Rodriguez, E., Gerashchenko, D., Shiromani, A.M., Salin-Pascual, R.J., Hof, P.R., and Shiromani, P.J. (2006). Adenosine and Sleep Homeostasis in the Basal Forebrain. J. Neurosci. *26*, 8092–8100.

Borbély, A.A., and Achermann, P. (1999). Sleep homeostasis and models of sleep regulation. J. Biol. Rhythms *14*, 557–568.

Borbély, A.A., Baumann, F., Brandeis, D., Strauch, I., and Lehmann, D. (1981). Sleep deprivation: effect on sleep stages and EEG power density in man. Electroencephalogr. Clin. Neurophysiol. *51*, 483–495.

Borbély, A.A., Daan, S., Wirz-Justice, A., and Deboer, T. (2016). The two-process model of sleep regulation: a reappraisal. J. Sleep Res. *25*, 131–143.

Boucetta, S., Cissé, Y., Mainville, L., Morales, M., and Jones, B.E. (2014). Discharge Profiles across the Sleep–Waking Cycle of Identified Cholinergic, GABAergic, and Glutamatergic Neurons in the Pontomesencephalic Tegmentum of the Rat. J. Neurosci. *34*, 4708–4727.

Boutrel, B., and Koob, G.F. (2004). What keeps us awake: the neuropharmacology of stimulants and wakefulness-promoting medications. Sleep *27*, 1181–1194.

Brown, R.E., Basheer, R., McKenna, J.T., Strecker, R.E., and McCarley, R.W. (2012). CONTROL OF SLEEP AND WAKEFULNESS. Physiol. Rev. *92*, 1087–1187.

Bushey, D., Tononi, G., and Cirelli, C. (2011). Sleep and synaptic homeostasis: structural evidence in Drosophila. Science *332*, 1576–1581.

Buzsáki, G., Anastassiou, C.A., and Koch, C. (2012). The origin of extracellular fields and currents — EEG, ECoG, LFP and spikes. Nat. Rev. Neurosci. *13*, 407–420.

Carskadon, M.A., Vieira, C., and Acebo, C. (1993). Association between puberty and delayed phase preference. Sleep *16*, 258–262.

Carskadon, M.A., Wolfson, A.R., Acebo, C., Tzischinsky, O., and Seifer, R. (1998). Adolescent sleep patterns, circadian timing, and sleepiness at a transition to early school days. Sleep *21*, 871–881.

Carter, M.E., Yizhar, O., Chikahisa, S., Nguyen, H., Adamantidis, A., Nishino, S., Deisseroth, K., and de Lecea, L. (2010). Tuning arousal with optogenetic modulation of locus coeruleus neurons. Nat. Neurosci. *13*, 1526–1533.

Castro-Alamancos, M.A., and Gulati, T. (2014). Neuromodulators Produce Distinct Activated States in Neocortex. J. Neurosci. *34*, 12353–12367.

Chemelli, R.M., Willie, J.T., Sinton, C.M., Elmquist, J.K., Scammell, T., Lee, C., Richardson, J.A., Williams, S.C., Xiong, Y., Kisanuki, Y., et al. (1999). Narcolepsy in orexin Knockout Mice: Molecular Genetics of Sleep Regulation. Cell *98*, 437–451.

Christie, M.A., McKenna, J.T., Connolly, N.P., McCarley, R.W., and Strecker, R.E. (2008). 24 hours of sleep deprivation in the rat increases sleepiness and decreases vigilance: introduction of the rat-psychomotor vigilance task. J. Sleep Res. *17*, 376–384.

Cirelli, C. (2006). Cellular consequences of sleep deprivation in the brain. Sleep Med. Rev. *10*, 307–321.

Cirelli, C., Gutierrez, C.M., and Tononi, G. (2004). Extensive and Divergent Effects of Sleep and Wakefulness on Brain Gene Expression. Neuron *41*, 35–43.

Cirelli, C., Huber, R., Gopalakrishnan, A., Southard, T.L., and Tononi, G. (2005). Locus Ceruleus Control of Slow-Wave Homeostasis. J. Neurosci. *25*, 4503–4511.

Connor, S.A., Wang, Y.T., and Nguyen, P.V. (2011). Activation of β-adrenergic receptors facilitates heterosynaptic translation-dependent long-term potentiation. J. Physiol. *589*, 4321–4340.

Dahan, L., Astier, B., Vautrelle, N., Urbain, N., Kocsis, B., and Chouvet, G. (2006). Prominent Burst Firing of Dopaminergic Neurons in the Ventral Tegmental Area during Paradoxical Sleep. Neuropsychopharmacology *32*, 1232–1241.

Dash, M.B., Tononi, G., and Cirelli, C. (2012). Extracellular Levels of Lactate, but Not Oxygen, Reflect Sleep Homeostasis in the Rat Cerebral Cortex. Sleep *35*, 909–919.

Dash, M.B., Bellesi, M., Tononi, G., and Cirelli, C. (2013). SLEEP/WAKE DEPENDENT CHANGES IN CORTICAL GLUCOSE CONCENTRATIONS. J. Neurochem. *124*, 79–89.

Dawson, D., and Reid, K. (1997). Fatigue, alcohol and performance impairment. Nature *388*, 235–235.

Deboer, T., Détári, L., and Meijer, J.H. (2007). Long term effects of sleep deprivation on the mammalian circadian pacemaker. Sleep *30*, 257–262.

van Diepen, H.C., Lucassen, E.A., Yasenkov, R., Groenen, I., Ijzerman, A.P., Meijer, J.H., and Deboer, T. (2014). Caffeine increases light responsiveness of the mouse circadian pacemaker. Eur. J. Neurosci. *40*, 3504–3511.

Dijk, D.J., and Czeisler, C.A. (1995). Contribution of the circadian pacemaker and the sleep homeostat to sleep propensity, sleep structure, electroencephalographic slow waves, and sleep spindle activity in humans. J. Neurosci. *15*, 3526–3538.

Dijk, D.J., Beersma, D.G.M., and Daan, S. (1987a). EEG Power Density during Nap Sleep: Reflection of an Hourglass Measuring the Duration of Prior Wakefulness. J. Biol. Rhythms *2*, 207–219.

Dijk, D.J., Beersma, D.G., Daan, S., Bloem, G.M., and Van den Hoofdakker, R.H. (1987b). Quantitative analysis of the effects of slow wave sleep deprivation during the first 3 h of sleep on subsequent EEG power density. Eur. Arch. Psychiatry Neurol. Sci. *236*, 323–328.

Dinges, D.F., and Powell, J.W. (1985). Microcomputer analyses of performance on a portable, simple, visual RT task during sustained operations. Behav. Res. Methods Instrum. Comput. *17*, 652–655.

Drummond, S.P.A., Brown, G.G., Gillin, J.C., Stricker, J.L., Wong, E.C., and Buxton, R.B. (2000). Altered brain response to verbal learning following sleep deprivation. Nature *403*, 655–657.

Drummond, S.P.A., Paulus, M.P., and Tapert, S.F. (2006). Effects of two nights sleep deprivation and two nights recovery sleep on response inhibition. J. Sleep Res. *15*, 261–265.

Eban-Rothschild, A., Rothschild, G., Giardino, W.J., Jones, J.R., and de Lecea, L. (2016). VTA dopaminergic neurons regulate ethologically relevant sleep-wake behaviors. Nat. Neurosci. *19*, 1356–1366.

Ernst, A.F., Gallo, G., Letourneau, P.C., and McLoon, S.C. (2000). Stabilization of Growing Retinal Axons by the Combined Signaling of Nitric Oxide and Brain-Derived Neurotrophic Factor. J. Neurosci. *20*, 1458–1469.

Esser, S.K., Hill, S.L., and Tononi, G. (2007). Sleep Homeostasis and Cortical Synchronization: I. Modeling the Effects of Synaptic Strength on Sleep Slow Waves. Sleep *30*, 1617–1630.

Faraguna, U., Vyazovskiy, V.V., Nelson, A.B., Tononi, G., and Cirelli, C. (2008). A Causal Role for Brain-Derived Neurotrophic Factor in the Homeostatic Regulation of Sleep. J. Neurosci. *28*, 4088–4095.

Feinberg, I., and Campbell, I.G. (2010). Sleep EEG changes during adolescence: An index of a fundamental brain reorganization. Brain Cogn. *72*, 56–65.

Feldberg, W., and Sherwood, S.L. (1954). Injections of drugs into the lateral ventricle of the cat. J. Physiol. *123*, 148–167.

Frank, M.G., and Heller, H.C. (1997). Development of REM and slow wave sleep in the rat. Am. J. Physiol. *272*, R1792-1799.

Frank, E., Sidor, M.M., Gamble, K.L., Cirelli, C., Sharkey, K.M., Hoyle, N., Tikotzky, L., Talbot, L.S., McCarthy, M.J., and Hasler, B.P. (2013). Circadian clocks, brain function, and development. Ann. N. Y. Acad. Sci. *1306*, 43–67.

Frank, M.G., Issa, N.P., and Stryker, M.P. (2001). Sleep Enhances Plasticity in the Developing Visual Cortex. Neuron *30*, 275–287.

Franken, P. (2013). A role for clock genes in sleep homeostasis. Curr. Opin. Neurobiol. *23*, 864–872.

Funk, C.M., Peelman, K., Bellesi, M., Cirelli, C., and Tononi, G. (Submitted). Induction of sleep slow waves by somatostatin-positive interneurons. Nat. Neurosci.

Gjedde, A., Marrett, S., and Vafaee, M. (2002). Oxidative and Nonoxidative Metabolism of Excited Neurons and Astrocytes. J. Cereb. Blood Flow Metab. *22*, 1–14.

Gu, Q. (2002). Neuromodulatory transmitter systems in the cortex and their role in cortical plasticity. Neuroscience *111*, 815–835.

Halász, P., Bódizs, R., Parrino, L., and Terzano, M. (2014). Two features of sleep slow waves: homeostatic and reactive aspects – from long term to instant sleep homeostasis. Sleep Med. *15*, 1184–1195.

Harris, J.J., Jolivet, R., and Attwell, D. (2012). Synaptic Energy Use and Supply. Neuron *75*, 762–777.

Hein, L. (2006). Adrenoceptors and signal transduction in neurons. Cell Tissue Res. *326*, 541–551.

Hengen, K.B., Torrado Pacheco, A., McGregor, J.N., Van Hooser, S.D., and Turrigiano, G.G. (2016). Neuronal Firing Rate Homeostasis Is Inhibited by Sleep and Promoted by Wake. Cell *165*, 180–191.

Hensch, T.K. (2005). Critical period plasticity in local cortical circuits. Nat. Rev. Neurosci. *6*, 877–888.

Hofle, N., Paus, T., Reutens, D., Fiset, P., Gotman, J., Evans, A.C., and Jones, B.E. (1997). Regional Cerebral Blood Flow Changes as a Function of Delta and Spindle Activity during Slow Wave Sleep in Humans. J. Neurosci. *17*, 4800–4808.

Huang, Z.-L., Qu, W.-M., Eguchi, N., Chen, J.-F., Schwarzschild, M.A., Fredholm, B.B., Urade, Y., and Hayaishi, O. (2005). Adenosine A2A, but not A1, receptors mediate the arousal effect of caffeine. Nat. Neurosci. *8*, 858–859.

Huang, Z.-L., Mochizuki, T., Qu, W.-M., Hong, Z.-Y., Watanabe, T., Urade, Y., and Hayaishi, O. (2006). Altered sleep–wake characteristics and lack of arousal response to H3 receptor antagonist in histamine H1 receptor knockout mice. Proc. Natl. Acad. Sci. U. S. A. *103*, 4687–4692.

Huber, R., Hill, S.L., Holladay, C., Biesiadecki, M., Tononi, G., and Cirelli, C. (2004). Sleep homeostasis in Drosophila melanogaster. Sleep *27*, 628–639.

Huber, R., Tononi, G., and Cirelli, C. (2007). Exploratory behavior, cortical BDNF expression, and sleep homeostasis. Sleep *30*, 129–139.

Hur, E.E., and Zaborszky, L. (2005). Vglut2 afferents to the medial prefrontal and primary somatosensory cortices: A combined retrograde tracing in situ hybridization. J. Comp. Neurol. *483*, 351–373.

Huttenlocher, P.R. (1979). Synaptic density in human frontal cortex - developmental changes and effects of aging. Brain Res. *163*, 195–205.

Innocenti, G.M., and Price, D.J. (2005). Exuberance in the development of cortical networks. Nat. Rev. Neurosci. *6*, 955–965.

Irmak, S.O., and de Lecea, L. (2014). Basal forebrain cholinergic modulation of sleep transitions. Sleep *37*, 1941–1951.

Jenni, O.G., Achermann, P., and Carskadon, M.A. (2005). Homeostatic sleep regulation in adolescents. Sleep *28*, 1446–1454.

John, J., Wu, M.-F., Boehmer, L.N., and Siegel, J.M. (2004). Cataplexy-Active Neurons in the Hypothalamus: Implications for the Role of Histamine in Sleep and Waking Behavior. Neuron *42*, 619–634.

Jones, B.E. (2005). From waking to sleeping: neuronal and chemical substrates. Trends Pharmacol. Sci. *26*, 578–586.

Kalinchuk, A.V., McCarley, R.W., Stenberg, D., Porkka-Heiskanen, T., and Basheer, R. (2008). The Role of Cholinergic Basal Forebrain Neurons in Adenosine-Mediated Homeostatic Control of Sleep: Lessons from 192 IgG-Saporin Lesions. Neuroscience *157*, 238–253.

Kamphuis, J., Baichel, S., Lancel, M., de Boer, S.F., Koolhaas, J.M., and Meerlo, P. (2016). Sleep restriction in rats leads to changes in operant behaviour indicative of reduced prefrontal cortex function. J. Sleep Res. n/a-n/a.

Killgore, W.D.S. (2010). Effects of sleep deprivation on cognition. In Progress in Brain Research, G.A.K. and H.P.A. van Dongen, ed. (Elsevier), pp. 105–129.

Killgore, W.D.S., Balkin, T.J., and Wesensten, N.J. (2006a). Impaired decision making following 49 h of sleep deprivation. J. Sleep Res. *15*, 7–13.

Killgore, W.D.S., McBride, S.A., Killgore, D.B., and Balkin, T.J. (2006b). The effects of caffeine, dextroamphetamine, and modafinil on humor appreciation during sleep deprivation. Sleep *29*, 841–847.

Killgore, W.D.S., Lipizzi, E.L., Kamimori, G.H., and Balkin, T.J. (2007). Caffeine Effects on Risky Decision Making After 75 Hours of Sleep Deprivation. Aviat. Space Environ. Med. *78*, 957–962.

King, D.P., and Takahashi, J.S. (2000). Molecular Genetics of Circadian Rhythms in Mammals. Annu. Rev. Neurosci. *23*, 713–742.

Kuhn, M., Wolf, E., Maier, J.G., Mainberger, F., Feige, B., Schmid, H., Bürklin, J., Maywald, S., Mall, V., Jung, N.H., et al. (2016). Sleep recalibrates homeostatic and associative synaptic plasticity in the human cortex. Nat. Commun. *7*, 12455.

Lazar, A.S., Lazar, Z.I., and Dijk, D.-J. (2015). Circadian regulation of slow waves in human sleep: Topographical aspects. Neuroimage *116*, 123–134.

Lee, M.G., Hassani, O.K., and Jones, B.E. (2005a). Discharge of Identified Orexin/Hypocretin Neurons across the Sleep-Waking Cycle. J. Neurosci. *25*, 6716–6720.

Lee, M.G., Hassani, O.K., Alonso, A., and Jones, B.E. (2005b). Cholinergic Basal Forebrain Neurons Burst with Theta during Waking and Paradoxical Sleep. J. Neurosci. *25*, 4365–4369.

Leger, D., Beck, F., Richard, J.-B., and Godeau, E. (2012). Total sleep time severely drops during adolescence. PloS One *7*, e45204.

Li, Y., Gao, X.-B., Sakurai, T., and van den Pol, A.N. (2002). Hypocretin/Orexin Excites Hypocretin Neurons via a Local Glutamate Neuron—A Potential Mechanism for Orchestrating the Hypothalamic Arousal System. Neuron *36*, 1169–1181.

Lim, J., and Dinges, D.F. (2008). Sleep Deprivation and Vigilant Attention. Ann. N. Y. Acad. Sci. *1129*, 305–322.

Lin, J. (2000). PHYSIOLOGICAL REVIEW ARTICLE: Brain structures and mechanisms involved in the control of cortical activation and wakefulness, with emphasis on the posterior hypothalamus and histaminergic neurons. Sleep Med. Rev. *4*, 471–503.

Malenka, R.C., and Bear, M.F. (2004). LTP and LTD: An Embarrassment of Riches. Neuron *44*, 5–21.

de Manacéine, M. (1894). Quelques observations experimentales sur l'influence de l'insomnie absolue. Arch. Ital. Biol. *21*, 322–325.

Maret, S., Faraguna, U., Nelson, A.B., Cirelli, C., and Tononi, G. (2011). Sleep and waking modulate spine turnover in the adolescent mouse cortex. Nat. Neurosci. *14*, 1418–1420.

Martindale, J.L., and Holbrook, N.J. (2002). Cellular response to oxidative stress: Signaling for suicide and survival*. J. Cell. Physiol. *192*, 1–15.

McGinty, D., and Szymusiak, R. (2000). The sleep–wake switch: A neuronal alarm clock. Nat. Med. *6*, 510–511.

Mileykovskiy, B.Y., Kiyashchenko, L.I., and Siegel, J.M. (2005). Behavioral Correlates of Activity in Identified Hypocretin/Orexin Neurons. Neuron *46*, 787–798.

Miller, J.D., Farber, J., Gatz, P., Roffwarg, H., and German, D.C. (1983). Activity of mesencephalic dopamine and non-dopamine neurons across stages of sleep and walking in the rat. Brain Res. *273*, 133–141.

Minges, K.E., and Redeker, N.S. (2016). Delayed school start times and adolescent sleep: A systematic review of the experimental evidence. Sleep Med. Rev. *28*, 86–95.

Mistlberger, R.E., Landry, G.J., and Marchant, E.G. (1997). Sleep deprivation can attenuate light-induced phase shifts of circadian rhythms in hamsters. Neurosci. Lett. *238*, 5–8.

Miyawaki, H., and Diba, K. (2016). Regulation of Hippocampal Firing by Network Oscillations during Sleep. Curr. Biol. *26*, 893–902.

Monti, J.M., and Jantos, H. (2008). The roles of dopamine and serotonin, and of their receptors, in regulating sleep and waking. In Progress in Brain Research, V.D.M. and E.E. Giuseppe Di Giovann, ed. (Elsevier), pp. 625–646.

Moruzzi, G., and Magoun, H.W. (1949). Brain stem reticular formation and activation of the EEG. Electroencephalogr. Clin. Neurophysiol. *1*, 455–473.

Musall, S., Pföstl, V. von, Rauch, A., Logothetis, N.K., and Whittingstall, K. (2014). Effects of Neural Synchrony on Surface EEG. Cereb. Cortex *24*, 1045–1053.

Neckelmann, D., and Ursin, R. (1993). Sleep stages and EEG power spectrum in relation to acoustical stimulus arousal threshold in the rat. Sleep *16*, 467–477.

Nelson, A.B., Faraguna, U., Zoltan, J.T., Tononi, G., and Cirelli, C. (2013). Sleep Patterns and Homeostatic Mechanisms in Adolescent Mice. Brain Sci. *3*, 318–343.

Nishino, S., Ripley, B., Overeem, S., Lammers, G.J., and Mignot, E. (2000). Hypocretin (orexin) deficiency in human narcolepsy. The Lancet *355*, 39–40.

Noudoost, B., and Moore, T. (2011). CONTROL OF VISUAL CORTICAL SIGNALS BY PREFRONTAL DOPAMINE. Nature *474*, 372–375.

Ohayon, M.M., Carskadon, M.A., Guilleminault, C., and Vitiello, M.V. (2004). Meta-analysis of quantitative sleep parameters from childhood to old age in healthy individuals: developing normative sleep values across the human lifespan. Sleep *27*, 1255–1273.

Paus, T., Keshavan, M., and Giedd, J.N. (2008). Why do many psychiatric disorders emerge during adolescence? Nat. Rev. Neurosci. *9*, 947–957.

Piper, D.C., Upton, N., Smith, M.I., and Hunter, A.J. (2000). The novel brain neuropeptide, orexin-A, modulates the sleep–wake cycle of rats. Eur. J. Neurosci. *12*, 726–730.

Porkka-Heiskanen, T., and Kalinchuk, A.V. (2011). Adenosine, energy metabolism and sleep homeostasis. Sleep Med. Rev. *15*, 123–135.

Porkka-Heiskanen, T., Strecker, R.E., and McCarley, R.W. (2000). Brain site-specificity of extracellular adenosine concentration changes during sleep deprivation and spontaneous sleep: an in vivo microdialysis study. Neuroscience *99*, 507–517.

Sagaspe, P., Sanchez-Ortuno, M., Charles, A., Taillard, J., Valtat, C., Bioulac, B., and Philip, P. (2006). Effects of sleep deprivation on Color-Word, Emotional, and Specific Stroop interference and on self-reported anxiety. Brain Cogn. *60*, 76–87.

Sakurai, T. (2013). Orexin deficiency and narcolepsy. Curr. Opin. Neurobiol. *23*, 760–766.

Saper, C.B. (2013). The central circadian timing system. Curr. Opin. Neurobiol. *23*, 747–751.

Saper, C.B., Chou, T.C., and Scammell, T.E. (2001). The sleep switch: hypothalamic control of sleep and wakefulness. Trends Neurosci. *24*, 726–731.

Saper, C.B., Scammell, T.E., and Lu, J. (2005). Hypothalamic regulation of sleep and circadian rhythms. Nature *437*, 1257–1263.

Sara, S.J. (2009). The locus coeruleus and noradrenergic modulation of cognition. Nat. Rev. Neurosci. *10*, 211–223.

Sasaki, K., Suzuki, M., Mieda, M., Tsujino, N., Roth, B., and Sakurai, T. (2011). Pharmacogenetic modulation of orexin neurons alters sleep/wakefulness states in mice. PloS One *6*, e20360.

Schmidt, C., Collette, F., Leclercq, Y., Sterpenich, V., Vandewalle, G., Berthomier, P., Berthomier, C., Phillips, C., Tinguely, G., Darsaud, A., et al. (2009). Homeostatic Sleep Pressure and Responses to Sustained Attention in the Suprachiasmatic Area. Science *324*, 516–519.

Steriade, M. (2004). Acetylcholine systems and rhythmic activities during the waking–sleep cycle. In Progress in Brain Research, K.K. Laurent Descarries and Mircea Steriade, ed. (Elsevier), pp. 179–196.

Steriade, M., and Hobson, J. (1976). Neuronal activity during the sleep-waking cycle. Prog. Neurobiol. *6*, 155–376.

Steriade, M., Timofeev, I., and Grenier, F. (2001). Natural Waking and Sleep States: A View From Inside Neocortical Neurons. J. Neurophysiol. *85*, 1969–1985.

Takahashi, K., Lin, J.-S., and Sakai, K. (2006). Neuronal Activity of Histaminergic Tuberomammillary Neurons During Wake–Sleep States in the Mouse. J. Neurosci. *26*, 10292–10298.

Takahashi, K., Kayama, Y., Lin, J.S., and Sakai, K. (2010). Locus coeruleus neuronal activity during the sleep-waking cycle in mice. Neuroscience *169*, 1115–1126.

Taylor, N.E., Dort, C.J.V., Kenny, J.D., Pei, J., Guidera, J.A., Vlasov, K.Y., Lee, J.T., Boyden, E.S., Brown, E.N., and Solt, K. (2016). Optogenetic activation of dopamine neurons in the ventral tegmental area induces reanimation from general anesthesia. Proc. Natl. Acad. Sci. 201614340.

Thannickal, T.C., Moore, R.Y., Nienhuis, R., Ramanathan, L., Gulyani, S., Aldrich, M., Cornford, M., and Siegel, J.M. (2000). Reduced Number of Hypocretin Neurons in Human Narcolepsy. Neuron *27*, 469–474.

Timofeev, I., Grenier, F., and Steriade, M. (2001). Disfacilitation and active inhibition in the neocortex during the natural sleep-wake cycle: An intracellular study. Proc. Natl. Acad. Sci. U. S. A. *98*, 1924–1929.

Tononi, G., and Cirelli, C. (2006). Sleep function and synaptic homeostasis. Sleep Med. Rev. *10*, 49–62.

Tononi, G., and Cirelli, C. (2012). Time to be SHY? Some comments on sleep and synaptic homeostasis. Neural Plast. *2012*, 415250.

Tononi, G., and Cirelli, C. (2014). Sleep and the Price of Plasticity: From Synaptic and Cellular Homeostasis to Memory Consolidation and Integration. Neuron *81*, 12–34.

Van Dongen, H.P.A., Maislin, G., Mullington, J.M., and Dinges, D.F. (2003). The cumulative cost of additional wakefulness: dose-response effects on neurobehavioral functions and sleep physiology from chronic sleep restriction and total sleep deprivation. Sleep *26*, 117–126.

Van Dort, C.J., Zachs, D.P., Kenny, J.D., Zheng, S., Goldblum, R.R., Gelwan, N.A., Ramos, D.M., Nolan, M.A., Wang, K., Weng, F.-J., et al. (2015). Optogenetic activation of cholinergic neurons in the PPT or LDT induces REM sleep. Proc. Natl. Acad. Sci. U. S. A. *112*, 584–589.

de Vivo, L., Bellesi, M., Marshall, W., Bushong, E.A., Ellisman, M.H., Tononi, G., and Cirelli, C. (2016a). Ultrastructural Evidence for Synaptic Scaling Across the Wake/sleep Cycle. Science *In press*.

de Vivo, L., Nelson, A.B., Bellesi, M., Noguti, J., Tononi, G., and Cirelli, C. (2016b). Loss of Sleep Affects the Ultrastructure of Pyramidal Neurons in the Adolescent Mouse Frontal Cortex. Sleep *39*, 861–874.

Von Economo, C. (1930). Sleep as a problem of localization. J. Nerv. Ment. Dis. *71*, 249–259.

Vyazovskiy, V.V., and Harris, K.D. (2013). Sleep and the single neuron: the role of global slow oscillations in individual cell rest. Nat. Rev. Neurosci. *14*, 443–451.

Vyazovskiy, V.V., Riedner, B.A., Cirelli, C., and Tononi, G. (2007). Sleep Homeostasis and Cortical Synchronization: II. A Local Field Potential Study of Sleep Slow Waves in the Rat. Sleep *30*, 1631–1642.

Vyazovskiy, V.V., Cirelli, C., Pfister-Genskow, M., Faraguna, U., and Tononi, G. (2008). Molecular and electrophysiological evidence for net synaptic potentiation in wake and depression in sleep. Nat. Neurosci. *11*, 200–208.

Vyazovskiy, V.V., Olcese, U., Lazimy, Y.M., Faraguna, U., Esser, S.K., Williams, J.C., Cirelli, C., and Tononi, G. (2009). Cortical firing and sleep homeostasis. Neuron *63*, 865–878.

Vyazovskiy, V.V., Cirelli, C., and Tononi, G. (2011). Electrophysiological correlates of sleep homeostasis in freely behaving rats. Prog. Brain Res. *193*, 17–38.

Watson, B.O., Levenstein, D., Greene, J.P., Gelinas, J.N., and Buzsáki, G. (2016). Network Homeostasis and State Dynamics of Neocortical Sleep. Neuron *90*, 839–852.

Werth, E., Dijk, D.J., Achermann, P., and Borbély, A.A. (1996). Dynamics of the sleep EEG after an early evening nap: experimental data and simulations. Am. J. Physiol. *271*, R501-510.

Chapter II:

Why does sleep slow wave activity increase after extended wake? Assessing the effects of increased cortical firing during wake and sleep

Alexander V. Rodriguez, Chadd M. Funk, Vladyslav Vyazovskiy, Yuval Nir, Giulio Tononi, and Chiara Cirelli

In press, *Journal of Neuroscience*

Abstract

During NREM sleep cortical neurons alternate between ON periods of firing and OFF periods of silence. This bistability, which is largely synchronous across neurons, is reflected in the EEG as slow waves. Slow wave activity (SWA) increases with wake duration and declines homeostatically during sleep, but the underlying mechanisms remain unclear. One possibility is neuronal 'fatigue': high, sustained firing in wake would force neurons to recover with more frequent and longer OFF periods during sleep. Another possibility is net synaptic potentiation during wake: stronger coupling among neurons would lead to greater synchrony and therefore higher SWA. Here we obtained a comparable increase in sustained firing (six hours) in cortex by: i) keeping mice awake by exposure to novel objects to promote plasticity; ii) optogenetically activating a local population of cortical neurons at wake-like levels during sleep. Sleep following extended wake led to increased SWA, higher synchrony, and more time spent OFF, with a positive correlation between SWA, synchrony, and OFF periods. Moreover, time spent OFF was correlated with cortical firing during prior wake. After local optogenetic stimulation, SWA and cortical synchrony decreased locally, time spent OFF did not change, and local SWA was not correlated with either measure. Moreover, laser-induced cortical firing was not correlated with time spent OFF afterwards. Overall, these results suggest that high sustained firing per se may not be the primary determinant of SWA increases observed after extended wake.

Significance statement

A long-standing hypothesis is that neurons fire less during slow wave sleep to recover from the “fatigue” accrued during wake, when overall synaptic activity is higher than in sleep. This idea, however, has rarely been tested and other factors, namely increased cortical synchrony, could explain why sleep slow wave activity is higher after extended wake. We forced neurons in the mouse cortex to fire at high levels for six hours in two different conditions, during active wake with exploration, and during sleep. We find that neurons need more time OFF only after sustained firing in wake, suggesting that fatigue due to sustained firing alone is unlikely to account for the increase in slow wave activity that follows sleep deprivation.

Introduction

During NREM sleep, cortical and thalamic neurons oscillate between ON states of firing and OFF periods of silence (Chauvette et al., 2011; Steriade et al., 2001). This bistability occurs more or less synchronously in many neurons and is recorded in the electroencephalogram (EEG) as slow waves. During NREM sleep, amplitude and incidence of slow waves are quantified using slow wave activity (SWA), the EEG power in the 0.5-4.0 Hz range. SWA increases with wake duration, peaks in early sleep and declines in late sleep. SWA is considered an index of the homeostatic process "S", reflecting the increase in sleep need/intensity with wake duration (in conjunction with the circadian factor "C", which affects primarily sleep timing and duration) (Borbély, 1982; Borbély et al., 2016).

However, the mechanisms linking wake duration to SWA remain unclear. Early hypotheses included the possible accumulation of "an endogenous sleep compound which is eliminated or inactivated during sleep" (Borbély et al., 1981) or of "metabolic processes" that need to be reversed in sleep (Feinberg et al., 1978). A long-standing hypothesis is that during wake neurons may accrue 'fatigue' due to overall higher firing, which would be reversed in NREM sleep as a result of reduced firing during OFF periods (Rechtschaffen, 1998; Vyazovskiy and Harris, 2013). Neuronal fatigue is usually conceptualized as temporary exhaustion triggered by intense activity, due to momentary run-down of energy resources (e.g. glycogen (Dalsgaard and Secher, 2007)), depletion of synaptic vesicles/calcium (O'Donovan and Rinzel, 1997), or accumulation of adenosine (Brambilla et al., 2005; Brundege and Dunwiddie, 1998; Lovatt et al., 2012). Indeed, it was explicitly suggested that SWA may reflect the build-up of adenosine and the subsequent potentiation of potassium currents that hyperpolarize cortical neurons during the OFF state (Benington and Heller, 1995).

Another hypothesis is that wake would lead to an overall increase in synaptic strength associated with learning, and that sleep would then be required to renormalize synaptic weights, with beneficial effects both at the cellular level (energy, supplies) and at the systems level (memory) (Cirelli et al., 2004; Tononi and Cirelli, 2006, 2012, 2014). The increase in SWA after wake would be due primarily to the increase in neuronal synchrony brought about by stronger synaptic coupling, just as its decrease during sleep would be due to reduced synchrony following net synaptic depression. The net increase in synaptic strength during wake and its decrease during sleep is supported by molecular, electrophysiological, as well as structural and ultrastructural evidence (Tononi and Cirelli, 2014; de Vivo et al., 2016). Moreover, computer simulations show that increased synaptic strength is sufficient to cause higher synchrony, higher SWA, as well as more numerous and prolonged OFF periods (Esser et al., 2007). Accordingly, the onset of ON and OFF periods is more synchronous after extended wake and less so after sleep (Vyazovskiy et al., 2009).

So far, many studies have demonstrated a global increase in SWA after extended wakefulness with object exploration, and local increases after specific learning tasks (Hanlon et al., 2011). However, the relative contribution of increased neuronal firing and synaptic plasticity to subsequent SWA cannot easily be disentangled. The occurrence of OFF periods during wake (‘local sleep’) after extended exploration of novel objects (Vyazovskiy et al., 2011) could also reflect either fatigue due to excessive firing and/or excessive synaptic potentiation. In this work, we set out to test directly whether a sustained increase in mean cortical firing rate during wake, obtained by having animals explore novel objects to promote plasticity, and a comparable increase obtained by optogenetic stimulation during sleep, lead to differential effects on neuronal synchrony, SWA, and OFF periods during subsequent NREM sleep.

Material and Methods

Surgery

Adult (~60-90 days old) male transgenic B6.Cg-Tg(Camk2a-Cre)T29-1Stl/J mice that express Cre recombinase in excitatory cortical neurons were used (Jackson Laboratory, JAX Stock number 005359, RRID:IMSR_JAX:005359). Animals were housed in single cages and kept on a 12h:12h light/dark cycle with lights on at 10 A.M. All animal procedures and experimental protocols followed the National Institutes of Health Guide for the Care and Use of Laboratory Animals and were approved by the licensing committee. All animal facilities were reviewed and approved by the institutional animal care and use committee (IACUC) of the University of Wisconsin-Madison, and were inspected and accredited by association for assessment and accreditation of laboratory animal care (AAALAC).

Virus injection and electrode implantation were performed in 2 separate surgeries, as adeno-associated viruses take up to 3 weeks to become fully expressed and cortical electrodes have a limited viable recording time once implanted, due to immune responses or glial buildup (Grill, 2008). Thus, we waited 3 weeks after virus injection before performing the electrode implant surgery. Both surgeries were performed under isoflurane anesthesia (2% for induction, 1-2% for maintenance) using proper sterile technique. After making a small craniotomy in the skull, the purified adeno-associated virus rAAV5-Ef1a-DIO hChR2 (C128S/D156A-EYFP) (4 x 10^{12} virus particles/ml) was stereotaxically injected into the right frontal cortex (from bregma, +1.28 A/P; +1.0 M/L; -1.5 D/V) at 0.1 µL/min for 20 min (total 2 µL of virus), with a 10-min wait following the end of the injection to allow for liquid diffusion into the cortex. This stable step function opsin (SSFO) virus was obtained from the UNC vector core (University of North

Carolina, RRID:SCR_002448) under an agreement with Dr. Karl Deisseroth at Stanford University. The small craniotomy was covered using the dental acrylic Fusio (Pentron Clinical) and the incision was closed using Vetbond (3M). For chronic polygraphic recordings, gold screws were inserted into the skull above left frontal (+1.4 AP, -1.5 M/L) and right parietal cortex (-2.5A/P, +1.7 M/L) to record EEG activity, and stainless steel wires were implanted into the nuchal muscles for electromyography (EMG). Moreover, a microwire electrode array with 16 electrodes (Tucker-Davis Technologies, RRID:SCR_006495) cemented to an optic fiber ferrule (Doric Lenses) was inserted into the right frontal hemisphere (+1.0 A/P; +1.0 M/L; -1.4 D/V; D/V measured from cortex), along with a laminar probe (Neuronexus) or a second microwire array into the left parietal cortex. Arrays were targeted to the deep cortical layers (mainly layer 5), while laminar probes spanned all layers. After one week of recovery from the second surgery, animals were connected to a wire bundle to record electrical signals and an optic patch cable to prepare for laser stimulation. Using the RZ2 amplifier and PZ2 pre-amplifier (Tucker-Davis Technologies, RRID:SCR_006495), EEG (256 Hz, bandpass filtered at 0.1-100 Hz) and EMG (256Hz, bandpass filtered at 10-50 Hz) signals were continuously collected for several weeks, together with local field potentials (LFPs, 256 Hz, bandpass filtered at 0.1-100 Hz) and multiunit activity (MUA, 24.4kHz, bandpass filtered at 300-5000 Hz). Thresholds for MUA were set manually below 0 mV, and waveforms for each threshold-crossing event were saved. Experiments started only after the sleep/wake cycle had normalized and mice were fully entrained to the light/dark cycle, sleeping mostly during the day and staying awake mainly at night. Percentage of sleep and wake (mean ± std) during the light phase in baseline were consistent with published values (e.g. (Bellesi et al., 2015; Franken et al., 1999; Huber et al., 2000)): Wake: 39.8% ± 5.0%, NREM sleep: 50.5% ± 4.6%, REM sleep: 9.7% ± 1.6%.

Sleep Deprivation (SD)

SD was performed for 6 hours starting at light onset using exposure to novel objects. Since the procedure can be stressful in naïve animals, mice were familiarized with the method by placing a new object in the cage every day for several days prior to the SD experiment. During SD, mice were given a new object or bedding every time they were inactive and slow waves became evident on real-time EEG monitoring. Mice were never disturbed when they were spontaneously awake, feeding, or drinking. As some mice continue to stay awake for variable amounts of time after all objects are removed, analysis started always at hour 7, but the exact time was adjusted to begin at the onset of consolidated sleep, defined as the first 30-min window in which sleep accounted for at least 50% of the time, and whose first 3 minutes also included at least 50% of time spent asleep.

Laser Stimulation during NREM sleep (laser-S)

To activate the stable step-function opsin (SSFO) rAAV5-Ef1a-DIO-hChR2 (C128S/D156A)-EYFP a 473 nm wavelength laser (OEM Laser Systems) was used. Laser stimulation was delivered remotely by an investigator who was outside the room housing the mice and was checking the polygraphic traces online. Short pulses of 2.3 ± 1.2 seconds (mean ± std) in duration and ~1mW in intensity (minimum 100µW, maximum 15mW, almost all pulses near 1mW) were given approximately every 5 min, always during NREM sleep. Laser power and pulse timing were titrated to maintain wake-like, tonic firing in the stimulated electrodes. To match the SD experiment the overall duration of the laser-S experiment was 6 hours; the last pulse was given no later than 20 min before the end of the sixth hour to allow SSFO channels to close, thus reducing the risk of carryover effects.

Data Analysis

Frontal and parietal EEG and local field potentials (LFPs), as well as EMG waveforms were exported to the graphic interface SleepSign (Kissei Comtec), where 4-sec epochs were manually scored as wake, NREM sleep or REM sleep according to established criteria. In wake, muscle activity was high and the EEG was dominated by low amplitude, high frequency activity, while NREM sleep was characterized by low muscle tone and high amplitude, low frequency EEG/LFP activity, and REM sleep by low EMG activity with occasional twitches and strong theta (6-9 Hz) activity. Scoring could not be blind to experimental condition, given the obvious unique features of SD (continuous wake for 6 hours) and laser-S (high gamma power, see Results). All further analyses were performed using custom scripts in MATLAB (Mathworks, RRID:SCR_001622). Fast Fourier transforms were calculated using Welch's approximation method on Hanning windows to gather power spectra data from 0 to 120 Hz for each 4-sec epoch. Multi-unit activity (MUA) was down sampled into 2-ms bins (500 Hz) before all analyses (no spikes were lost due to downsampling). To calculate OFF period measures for MUA (number of OFF periods per minute of NREM sleep, average duration of OFF periods, and percent of time in NREM sleep spent OFF), each electrode was assigned an OFF period threshold, where all periods of silence equal to or longer than that threshold were counted as OFF periods. The OFF period threshold for an electrode was calculated by fitting the interspike intervals (ISIs) for an electrode to a gamma distribution using the MATLAB function 'gamfit'. A number of ISIs equal to the number of ISIs used for fitting were drawn from this distribution, and the 99th percentile for ISI length from this set of ISIs was the OFF period threshold. A close variation of this process was used in previously published work (Vyazovskiy et al., 2011). However, the current analysis was performed at the single electrode level, whereas previously

(Vyazovskiy et al., 2011) OFF measures were calculated on MUA collapsed across several electrodes (for validation of the current method, see Results). We also performed OFF period analysis on spike data collapsed across all electrodes of an array for each mouse. This collapsed spike train was then treated as firing from a single electrode, and the analysis was performed as above.

To calculate synchrony of ON periods between electrodes, contributing electrodes from each mouse were considered in groups. Each electrode from a mouse in turn was the 'target' electrode, while all other electrodes from the same array were 'other' electrodes (mice that contributed only one electrode were excluded from this analysis). ON periods were defined for each electrode as the entire time spent in NREM sleep that was not classified as an OFF period for that electrode (as defined above). The start of each ON period (that is, end of each OFF period) in the target electrode was the center of a time window of 48 ms. Other electrodes that also had ON periods starting within this 48 ms window were counted as 'synchronous'. The proportion of other electrodes marked 'synchronous' provided a synchrony score for the beginning of each ON period in the target electrode. For example, if 4 of 4 other electrodes were synchronous, the score for that ON period was 1. If only 1 of 4 other electrodes were synchronous, the score was instead 0.25. The total synchrony score for an electrode was the average of the synchrony score across all of the ON period onsets for a given time period. This process was repeated for the ends of the ON periods.

Histology and colocalization studies

Mice were deeply anesthetized under 3% isoflurane and transcardially perfused with 0.9% saline followed by 4% paraformaldehyde (PFA) in phosphate buffer. Brains were removed and placed in 4% PFA for at least 24 hours, then sliced into 50-µm-thick sections on a vibratome, mounted onto glass slides, covered in Vectashield (Vector Labs, H-1000, RRID:AB_2336789), and imaged using a light microscope (Leica Microsystems, RRID:SCR_008960) to verify virus expression and electrode placement in the cortex. To estimate the percentage of cells infected by the virus we injected 4 additional mice of the same strain, sex, and age as above with a nearly identical virus containing only EYFP (rAAV5-EF1a-DIO-EYFP) (University of North Carolina, RRID:SCR_002448). After allowing ~1 month for viral expression, mice were perfused and brains were sliced as above. A subset of slices was then selected for NeuN staining. Infection rate was estimated in the 'main injection area', which could be easily identified as the homogenous bright fluorescent area surrounding the injection. In all mice this region spanned more than 1 mm rostro-caudally, and corresponded to the area where the recording electrodes were located in implanted mice. To estimate the infection rate, we took 3 sections from each mouse within this area: 1 section that included the injection track, and 2 other sections located 0.5 mm rostral and 0.5 mm caudal to the central section. Sections were first left for 1 hour in 10% normal goat serum (NGS; MP Biomedicals, Catalog #08642921, RRID:AB_2335031) in 0.05 M phosphate buffered saline (PBS), then incubated in rabbit anti-NeuN overnight at room temperature (Millipore, ABN78, RRID:AB_10807945, 1:200 in PBS). The next day, sections were washed 5 times for 5 min each in PBS and then left in 10% NGS for 25 min. Next, sections were incubated in anti-rabbit Alexa Fluor 568 for 1 hour at room temperature (Life Technologies, A11011, RRID:AB_2534078, 1:1000 in PBS), then washed

again, mounted onto glass slides and covered in Vectashield. One mouse was excluded due to faint viral expression. Within the remaining 3 mice, images from the main injection area of each section were taken using a confocal microscope (Olympus). Several (3 to 5) non-overlapping image stacks (5-10 µm thick) were taken per section, depending on image quality and injection area, for a total of 39 stacks across the 3 mice. Images were analyzed with ImageJ using an algorithm that first collapsed stacks into a maximum projection, then automatically detected NeuN+ spots and marked them as regions of interest (ROIs). ROIs that contacted any of the 4 margins of the image were discarded, as mean EYFP fluorescence inside them could not be fully assessed. A fluorescence threshold was manually set after visual inspection and applied uniformly to all images. EYFP fluorescence was then measured across all ROIs. NeuN+ cells that contained an average EYFP fluorescence above threshold were counted as double-labeled (NeuN+ EYFP+) cells.

Results

We compared 2 experimental conditions associated with a similar sustained increase in cortical neuronal activity, 6 hours of extended wake with exposure to novel objects, and 6 hours of optogenetic stimulation of cortical pyramidal neurons during sleep. Twenty adult male Camk2a-Cre mice were used in the study, all of which showed fairly widespread virus expression in the frontal cortex, limited to the right hemisphere, and had microwire arrays well placed within the expression area, as determined by histological examination (Figure 1A). The arrays in the right frontal cortex each included 16 electrodes that are referred to as “ipsilateral” electrodes. These electrodes spanned the cortical area injected with the virus that was subjected to optogenetic stimulation. Electrodes placed in the left parietal cortex are referred to as “contralateral” electrodes (with neither viral expression nor optogenetic stimulation; Figure 1B).

The 16 ipsilateral electrodes were organized into 2 parallel rows of 8 that spanned 1.4 mm in the anteroposterior direction and 0.5 mm mediolaterally, and their tips were located at the same cortical depth, mainly in layer 5 (Figure 1B). The extent of virus infection was estimated in 3 other Camk2a-Cre mice, not used for the 2 main experiments, in which we counted how many cells in the main injected area expressed the neuronal nuclear marker NeuN and contained rAAV5-EF1a-DIO-EYFP (see Methods for details). This virus localizes throughout the cell, especially within the nucleus, and is almost identical to the one we used for the laser experiment, whose expression is instead excluded from the nucleus (Yizhar et al., 2011a). In the 3 animals, 62.7 ± 19.6% of NeuN+ cells were also EYFP+ (39 images, mean ± std; Figure 1C), suggesting that, within the main injection area, most excitatory neurons were infected.

In each mouse, 2 experiments were performed: sleep deprivation (SD) and laser stimulation during NREM sleep (laser-S), usually spaced ~ 4-5 days apart and run in counterbalanced order. Both experiments lasted two days, with the first day being the baseline day in which mice were allowed to sleep undisturbed (Figure 1D). On day two, during the first 6 hours of the light period, mice were either kept awake by exposure to novel objects (SD) or allowed to sleep but received laser stimulation during NREM sleep (laser-S). Sleep that followed SD or laser-S was analyzed starting at hour 7 of the light period and compared to the same time period of the preceding baseline day. Firing from all electrodes was manually inspected across both experimental days, and only those electrodes that showed a stable signal across both days were selected for analysis. Most mice (13 out of 20) contributed electrodes for both experimental conditions; in the remaining 7 mice, data from only SD or laser-S could be used, due to decreased quality and stability of the recordings (see below). Overall, 16 mice contributed data for SD, and 17 mice contributed for laser-S. Three measures were used to assess the effects of

SD or laser-S: 1) the left frontal and right parietal EEG, to detect broad changes in brain activity outside the virus expression/stimulated area; 2) LFP recordings from ipsilateral and contralateral electrodes; 3) multi-unit activity (MUA) from the same electrodes.

Sleep deprivation increases cortical firing and is followed by increases in SWA and time spent OFF during sleep

SD by novel objects reduced the total time spent asleep to <1% of the 6 hours, with the few minutes of sleep spent in NREM sleep (not shown). To obtain an overall estimate of neuronal activity during SD we focused on the ipsilateral electrodes, the same ones targeted by laser stimulation (n=59, 16 mice), and for each of them we expressed the mean firing rate for hours 1-6 of the SD day as a percentage of the corresponding firing rate during hours 1-6 of the baseline day. In most electrodes, neuronal activity during SD increased relative to the same circadian time in baseline, when mice are mostly asleep. As a result, mean firing rate during SD increased by 72.13 ± 47.49 % (mean ± std, 59 electrodes, 16 mice; Wilcoxon signed rank test, $p=2.65*10^{-11}$; Figure 2A). Not surprisingly, a similar increase was present in contralateral channels (not shown).

As expected, mice showed a sleep rebound when they were allowed to sleep. During the first 2 hours after SD, time spent in NREM sleep increased at the expense of wake (% of time spent in each state, hours 7-8 of baseline day vs. hours 7-8 SD day, mean ± std; wake: 37.5 ± 9.5 % vs. 17.6 ± 7.9 %, NREM: 52.1 ± 7.6 % vs. 71.8 ± 7.1 %, REM: 10.4 ± 2.8 % vs. 10.5 ± 2.7 %). SWA also increased at the beginning of the recovery period in both the left frontal EEG (Figure 2B) and the right parietal EEG (% increase in SD vs. baseline; 15 electrodes, 15 mice; 32.3 ± 23.3%, mean ± std; Wilcoxon signed rank test, $p=6.10*10^{-5}$), and this increase was

specific for the low EEG frequencies (Figure 2B). A similar specific increase in SWA was seen in the LFPs from all ipsilateral electrodes (Figure 2C). We then focused on measures of OFF periods (Figure 2D). First, we tested whether "OFF periods" as identified at the single-electrode level correspond to OFF periods as previously defined based on the positive peak of the LFP slow waves (negative peak of the scalp EEG slow waves), or on a pre-selected time of silence across all electrodes (Vyazovskiy et al., 2009). We found that this was the case. Specifically, we isolated single electrodes and examined the OFF period-triggered average of LFP traces and found that single-electrode OFF periods aligned well with LFP positive peaks (Figure 2E). Next, to measure changes in neuronal activity during recovery sleep we calculated, for each ipsilateral electrode, the incidence of OFF periods (number/min of NREM sleep), their average duration, as well as the "percentage of time OFF" (total time spent in OFF periods, expressed as % of total time in NREM sleep) in hours 7-8 of the SD day, and compared these measures to the same circadian time in the baseline day (Figure 2D). Time spent in OFF periods increased in the first 2 hours following SD relative to the same circadian time in baseline, due to an increase in both number and duration of OFF periods (Figure 2F) and all changes had returned to baseline levels or lower by the first 2 hours of the dark period (Figure 2G). Moreover, time spent OFF in the first 2 hours after SD was correlated with mean firing rates during the 6 hours of extended wake (Figure 2H). Thus, after sustained high firing in wake for 6 hours, neurons spent more time OFF, a change that was reversible in a few hours. This change was detectable at the level of individual electrodes. We also calculated OFF period measures after collapsing all electrodes within each mouse and treating the collapsed MUA as a single MUA trace, similar to previous work (Vyazovskiy et al., 2009). Results were similar: number and duration of OFF periods, as well as percent of time spent OFF, significantly increased in hours 7-8 after SD relative to baseline (16

mice; mean ± std, Wilcoxon signed rank test, N: +10.1 ± 17.9 %; p=0.03; duration: +7.3 ± 9.2 %; p=0.008; % OFF: +18.8 ± 24.5 %; p=0.009). As previously reported in rats (Vyazovskiy et al., 2009), firing rate during the ON periods also increased in the first 2 hours after SD relative to baseline (+7.2 ± 11.9 %; Wilcoxon signed rank test, $p=6.74*10^{-5}$).

Laser stimulation during sleep increases local cortical firing without causing arousal, and is followed by a decrease in SWA and no changes in time spent OFF during sleep

The goal of the laser-S experiment was to force neurons in a small cortical area to fire during NREM sleep at levels comparable to those reached during SD, but without waking up the mice. Since high firing had to be maintained for several hours, a stable step function opsin (SSFO) was used, which introduces a steady cationic current into neurons and thus increases their overall excitability (Yizhar et al., 2011a). An advantage of SSFOs is that affected neurons are more likely to still fire in their natural patterns, albeit at a higher rate, making the increased activity more physiologically relevant compared to repeated electrical stimulation or acute optogenetic stimulation using opsins with fast kinetics (Yizhar et al., 2011a). Brief laser pulses (mostly ~2 sec at ~1mW) were delivered only during NREM sleep, on average every 5 min, for a total of ~60 pulses during hours 1-6 of the laser-S day. During this time, the percentage of wake, NREM sleep, and REM sleep did not differ from baseline (Figure 3A). The average duration of sleep and wake episodes, as well as number of brief awakenings (wake bouts of ≤ 16 sec), also did not change between hours 1-6 of the baseline and laser-S days (Figure 3A). SWA during NREM sleep showed a small but significant decrease in the ipsilateral (right) parietal EEG (percent change in laser-S vs. baseline = -7.4 ± 9.8 %; Wilcoxon signed rank test, p=0.007) and the contralateral (left) frontal EEG (Figure 3B), while gamma power (30-55 Hz) was significantly increased in frontal EEG only (Figure 3B). In contrast to the small changes in

global measures of sleep, laser stimulation clearly affected LFP spectral power and neuronal activity at the local level. As mentioned, we estimated that ~63% of neurons were infected with the virus in the main injected area, and because of the especially low power required for SSFO activation (Yizhar et al., 2011b), and the fact that our laser light was focused on this area, we assume that most of them were activated. However, due to the complex nature of light diffusion within the cortex, we cannot estimate the total number of neurons activated by laser stimulation, nor can we be sure that all infected neurons were activated to the same extent. Indeed, the effects of the optogenetic stimulation varied across electrodes, either because of variable levels of virus expression and/or because of changes in light intensity at the different electrode sites. Thus, some electrodes were strong responders, showing a sustained increase in firing across the 6 hours, while others showed weak or no responses, or even a decrease in firing during laser stimulation (Figure 3C). When all ipsilateral electrodes were considered together (n=66, 15 mice) across the entire 6 hours, including both sleep and wake, there was an overall significant increase in mean firing rate of 53.6 ± 57.8 % relative to baseline (percent change hours 1-6 laser-S vs. hours 1-6 baseline, mean ± std; Wilcoxon signed rank test, $p=8.82*10^{-10}$). This increase, however, was significantly smaller than the increase seen during SD. Since matching the 2 experimental conditions (SD and laser-S) by overall increase in firing rate was key to the goal of the study, we then selected, among all ipsilateral electrodes (n=66), only those whose laser-induced increase in firing rate was within the mean ± std observed during SD (72.1 ± 47.5 %). This selection resulted in 32 “SD-matched” electrodes, with an overall increase in mean firing rate of 66.1 ± 28.3 % (Figure 3D). During baseline, SD-matched electrodes did not show any obvious difference relative to the remaining ipsilateral electrodes: for instance, during hours 1-6 of the baseline day their mean firing rates and SWA power in NREM sleep varied within the

same range as the other electrodes (not shown). During laser stimulation, firing in these SD-matched responders was wake-like with little evidence of bistability, and indeed during the 6 hours of laser stimulation, the incidence of OFF periods during NREM sleep decreased by ~ 90% and the few remaining OFF periods were shorter, resulting in an almost complete lack of time OFF (Figure 3E). SD-matched electrodes also showed a noticeable shift in LFP power throughout the entire duration of the experiment, including a ~30% decrease in SWA and a ~100% increase in gamma power (Figure 3F). There was no correlation between changes in SWA and gamma power during the 6 hours of laser stimulation, and both changes were also visible in raw spectrograms in which LFP power was not normalized by the total power during baseline. During the 6 hours of laser stimulation contralateral channels showed no significant changes in firing rate (3.0 ± 15.8%, mean ± std; Wilcoxon signed rank test, p=0.36), OFF measures (% OFF: 9.2 ± 26.1%, p=0.30), or LFP SWA power (1.1 ± 6.4 %, p=0.50) relative to baseline.

During the first two hours after laser-S (hours 7-8), SWA was slightly decreased in both left frontal EEG (Figure 3G) and right parietal EEG (not shown) as compared to baseline. The LFPs of the SD-matched channels no longer had elevated gamma power, but still showed a significant decline in SWA relative to baseline, albeit smaller than during stimulation (Figure 3H). As before, we found that OFF periods were well correlated with positive LFP peaks (Figure 3I). However, in SD-matched electrodes, none of the OFF measures changed significantly in the first two hours after Laser-S (Figure 3J), or later (not shown). Moreover, time spent OFF in the first 2 hours after laser stimulation did not correlate with mean firing rates during the 6 hours of optogenetic stimulation (Figure 3K). OFF measures also did not change if all ipsilateral electrodes were considered (Figure 3L). Electrodes placed in the contralateral parietal cortex,

which received neither light exposure nor virus injection, showed no change in firing rate during laser-S (3.0 ± 15.8%, mean ± std; Wilcoxon signed rank test, p=0.36), and no changes in OFF periods following laser stimulation (not shown). These results were confirmed when calculating OFF period measures after collapsing across all electrodes for each mouse (SD-matched electrodes, 11 mice; mean ± std, Wilcoxon signed rank test; Number: 12.6 ± 45.4 %, p=0.76; Duration: 1.3 ± 4.6 %, p=0.70; % time OFF: 16.0 ± 53.4, p=0.64). In contrast to the recovery sleep after SD, after laser stimulation, mean firing rates during the ON periods in hours 7-8 showed no change relative to baseline in SD-matched electrodes (-1.9 ± 14.4 %; p=0.21).

Cortical synchrony increases after sleep deprivation but not after laser stimulation

Next we looked at the effects of SD and laser-S on neuronal coupling by measuring the extent to which the onset and offset of ON periods in each electrode were locked to those in the other electrodes of the same array (Figure 4A; see Methods for details). Consistent with previous work in rats (Vyazovskiy et al., 2009), neurons were significantly more likely to start and end their ON periods synchronously in the first 2 hours of recovery sleep after SD (Figure 4B; ON Starts, 48 ms window; 55 electrodes, 12 mice; 23.9 ± 31.8 %, mean ± std; Wilcoxon signed rank test, $p=1.72*10^{-6}$) and these results were robust across a series of time windows used to define synchronicity, from 48 ms to 148 ms. Moreover, SWA and synchrony measures were correlated (Figure 4C). By contrast, no increase in synchrony measures was seen after laser stimulation. In fact, the onset of the ON periods was significantly less synchronous across SD-matched electrodes (30 electrodes, 9 mice; -2.5 ± 25.8 %, mean ± std; Wilcoxon signed rank test, p=0.03), and both onsets and offsets showed less synchrony when calculated across all ipsilateral electrodes (Figure 4D; 63 electrodes, 14 mice; 0.6 ± 25.6 %, mean ± std; Wilcoxon signed rank test, p = 0.001). Thus, both SWA and synchrony measures decreased after

optogenetic stimulation, but they were not correlated (Figure 4E). No changes were present in the contralateral electrodes (Figure 4F). The results again were confirmed using different time windows (100 and 148 ms, not shown).

Discussion

Changes in SWA and cortical synchrony after sleep deprivation

We measured sleep SWA, OFF measures and cortical synchrony after extended wake with exposure to novel objects and after optogenetic cortical stimulation during NREM sleep. Both experimental conditions induced a comparable, sustained (6 hours) increase in mean cortical firing (~ 70% relative to baseline). As expected, the increase in firing rate was widespread in both left and right cortex during sleep deprivation, and restricted to the targeted area during laser stimulation. The results show that sustained high firing induced by exposure to novel objects during wake was followed, during subsequent sleep, by an increase in SWA, cortical neuronal synchrony, and number and duration of OFF periods. Moreover, the increase in SWA was correlated with both neuronal synchrony and time spent OFF. These findings are fully in line with the results observed in the rat cortex (Vyazovskiy et al., 2009), confirming in two rodent species that homeostatic changes in SWA due to sleep deprivation are linked to changes in both cortical synchrony and OFF periods measures. Based on previous studies, we hypothesize that increased synchrony in the transition into ON and OFF periods is a reflection of increased neuronal coupling due to net synaptic potentiation occurring during prior wake (Tononi and Cirelli, 2014; Vyazovskiy et al., 2009).

Changes in SWA and cortical synchrony after optogenetic stimulation during sleep

After laser stimulation high firing was confined to the main injection area, where we estimate that ~63% of neurons were infected by the virus. Of note, in the same area, and only during laser stimulation, we also found an increase in gamma power (Figure 3), which has frequently been observed as a result of inhibitory firing (Buzsáki and Wang, 2012; Whittington et al., 2011). Thus, although our stimulation targeted excitatory cells, most likely it also led to increased compensatory firing of fast spiking inhibitory interneurons, recruited to maintain the balance between excitation and inhibition.

None of the effects observed after sleep deprivation was observed following sustained firing induced by optogenetic stimulation during sleep: SWA and cortical synchrony decreased, the number and duration of OFF periods did not change, and SWA was not correlated with cortical synchrony and time spent OFF. Thus, a wake-like, tonic increase in firing comparable to that observed during active exploration, but produced by optogenetic activation during sleep, fails to trigger homeostatic changes in subsequent SWA and associated neural signatures. In fact, SWA and neural synchrony not only failed to increase, but declined significantly. Just like wake leads to a net increase in synaptic strength, presumably because of a neuromodulatory milieu that favors learning through synaptic potentiation, NREM sleep leads to a net decrease in synaptic strength, presumably through a neuromodulatory milieu that favors synaptic depression (Harley, 1991; Seol et al., 2007). It has been hypothesized that, at least in mammalian cortex, this sleep-dependent down-selection of synaptic strength would be activity-dependent (Tononi and Cirelli, 2014). Thus, we speculate that increased firing induced by optogenetic stimulation during sleep may have promoted additional synaptic depression, thereby explaining the decline in SWA and neuronal synchrony. In pilot experiments, optogenetic stimulation for several hours during wake,

in conjunction with active exploration, often resulted in seizures or cortical spreading depression and prevented the analysis of subsequent sleep.

Mechanisms underlying the decline in SWA after optogenetic stimulation during sleep

In general, the synchrony of neuronal firing is strongly correlated with the amplitude of EEG signals (Musall et al., 2014). Since the effects of extended wake are global, they are expected to be similar, hence correlated, at every scale: from the synchrony of firing of the few units near the recording tip, to the amplitude of the local LFP, reflecting the input (mainly postsynaptic potentials) from thousands of neurons surrounding the recording electrode (Buzsáki et al., 2012), to the overall EEG. Indeed, extended wake increased both SWA and synchrony measures in a correlated manner, and the increase in SWA was also observed in the contralateral hemisphere, with no statistical differences between left and right cortex (Figure 2B,C). By contrast, optogenetic stimulation primarily affects neurons locally, which may lead to complex interactions between direct local effects on firing synchrony and indirect effects on inputs from neighboring regions. This may account for the observation that after optogenetic stimulation both SWA and synchrony measures declined, but not in a correlated manner. Moreover, the decline in SWA was significantly larger ipsi- than contralaterally (Figure 3G,H).

Changes in intrinsic excitability might also contribute to the decline of SWA after optogenetic stimulation. For instance, the non-inactivating hyperpolarization-activated cation current I_h plays a crucial role in the generation of the slow oscillation (Blethyn et al., 2006; McCormick and Bal, 1997). In the hippocampus, I_h is decreased by stimulation paradigms that induce LTD and increased by LTP (Brager and Johnston, 2007; Fan et al., 2005), but only in

association with strong firing (theta bursts but not tetanus, which elicits few action potentials). However, while long-lasting homeostatic changes in intrinsic excitability mediated by I_h (Fan et al., 2005) might affect SWA after optogenetic stimulation, they cannot easily account for the associated decline of neuronal synchrony.

Several recent studies have shown that increased activation of specific cortical areas during wake results in a local increase in SWA during subsequent sleep, but in most cases it is not straightforward to tease apart the role of neuronal activity from that of synaptic plasticity (reviewed in (Hanlon et al., 2011)). However, a few studies contrasted conditions providing similar amounts of wake stimulation (activity) with or without a learning component (plasticity). In humans, SWA increased over right parietal cortex after a visuomotor task requiring learning compared to a kinematically identical task that did not require learning (Huber et al., 2004; Landsness et al., 2009). Similar results have been obtained using a reaching task in rodents and comparing the training and the post-training phase (Hanlon et al., 2009), indicating that changes in SWA reflect the effects of synaptic plasticity above and beyond any effect of neuronal activity. Finally, a study in humans used transcranial paired-associative stimulation (PAS) in wake to deliver the same number of paired stimuli, but at time intervals meant to induce spike-timing dependent synaptic potentiation or depression, respectively (Huber et al., 2008). The potentiation paradigm locally increased SWA during subsequent sleep, whereas the depression paradigm decreased it, suggesting that changes in SWA are driven primarily by changes in synaptic plasticity, in line with the present results.

Conclusions

In summary, our findings demonstrate that sustained neuronal activation induced by active exploration in wake leads to an increase in SWA, neuronal synchrony, and neuronal OFF periods during subsequent sleep, consistent with the expected consequences of a net increase in synaptic strength in cortical circuits (Tononi and Cirelli, 2014). By contrast, a comparable, wake-like local increase in neuronal activity obtained by optogenetic stimulation during sleep was followed by a local decrease in SWA and neuronal synchrony, with no change in OFF periods. Thus, the increase in SWA and OFF periods after extended wake is unlikely to result from neuronal 'fatigue' induced by excessive firing as such. Instead, it appears that neuronal activation leads to homeostatic changes in sleep SWA only if it occurs in the neuromodulatory, metabolic, and neurochemical milieu of active wake, which influences multiple cellular functions including the ionic balance of interstitial spaces (Ding et al., 2016), and favors learning through synaptic potentiation (Tononi and Cirelli, 2014; de Vivo et al., 2016). Indeed, in previous studies we found that rats whose cortical noradrenergic levels had been depleted using chronic lesions of the locus coeruleus did not show the expected cortical induction of plasticity-related genes during wake, and had a blunted SWA response during subsequent sleep (Cirelli and Tononi, 2000, 2004, Cirelli et al., 1996, 2005). In the current study, the tone of the noradrenergic and other neuromodulatory systems was low because the mice were asleep, and thus laser-induced high firing occurred in a state that as a whole is not conducive to synaptic potentiation (Bramham and Srebro, 1989; Leonard et al., 1987). We cannot rule out, however, that laser stimulation also caused neurons to fire in a "random" pattern, uncoupled from wake behavior and physiological sensory inputs. While this may have contributed to the observed decrease in SWA after optogenetic stimulation, SSFO was chosen specifically to increase neuronal

excitability while preserving as much as possible the endogenous pattern of firing. Finally, a recent study found that even ‘sleep-like’ slow waves occurring during wake due to systemic atropine injections can lead to an increase in NREM sleep duration as long as subcortical areas are activated and the experimental animals are actively behaving (Qiu et al., 2015). This possibility should be tested further by experiments aimed at decoupling the effects of neuronal activity and plasticity during wake.

Figure 1. Experimental design. **A**. Representative example of virus expression in one mouse. Virus expression spread 2-3 mm in the anterior/posterior direction and remained within the right hemisphere. Red arrow denotes visible electrode tracks. Scale bar = 1mm. **B**. Placement of electrodes and screws in reference to the virus expression, as well as details of the microwire electrode array with 16 electrodes, of which only one row of 8 is shown. **C**. Example of EYFP (left) and NeuN (middle) expression in a confocal image taken near the injection site, and combined overlay of both images (right). Scale bars = 100 μm. **D**. Experimental design. The two experiments (baseline+SD and baseline+laser-S) were spaced ~ 4-5 days apart and their order was counterbalanced. Vertical grey boxes indicate the time window in which most of the analysis was done, corresponding to the first 2 hours after SD or laser-S and the same time of day during baseline (hours 7-8 of the light period).

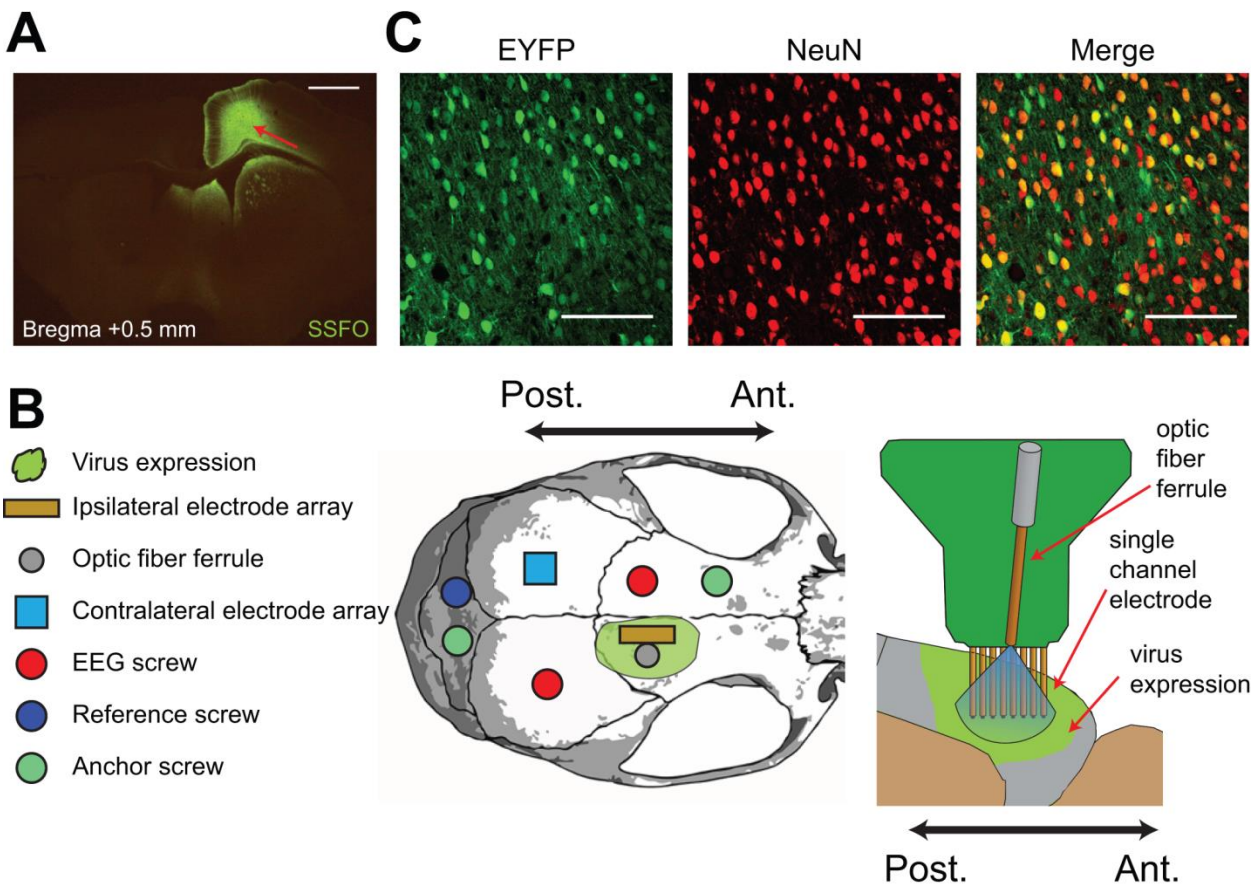
A
Bregma +0.5 mm
SSFO
C
EYFP
NeuN
Merge
B
Virus expression
Ipsilateral electrode array
Optic fiber ferrule
Contralateral electrode array
EEG screw
Reference screw
Anchor screw
Post.
Ant.
optic fiber ferrule
single channel electrode
virus expression
Post.
Ant.

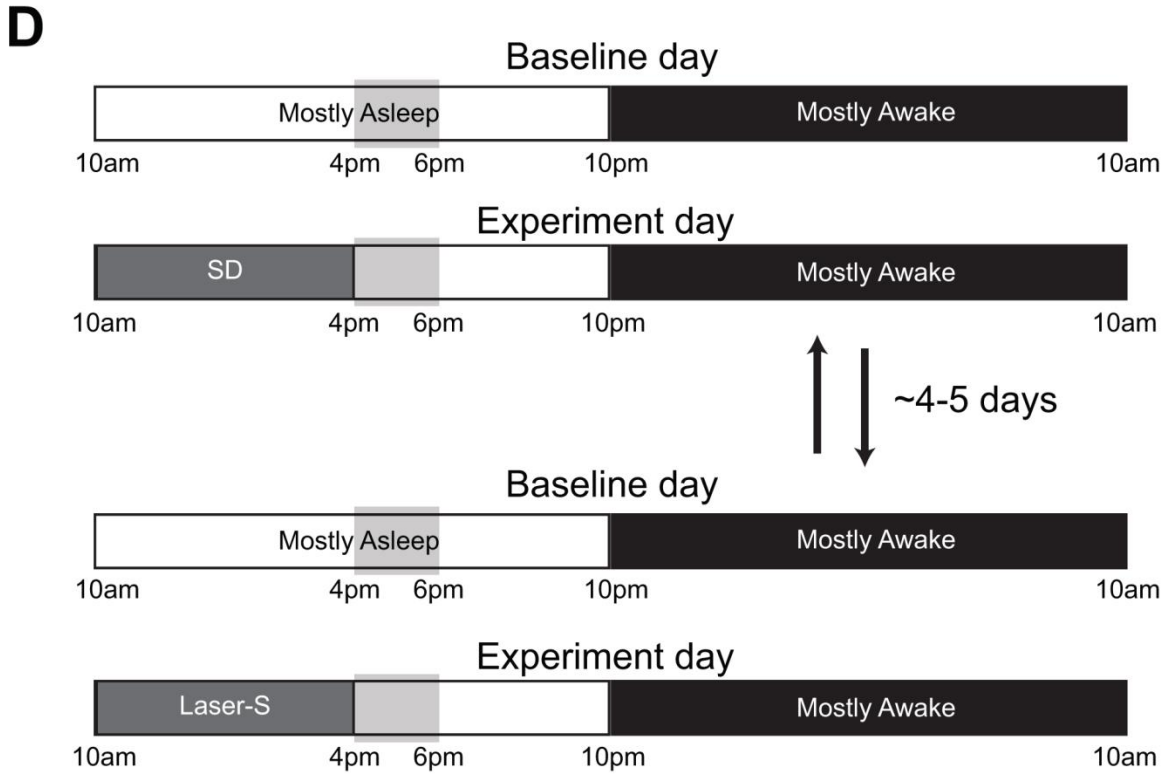
D
Baseline day
Mostly Asleep
Mostly Awake
10am
4pm
6pm
10pm
10am
Experiment day
SD
Mostly Awake
10am
4pm
6pm
10pm
10am
~4-5 days
Baseline day
Mostly Asleep
Mostly Awake
10am
4pm
6pm
10pm
10am
Experiment day
Laser-S
Mostly Awake
10am
4pm
6pm
10pm
10am

Figure 2. Sleep deprivation experiment. **A**. Left, firing rate in a representative electrode during the light period of baseline and SD days. Firing rate is plotted for each 4-sec epoch, and expressed as a percent of hours 1-12 NREM average firing rate during the baseline day. Right, firing rate for all electrodes during SD hours 1-6, plotted as percent change from the corresponding firing rate in baseline (59 electrodes, 16 mice). In this and the following boxplots, red and green lines denote median and mean, respectively; the blue box extends from the 25^{th} to 75^{th} percentile, and the black whiskers extend to 2.7 standard deviations. **B**. Left, mean spectrograms for frontal left EEG during hours 7-8 of the SD day (as % of total spectral power during hours 1-12 of the baseline day) (15 electrodes, 15 mice; Wilcoxon signed rank test, $p=6.10*10^{-5}$). Here and in panel C, frequencies from 57-63 Hz are not displayed due to an artifact from a notch filter used to suppress 60 Hz electrical noise. Right, power in the SWA band (0.5-4 Hz) in NREM sleep during hours 7-8 of the SD day plotted as percent change from the corresponding baseline value. **C**. Same as in B, for ipsilateral (right) LFPs (59 electrodes, 16 mice; Wilcoxon signed rank test, $p=2.39*10^{-11}$). **D**. Representative example of electrophysiological measures at ~ hour 7.5 in the baseline day and SD day. OFF periods are shown as gray bars under spike rasters. **E**. Average LFP waveform locked to all detected OFF periods from all electrodes in hours 7-8 of the SD day. **F**. OFF period measures after SD (hours 7-8) plotted as a percent change from the corresponding baseline. Number of OFF periods is per minute of NREM sleep (59 electrodes, 16 mice; Wilcoxon signed rank test, p=0.0003). Duration is the average duration of all OFF periods (p=0.0001). Percent of time spent in OFF periods is expressed as a percent of total time spent in NREM sleep ($p=4.44*10^{-5}$). **G**. As F, for the first 2 hours of the dark period (hours 13-14) (59 electrodes, 16 mice; Wilcoxon signed rank test; Number: p=0.03, Duration: p=0.52, Percent: p=0.05). **H**. Correlation plot between firing rates

during hours 1-6 of SD day and percent of NREM time spent in OFF periods in hours 7-8 of the same day for all 59 electrodes. 'r' shown is Pearson's rho, the black line is a least-squares fit (59 electrodes, 16 mice; Linear correlation; $r=0.64$ $p=4.72*10^{-8}$).

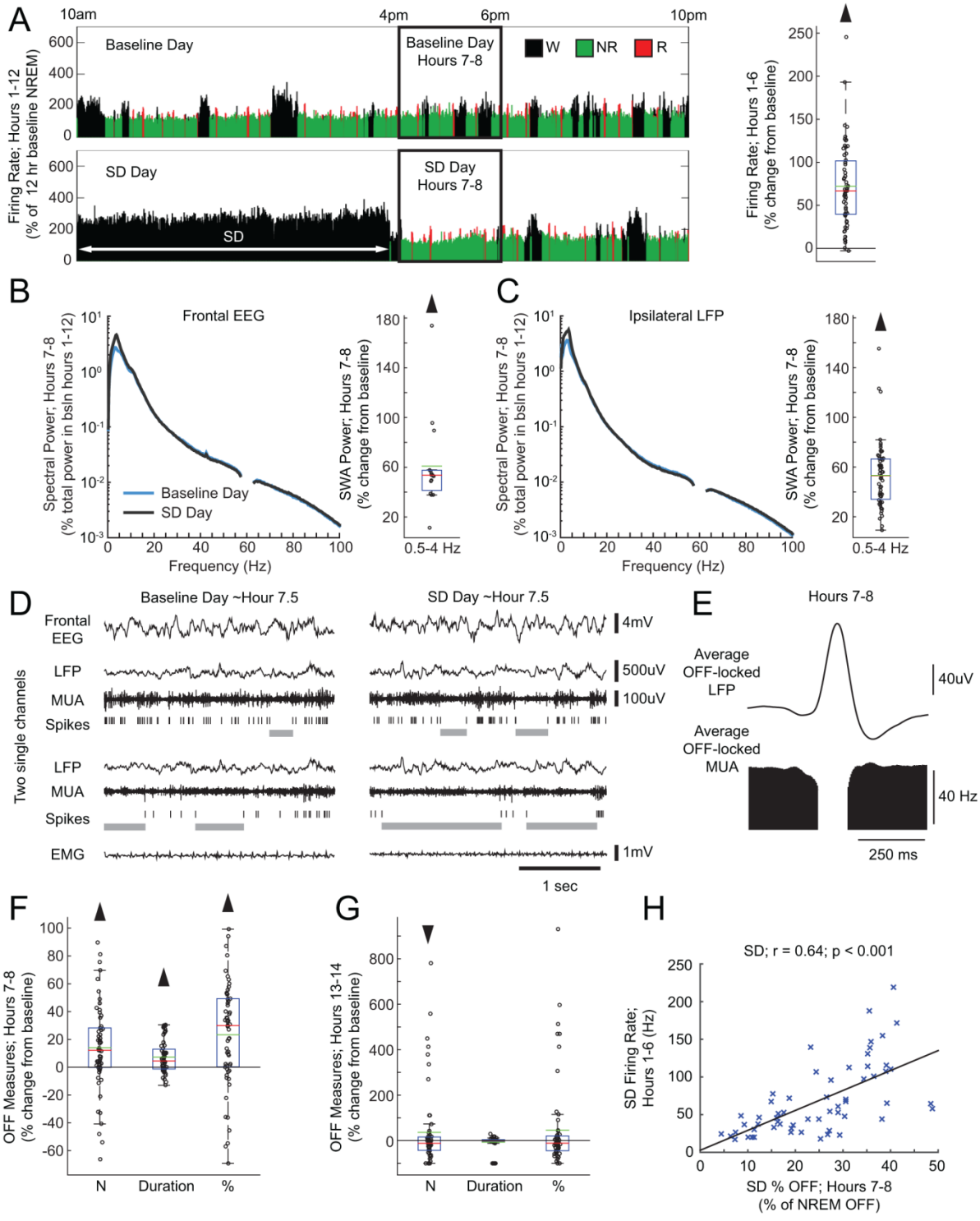

Figure 3. Laser-S experiment. **A**. Left, % of time spent in wake, NREM sleep and REM sleep in hours 1-6 (17 mice; Wilcoxon signed rank test; Wake: p=0.55, NREM: p=0.24, REM: p=0.28). Middle: average bout duration for wake and sleep in hours 1-6 (Wilcoxon signed rank test; Wake: p=0.55, NREM: p=0.49, REM: p=0.08), Right, number of brief awakenings (wake bouts ≤ 16 sec) per minute of NREM sleep in hours 1-6 (Wilcoxon signed rank test; p=0.69). All bars are mean, error bars show standard deviation. **B**. Left, mean spectrogram for frontal left EEG in hours 1-6 (% of total spectral power during hours 1-12 of the baseline day). Here and in other panels, frequencies from 57-63 Hz are not displayed due to an artifact from a notch filter used to suppress 60 Hz electrical noise. Right, power in SWA (0.5-4 Hz) and gamma (30-55 Hz) bands for each frontal EEG in laser-S day plotted as percent change from the baseline day (15 electrodes, 15 mice; Wilcoxon signed rank test; SWA: p=0.02, Gamma: p=0.03). In this and the following boxplots, red and green lines denote the median and the mean, respectively; the blue box extends from the 25^{th} to 75^{th} percentile, and the black whiskers extend to 2.7 standard deviations. **C**. Representative example of electrophysiological measures in strong and weak responding electrodes at onset of laser stimulation. OFF periods are shown as gray bars under spike rasters. The blue box denotes the duration of a blue laser pulse. **D**. Left, firing rate in a representative strong responding electrode during the light period of the baseline and laser-S days. Firing rate is plotted for each 4-sec epoch, and expressed as a percent of hours 1-12 NREM average firing rate during the baseline day. Right, firing rate for all electrodes and SD-matched electrodes during laser-S hours 1-6, plotted as a percent change from the corresponding firing rate in baseline (Wilcoxon signed rank test; All: n=66, $p=8.82*10^{-10}$, SD-matched: n=32, $p=7.95*10^{-7}$). **E**. OFF period measures during hours 1-6 of laser-S for SD-matched electrodes. Percent change in laser-S from the baseline day is plotted for each OFF measure. Number of

OFF periods is per minute of NREM sleep (32 electrodes, 11 mice; Wilcoxon signed rank test, $p=7.95*10^{-7}$). Duration is the average duration of all OFF periods ($p=7.95*10^{-7}$). Percent of time spent in OFF periods is expressed as a percent of total time spent in NREM sleep ($p=7.95*10^{-7}$). **F**. Left, mean spectrogram for the LFPs of SD-matched electrodes during hours 1-6 (% of total spectral power during hours 1-12 of the baseline day) (32 electrodes, 11 mice; Wilcoxon signed rank test; Delta: $p=7.95*10^{-7}$, Gamma: $p=7.95*10^{-7}$). Right, power in SWA and gamma bands for the laser-S day plotted as percent change from the baseline. Note that the spectrograms shown are all scaled uniformly 0-100 Hz by a single value, the total power across all frequency bins in the baseline day hours 1-12. **G**. Left, mean spectrograms for frontal EEG during hours 7-8 of the laser-S day (% of total spectral power during hours 1-12 of the baseline day). Right, power in the SWA and gamma bands plotted as percent change from the baseline (9 electrodes, 9 mice; Wilcoxon signed rank test, Delta: p=0.03 Gamma: p=0.91). **H**. Same as in G for the LFPs of SD-matched electrodes (32 electrodes, 11 mice; Wilcoxon signed rank test; SWA: $p=6.59*10^{-7}$, Gamma: p=0.24). **I**. Average LFP waveform in SD-matched electrodes locked to all detected OFF from all electrodes in hours 7-8 of the laser-S day. **J**. OFF period measures in SD-matched electrodes after laser-S (hours 7-8) plotted as a percent change from the corresponding baseline. Number of OFF periods is per minute of NREM sleep (32 electrodes, 11 mice; Wilcoxon signed rank test, p=0.68). Duration is the average duration of all OFF periods (p=0.91). Percent of time spent in OFF periods is expressed as a percent of total time spent in NREM sleep (p=0.55). **K**. Correlation plot between firing rates during hours 1-6 of laser-S day and percent of time spent in OFF periods in hours 7-8 for SD-matched electrodes. 'r' shown is Pearson's rho, the black line is a least-squares fit (59 electrodes, 16 mice; Linear correlation; r=-0.04 p=0.81). **L**. As in J, for all

ipsilateral electrodes in Laser-S (66 electrodes, 17 mice; Wilcoxon signed rank test; Number: p=0.34, Duration: p=0.19, Percent: p=0.28).

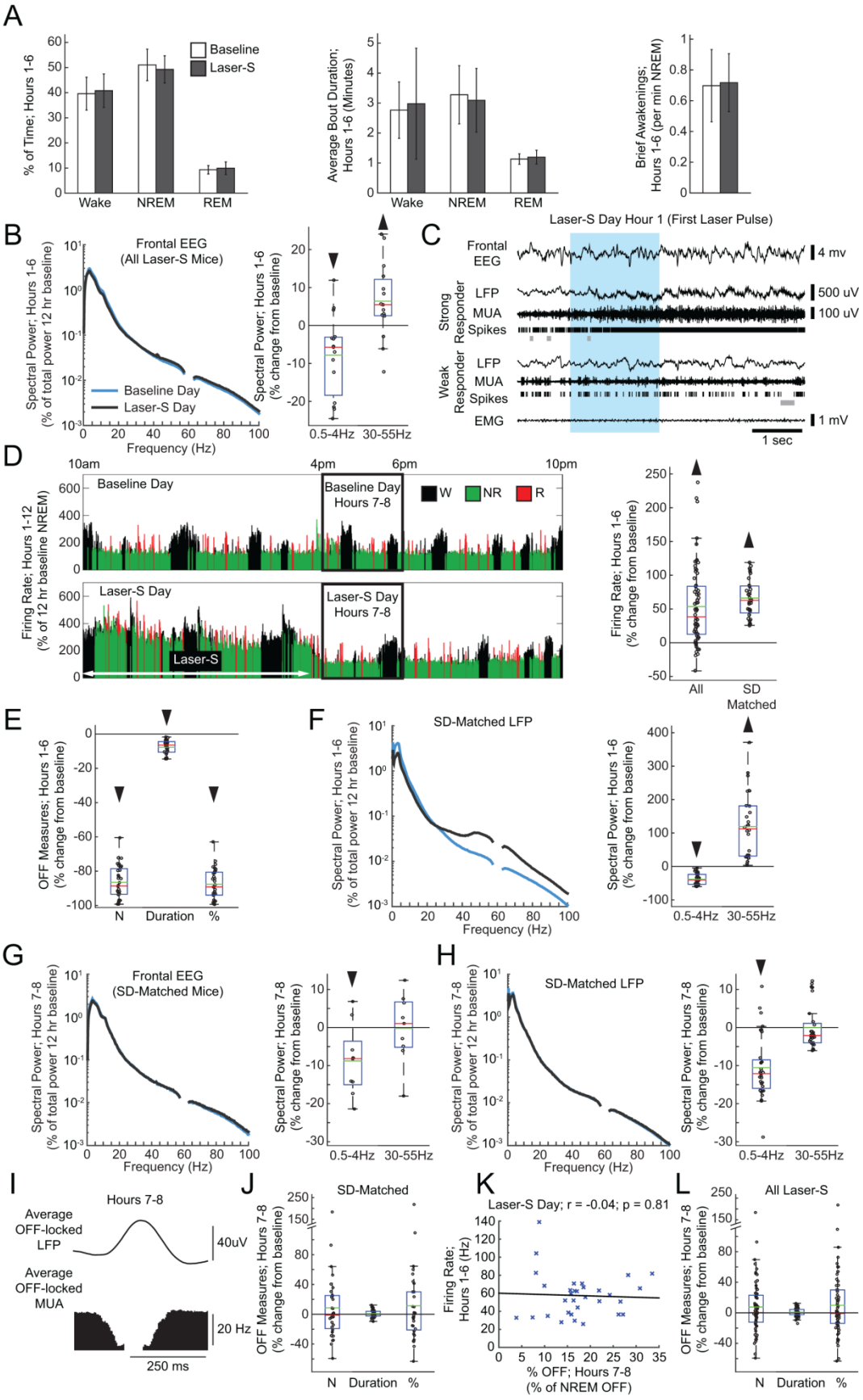
A
% of Time; Hours 1-6
Baseline
Laser-S
Wake
NREM
REM
Average Bout Duration; Hours 1-6 (Minutes)
Brief Awakenings; Hours 1-6 (per min NREM)
B
Frontal EEG (All Laser-S Mice)
Spectral Power; Hours 1-6 (% of total power 12 hr baseline)
Baseline Day
Laser-S Day
Frequency (Hz)
Spectral Power; Hours 1-6 (% change from baseline)
0.5-4Hz
30-55Hz
C
Laser-S Day Hour 1 (First Laser Pulse)
Frontal EEG
4 mv
Strong Responder
LFP
MUA
Spikes
500 uV
100 uV
Weak Responder
EMG
1 mV
1 sec
D
10am
4pm
6pm
10pm
Baseline Day
Baseline Day Hours 7-8
W
NR
R
Laser-S Day
Laser-S Day Hours 7-8
Laser-S
Firing Rate; Hours 1-12 (% of 12 hr baseline NREM)
Firing Rate; Hours 1-6 (% change from baseline)
All
SD Matched
E
OFF Measures; Hours 1-6 (% change from baseline)
N
Duration
%
F
SD-Matched LFP
Spectral Power; Hours 1-6 (% of total power 12 hr baseline)
Frequency (Hz)
Spectral Power; Hours 1-6 (% change from baseline)
0.5-4Hz
30-55Hz
G
Frontal EEG (SD-Matched Mice)
Spectral Power; Hours 7-8 (% of total power 12 hr baseline)
Frequency (Hz)
Spectral Power; Hours 7-8 (% change from baseline)
0.5-4Hz
30-55Hz
H
SD-Matched LFP
Spectral Power; Hours 7-8 (% of total power 12 hr baseline)
Frequency (Hz)
Spectral Power; Hours 7-8 (% change from baseline)
0.5-4Hz
30-55Hz
I
Hours 7-8
Average OFF-locked LFP
40uV
Average OFF-locked MUA
20 Hz
250 ms
J
SD-Matched
OFF Measures; Hours 7-8 (% change from baseline)
N
Duration
%
K
Laser-S Day; r = -0.04; p = 0.81
Firing Rate; Hours 1-6 (Hz)
% OFF; Hours 7-8 (% of NREM OFF)
L
All Laser-S
OFF Measures; Hours 7-8 (% change from baseline)
N
Duration
%

***Figure 4. Changes in ON period synchrony after SD and laser stimulation*. A**. Examples of synchrony measurements across the onset and offset of ON periods. The top electrode is the one being evaluated (the target electrode), with ON periods (spikes) shown in red and OFF periods shown in blue. In the other 5 electrodes of the same array, spikes are shown in black, except when a corresponding ON period starts or ends in synchrony with the target electrode, in which case spikes are shown in red. Synchrony was measured within a window of 48 ms centered over the beginning and ending of the ON periods of the target electrode (yellow area). For better visualization, the size of this window is not drawn to scale. Note that only the start and end of ON periods count as possible synchrony events, and that shorter silences within an ON period that do not pass the OFF period threshold are not ON period boundaries. **B**. Synchrony measures in hours 7-8 after SD, shown for each electrode as a percent of the synchrony in the baseline day hours 7-8 (55 electrodes, 12 mice; Wilcoxon signed rank test; ON Starts: $p=1.72*10^{-6}$, ON Ends: $p=6.51*10^{-8}$). In the boxplots, data points are shown as black circles, red and green lines denote the median and the mean, respectively; the blue box extends from the 25^{th} to 75^{th} percentile, and the black whiskers extend to 2.7 standard deviations from the mean. **C**. Correlation plot between average LFP SWA and average synchrony for start of ON periods in hours 7-8 of the SD day for all 12 mice used for synchrony analysis. 'r' shown is Pearson's rho, the black line is a least-squares fit (12 mice; Linear correlation; r=-0.84 p=0.0006). **D**. As in B, for laser-S electrode subsets (SD-matched: 30 electrodes, 9 mice; Wilcoxon signed rank test; ON Starts: p=0.03, ON Ends: p=0.37) (All Laser-S: 63 electrodes, 14 mice; Wilcoxon signed rank test; ON Starts: p=0.001, ON Ends: p=0.04). **E**. Correlation plot between average LFP SWA and average synchrony for start of ON periods in hours 7-8 of the laser-S day (9 mice; Linear correlation; r=-

0.04 p=0.93). **F**. As in B, for contralateral laser-S electrodes (22 electrodes, 5 mice; Wilcoxon signed rank test; ON Starts: p=0.66, ON Ends: p=0.12).

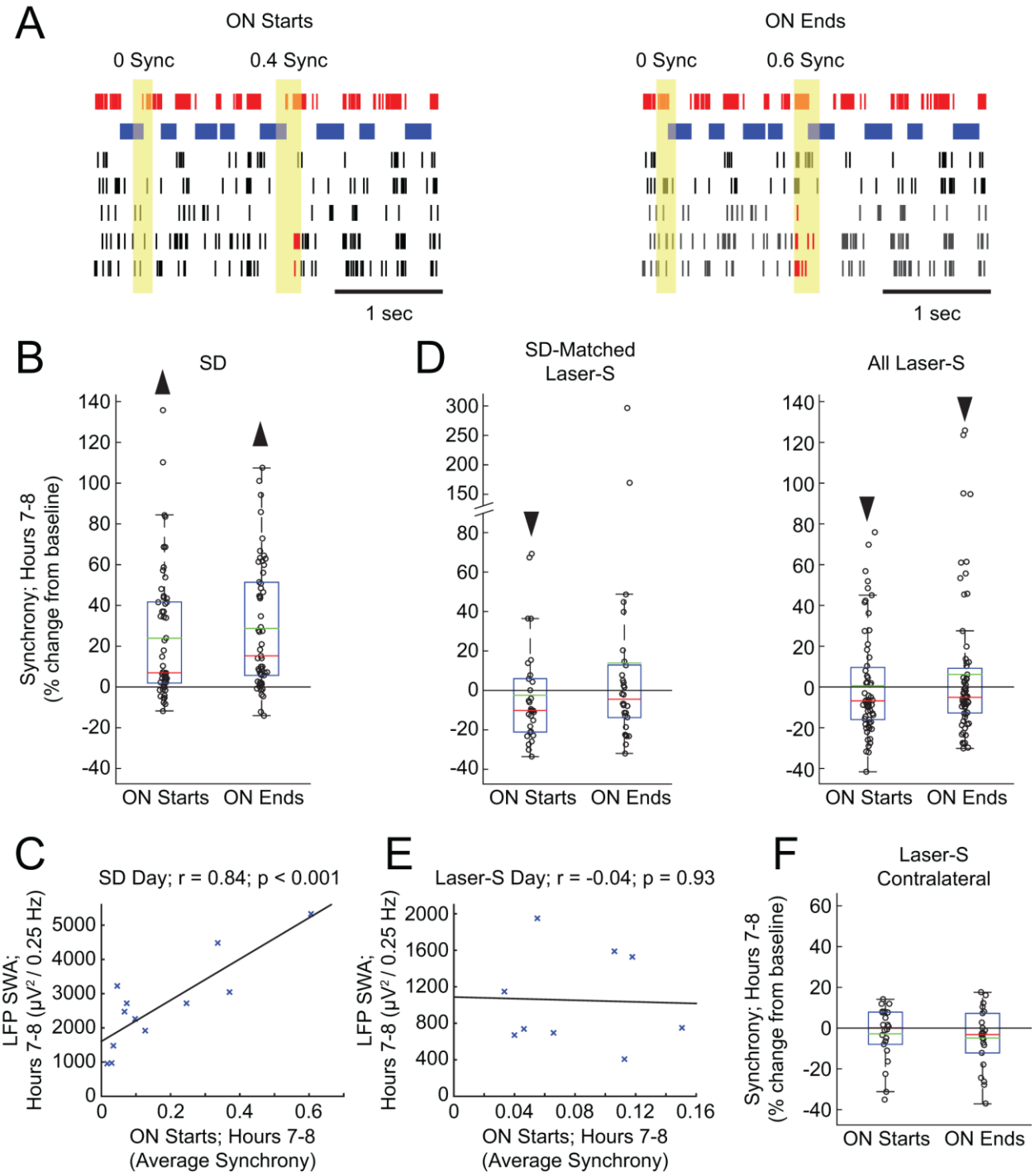

References

Bellesi, M., de Vivo, L., Tononi, G., and Cirelli, C. (2015). Effects of sleep and wake on astrocytes: clues from molecular and ultrastructural studies. BMC Biol. *13*, 66.

Benington, J.H., and Heller, H.C. (1995). Restoration of brain energy metabolism as the function of sleep. Prog. Neurobiol. *45*, 347–360.

Blethyn, K.L., Hughes, S.W., Tóth, T.I., Cope, D.W., and Crunelli, V. (2006). Neuronal basis of the slow (<1 Hz) oscillation in neurons of the nucleus reticularis thalami in vitro. J. Neurosci. Off. J. Soc. Neurosci. *26*, 2474–2486.

Borbély, A.A. (1982). A two process model of sleep regulation. Hum. Neurobiol. *1*, 195–204.

Borbély, A.A., Baumann, F., Brandeis, D., Strauch, I., and Lehmann, D. (1981). Sleep deprivation: effect on sleep stages and EEG power density in man. Electroencephalogr. Clin. Neurophysiol. *51*, 483–495.

Borbély, A.A., Daan, S., Wirz-Justice, A., and Deboer, T. (2016). The two-process model of sleep regulation: a reappraisal. J. Sleep Res. *25*, 131–143.

Brager, D.H., and Johnston, D. (2007). Plasticity of intrinsic excitability during long-term depression is mediated through mGluR-dependent changes in I(h) in hippocampal CA1 pyramidal neurons. J. Neurosci. Off. J. Soc. Neurosci. *27*, 13926–13937.

Brambilla, D., Chapman, D., and Greene, R. (2005). Adenosine mediation of presynaptic feedback inhibition of glutamate release. Neuron *46*, 275–283.

Bramham, C.R., and Srebro, B. (1989). Synaptic plasticity in the hippocampus is modulated by behavioral state. Brain Res. *493*, 74–86.

Brundege, J.M., and Dunwiddie, T.V. (1998). Metabolic regulation of endogenous adenosine release from single neurons. Neuroreport *9*, 3007–3011.

Buzsáki, G., and Wang, X.-J. (2012). Mechanisms of gamma oscillations. Annu. Rev. Neurosci. *35*, 203–225.

Buzsáki, G., Anastassiou, C.A., and Koch, C. (2012). The origin of extracellular fields and currents — EEG, ECoG, LFP and spikes. Nat. Rev. Neurosci. *13*, 407–420.

Chauvette, S., Crochet, S., Volgushev, M., and Timofeev, I. (2011). Properties of slow oscillation during slow-wave sleep and anesthesia in cats. J. Neurosci. Off. J. Soc. Neurosci. *31*, 14998–15008.

Cirelli, C., and Tononi, G. (2000). Differential Expression of Plasticity-Related Genes in Waking and Sleep and Their Regulation by the Noradrenergic System. J. Neurosci. *20*, 9187–9194.

Cirelli, C., and Tononi, G. (2004). Locus Ceruleus Control of State-Dependent Gene Expression. J. Neurosci. *24*, 5410–5419.

Cirelli, C., Pompeiano, M., and Tononi, G. (1996). Neuronal Gene Expression in the Waking State: A Role for the Locus Coeruleus. Science *274*, 1211–1215.

Cirelli, C., Gutierrez, C.M., and Tononi, G. (2004). Extensive and Divergent Effects of Sleep and Wakefulness on Brain Gene Expression. Neuron *41*, 35–43.

Cirelli, C., Huber, R., Gopalakrishnan, A., Southard, T.L., and Tononi, G. (2005). Locus Ceruleus Control of Slow-Wave Homeostasis. J. Neurosci. *25*, 4503–4511.

Dalsgaard, M.K., and Secher, N.H. (2007). The brain at work: a cerebral metabolic manifestation of central fatigue? J. Neurosci. Res. *85*, 3334–3339.

Ding, F., O'Donnell, J., Xu, Q., Kang, N., Goldman, N., and Nedergaard, M. (2016). Changes in the composition of brain interstitial ions control the sleep-wake cycle. Science *352*, 550–555.

Esser, S.K., Hill, S.L., and Tononi, G. (2007). Sleep Homeostasis and Cortical Synchronization: I. Modeling the Effects of Synaptic Strength on Sleep Slow Waves. Sleep *30*, 1617–1630.

Fan, Y., Fricker, D., Brager, D.H., Chen, X., Lu, H.-C., Chitwood, R.A., and Johnston, D. (2005). Activity-dependent decrease of excitability in rat hippocampal neurons through increases in I(h). Nat. Neurosci. *8*, 1542–1551.

Feinberg, I., March, J.D., Fein, G., Floyd, T.C., Walker, J.M., and Price, L. (1978). Period and amplitude analysis of 0.5-3 c/sec activity in NREM sleep of young adults. Electroencephalogr. Clin. Neurophysiol. *44*, 202–213.

Franken, P., Malafosse, A., and Tafti, M. (1999). Genetic determinants of sleep regulation in inbred mice. Sleep *22*, 155–169.

Grill, W.M. (2008). Signal Considerations for Chronically Implanted Electrodes for Brain Interfacing. In Indwelling Neural Implants: Strategies for Contending with the In Vivo Environment, W.M. Reichert, ed. (Boca Raton (FL): CRC Press/Taylor & Francis), pp. 41–62.

Hanlon, E.C., Faraguna, U., Vyazovskiy, V.V., Tononi, G., and Cirelli, C. (2009). Effects of Skilled Training on Sleep Slow Wave Activity and Cortical Gene Expression in the Rat. Sleep *32*, 719–729.

Hanlon, E.C., Vyazovskiy, V.V., Faraguna, U., Tononi, G., and Cirelli, C. (2011). Synaptic potentiation and sleep need: clues from molecular and electrophysiological studies. Curr. Top. Med. Chem. *11*, 2472–2482.

Harley, C. (1991). Noradrenergic and locus coeruleus modulation of the perforant path-evoked potential in rat dentate gyrus supports a role for the locus coeruleus in attentional and memorial processes. Prog. Brain Res. *88*, 307–321.

Huber, R., Deboer, T., and Tobler, I. (2000). Effects of sleep deprivation on sleep and sleep EEG in three mouse strains: empirical data and simulations. Brain Res. *857*, 8–19.

Huber, R., Felice Ghilardi, M., Massimini, M., and Tononi, G. (2004). Local sleep and learning. Nature *430*, 78–81.

Huber, R., Määttä, S., Esser, S.K., Sarasso, S., Ferrarelli, F., Watson, A., Ferreri, F., Peterson, M.J., and Tononi, G. (2008). Measures of cortical plasticity after transcranial paired associative stimulation predict changes in electroencephalogram slow-wave activity during subsequent sleep. J. Neurosci. Off. J. Soc. Neurosci. *28*, 7911–7918.

Landsness, E.C., Crupi, D., Hulse, B.K., Peterson, M.J., Huber, R., Ansari, H., Coen, M., Cirelli, C., Benca, R.M., Ghilardi, M.F., et al. (2009). Sleep-dependent improvement in visuomotor learning: a causal role for slow waves. Sleep *32*, 1273–1284.

Leonard, B.J., McNaughton, B.L., and Barnes, C.A. (1987). Suppression of hippocampal synaptic plasticity during slow-wave sleep. Brain Res. *425*, 174–177.

Lovatt, D., Xu, Q., Liu, W., Takano, T., Smith, N.A., Schnermann, J., Tieu, K., and Nedergaard, M. (2012). Neuronal adenosine release, and not astrocytic ATP release, mediates feedback inhibition of excitatory activity. Proc. Natl. Acad. Sci. U. S. A. *109*, 6265–6270.

McCormick, D.A., and Bal, T. (1997). Sleep and arousal: thalamocortical mechanisms. Annu. Rev. Neurosci. *20*, 185–215.

Musall, S., Pföstl, V. von, Rauch, A., Logothetis, N.K., and Whittingstall, K. (2014). Effects of Neural Synchrony on Surface EEG. Cereb. Cortex *24*, 1045–1053.

O'Donovan, M.J., and Rinzel, J. (1997). Synaptic depression: a dynamic regulator of synaptic communication with varied functional roles. Trends Neurosci. *20*, 431–433.

Qiu, M.-H., Chen, M.C., and Lu, J. (2015). Cortical neuronal activity does not regulate sleep homeostasis. Neuroscience *297*, 211–218.

Rechtschaffen, A. (1998). Current perspectives on the function of sleep. Perspect. Biol. Med. *41*, 359–390.

Seol, G.H., Ziburkus, J., Huang, S., Song, L., Kim, I.T., Takamiya, K., Huganir, R.L., Lee, H.-K., and Kirkwood, A. (2007). Neuromodulators control the polarity of spike-timing-dependent synaptic plasticity. Neuron *55*, 919–929.

Steriade, M., Timofeev, I., and Grenier, F. (2001). Natural Waking and Sleep States: A View From Inside Neocortical Neurons. J. Neurophysiol. *85*, 1969–1985.

Tononi, G., and Cirelli, C. (2006). Sleep function and synaptic homeostasis. Sleep Med. Rev. *10*, 49–62.

Tononi, G., and Cirelli, C. (2012). Time to be SHY? Some comments on sleep and synaptic homeostasis. Neural Plast. *2012*, 415250.

Tononi, G., and Cirelli, C. (2014). Sleep and the Price of Plasticity: From Synaptic and Cellular Homeostasis to Memory Consolidation and Integration. Neuron *81*, 12–34.

de Vivo, L., Nelson, A.B., Bellesi, M., Noguti, J., Tononi, G., and Cirelli, C. (2016). Loss of Sleep Affects the Ultrastructure of Pyramidal Neurons in the Adolescent Mouse Frontal Cortex. Sleep *39*, 861–874.

Vyazovskiy, V.V., and Harris, K.D. (2013). Sleep and the single neuron: the role of global slow oscillations in individual cell rest. Nat. Rev. Neurosci. *14*, 443–451.

Vyazovskiy, V.V., Olcese, U., Lazimy, Y.M., Faraguna, U., Esser, S.K., Williams, J.C., Cirelli, C., and Tononi, G. (2009). Cortical firing and sleep homeostasis. Neuron *63*, 865–878.

Vyazovskiy, V.V., Olcese, U., Hanlon, E.C., Nir, Y., Cirelli, C., and Tononi, G. (2011). Local sleep in awake rats. Nature *472*, 443–447.

Whittington, M.A., Cunningham, M.O., LeBeau, F.E.N., Racca, C., and Traub, R.D. (2011). Multiple origins of the cortical γ rhythm. Dev. Neurobiol. *71*, 92–106.

Yizhar, O., Fenno, L.E., Davidson, T.J., Mogri, M., and Deisseroth, K. (2011a). Optogenetics in neural systems. Neuron *71*, 9–34.

Yizhar, O., Fenno, L.E., Prigge, M., Schneider, F., Davidson, T.J., O'Shea, D.J., Sohal, V.S., Goshen, I., Finkelstein, J., Paz, J.T., et al. (2011b). Neocortical excitation/inhibition balance in information processing and social dysfunction. Nature *477*, 171–178.

Chapter III:

Effects of Chronic Sleep Restriction during Early Adolescence on the Adult Pattern of Connectivity of Mouse Secondary Motor Cortex

Yazan N. Billeh*, Alexander V. Rodriguez*, Michele Bellesi, Amy Bernard, Luisa de Vivo, Chadd M. Funk, Julie Harris, Sakiko Honjoh, Stafan Mihalas, Lydia Ng, Christof Koch, Chiara Cirelli, and Giulio Tononi

*Indicates co-first authors; Published in *eNeuro* (2016). *3*.

Abstract

Cortical circuits mature in stages, from early synaptogenesis and synaptic pruning to late synaptic refinement, resulting in the adult anatomical connection matrix. Because the mature matrix is largely fixed, genetic or environmental factors interfering with its establishment can have irreversible effects. Sleep disruption is rarely considered among those factors, and previous studies have focused on very young animals and the acute effects of sleep deprivation on neuronal morphology and cortical plasticity. Adolescence is a sensitive time for brain remodeling, yet whether chronic sleep restriction (CSR) during adolescence has long-term effects on brain connectivity remains unclear. We used viral-mediated axonal labeling and serial two-photon tomography to measure brain-wide projections from secondary motor cortex (MOs), a high-order area with diffuse projections. For each MOs target, we calculated the projection fraction, a combined measure of passing fibers and axonal terminals normalized for the size of each target. We found no homogeneous differences in MOs projection fraction between mice subjected to 5 days of CSR during early adolescence (P25-P30, ≥ 50% decrease in daily sleep, n=14) and siblings that slept undisturbed (n=14). Machine learning algorithms, however, classified animals at significantly above chance levels, indicating that differences between the two groups exist, but are subtle and heterogeneous. Thus, sleep disruption in early adolescence may affect adult brain connectivity. However, because our method relies on a global measure of projection density and was not previously used to measure connectivity changes due to behavioral manipulations, definitive conclusions on the long-term structural effects of early CSR require additional experiments.

Keywords: adolescence; secondary motor cortex; sensitive period; sleep loss

Significance Statement

Adolescence is a sensitive period of intense brain remodeling but it is unknown whether chronic disruption of sleep at this age has long-term structural effects on neural circuits. We measured the density of projections between the mouse secondary motor cortex and the rest of the brain, using viral-mediated axonal labeling followed by serial two-photon tomography. Mice underwent 5 days of chronic sleep restriction during early adolescence or slept undisturbed, and brain connectivity was assessed after the mice reached adulthood. The two groups did not differ in any global or homogeneous way. However, machine learning classification performance allows us to conclude that intricate and local heterogeneous changes do persist in adulthood due to chronic sleep restriction.

Introduction

From early development to the end of adolescence, cortical circuits mature in stages, from early massive synaptogenesis and synaptic pruning, which result in large changes in the absolute number of synapses, to late synaptic refinement, when the initially homogeneous connectivity is reorganized without major changes in synaptic density (Innocenti and Price, 2005; Sanes and Yamagata, 2009; Tau and Peterson, 2010; Uddin et al., 2010). The end result of these processes is the adult anatomical connection matrix. Because this matrix is largely fixed, genetic or environmental factors that interfere with its establishment during development can have irreversible effects. Sleep disruption is rarely considered among these factors, perhaps because one can always sleep longer or deeper at a later time. Thus, few studies have tested the hypothesis that sleep disruption during development may impair the maturation and maintenance of brain circuits (Roffwarg et al., 1966). For example, early experiments used drugs to disturb

neonatal sleep, and found long-term neurochemical and behavioral effects, for instance on anxious behavior (for review, see (Frank, 2011)). However, these changes were likely caused not only by sleep loss, but also by other effects of the drugs used to enforce wake, many of which affect monoaminergic transmission (Frank, 2011). More recent experiments in kittens combined monocular deprivation with 1 week of rapid eye movement (REM) sleep deprivation before the end of the critical period and found a decrease in the size of neurons in the lateral geniculate nucleus of the thalamus (Shaffery et al., 1998), and similar results were obtained after total sleep deprivation (Pompeiano et al., 1995). Chronic REM sleep deprivation alone also leads to the persistence of an immature form of synaptic potentiation in primary visual cortex, suggesting that sleep loss slows down the maturation of cortical circuits (Roffwarg et al., 1966; Shaffery et al., 2002, 2012). Other studies in kittens found that a few hours of total sleep deprivation can immediately impair ocular dominance plasticity when sleep is prevented at the height of the critical period (Frank, 2011; Frank et al., 2001), and acute sleep deprivation in adolescent mice impairs the growth and maintenance of a subset of cortical spines formed after learning (Yang et al., 2014). Most of these experiments focused on preadolescent animals, and morphological and electrophysiological effects were assessed immediately or soon after the end of sleep deprivation. Thus, whether sleep loss during development leaves permanent structural changes in the adult brain was unknown, and even less known were the consequences of sustained sleep disruption during the sensitive period of adolescence (Paus et al., 2008).

Here we tested in mice whether the occurrence of chronic sleep restriction (CSR) during early adolescence has long-term effects on the adult anatomical connection matrix. In rodents, adolescence can be broadly defined as the period from weaning at postnatal day (P)21 to sexual maturity (~P50–P60; (Spear, 2000)). Massive synaptogenesis and synaptic pruning occur mainly

during the second postnatal week (Aghajanian and Bloom, 1967; Ashby and Isaac, 2011; De Felipe et al., 1997; Koester and O'Leary, 1992; Maravall et al., 2004; Micheva and Beaulieu, 1996; Romand et al., 2011). Synaptic refinement follows in the third and fourth postnatal week, when the initially homogeneous connectivity is reorganized without major changes in synaptic density, and the functional optimization of cortical circuits continues throughout adolescence (Cancedda et al., 2004; Ko et al., 2013; Seelke et al., 2012; Zhang et al., 2002). Thus, during early adolescence (~P21–P34) the anatomical connection matrix is still being refined. During the same time electroencephalographic (EEG) patterns across the sleep/wake cycle are similar to those seen in adults, and so are total daily sleep amounts ((Frank and Heller, 1997; Gramsbergen, 1976; Nelson et al., 2013); see Materials and Methods for details).

Materials and Methods

Animals

Five litters of C57BL/6J mice of the same age (n=32) were used in one single experiment that included 5 days of chronic sleep restriction (or sleep *ad libitum*) between P25 and P30, surgery for cortical injection of viral tracer at P44–P47, and perfusion for brain collection at P65–P68 (Figure 1A). All animal procedures followed the National Institutes of Health *Guide for the Care and Use of Laboratory Animals* and facilities were reviewed and approved by the IACUC of the University of Wisconsin-Madison, and were inspected and accredited by AAALAC.

Experimental procedure

At P21 mice were weaned, weighed, and housed in groups (4 per cage) in environmentally controlled conditions (12 h light/dark cycle; lights on at 8:00 A.M., room

temperature 23 ± 1°C). At P24 body weight was rechecked and two groups of 16 animals, weight-balanced and sex-balanced, were created from the total pool of 32 mice. Each group was moved into a large cage (60 × 60 × 40 cm) where mice were free to interact. Food and water were provided *ab libitum* and replaced daily at 8 A.M. At P25, the control group was left undisturbed and video-monitored for 5 days, whereas the second group was subjected to 5 days of CSR starting at 8 A.M. At that time adolescent mice show EEG patterns across the sleep/wake cycle similar to those of adult mice, with low-voltage fast activity during wake and REM sleep and large slow waves during NREM sleep (Frank and Heller, 1997; Gramsbergen, 1976). Total daily sleep amounts in young adolescent mice are also at adult levels (Nelson et al., 2013). On the other hand, REM sleep in mice continues to decline during early adolescence, and sleep deprivation is followed by an increase in sleep duration but not in sleep intensity, suggesting that the mechanisms of homeostatic sleep regulation are not fully mature (Nelson et al., 2013).

CSR was enforced using multiple strategies to disrupt sleep. During the day, ecologically relevant stimuli were selected and presented to mice, including continuous exposure to novel objects, changes of cage and bedding, social interaction, and free access to multiple running wheels. Mild forced locomotion on a slowly rotating platform was used to restrict sleep during some parts of the night. The platform was located above a tray filled with 2–3 cm of water, and the rotation speed was low enough that mice could easily avoid falling into the water as long as they moved continuously. Heat lamps were placed ~2 m above the platform to keep mice at the proper temperature. Video cameras and/or direct visual observation were used to monitor the mice at all times. Several mice were placed on the platform at the same time, and we estimate that each mouse fell into the water no more than 5 times per hour. If a mouse fell often enough such that it did not have a chance to dry, it was removed to a cage filled with novel objects and

allowed to dry before being placed back onto the rotating platform. A previous CSR study that lasted 4 days (P25–P29) and used mice implanted with EEG electrodes found that total sleep time throughout the experiment was decreased by ~70% (de Vivo et al., 2016). After CSR (or sleep *ad libitum*) mice were returned in their home cages (4 per cage), and continued to have access to novel objects (new sets of objects every morning) and running wheels until the end of the experiment at P65–P68. All mice gained weight between P21 (weaning day) and P30 (end of CSR), but controls did so more than CSR mice (C: +44.2 ± 12.2%; CSR: +20.7 ± 9.3%; t-test, $p < 0.0001$), and in each group males grew more than females (C/F +34.8 ± 12.7%; C/M +51.1 ± 12.2%; t-test, $p = 0.007$; CSR/F +15.8 ± 9.8%; CSR/M +27.9 ± 8.3%; t-test, $p = 0.008$).

Stereotaxic injection of AAV for anterograde axonal tracing

Surgery occurred over the course of 4 days (8 mice/day) between P44 and P47. Anterograde axonal tracing from MOs was performed by injecting AAV1.hSyn.eGFP.WPRE.bGH (1.79×10^{13} GC/mL) at two different depths using iontophoresis, which allows for small, focal injections (Harris et al., 2012). The day before surgery, glass capillary tubing was heat-pulled to create pipet tips that were then cut and verified under a microscope to obtain tip widths of 10–30 μm. Just prior to surgery, these pipets were filled with virus using capillary action to prevent formation of bubbles. Mice were anesthetized under 2% isoflurane and maintained at 1–2% isoflurane for the duration of surgery. Using sterile technique, mice were fitted into a stereotaxic frame and an incision was made to expose the skull. The skull was cleaned with saline and hydrogen peroxide, and a small burr hole was made in the skull using a dental drill. Any exposed brain was kept moist by saline at all times. The filled pipet was then prepared by lowering a silver wire into the pipet until it contacted virus. An electrical lead was attached to the silver wire, and an electrical ground was connected to a metal

clip placed on the skin near the skull. The pipet was then lowered to the surface of the brain 1.7 mm anterior and 0.75 mm lateral (right) from bregma. From the cortical surface, the pipet tip was lowered through the dura and into the brain 0.4 mm. A pause of 2 min was given to allow for a weak seal to form between the brain and the glass of the pipet. Current was then delivered through the pipet tip at 3 μA, alternating 7 s on and 7 s off, and repeating for 5 min to inject viral particles. The pipet tip was then lowered another 0.4 mm (to a total depth of 0.8 mm from the surface of the cortex) and the 5 min current delivery was repeated. After the current was stopped, the pipet tip was kept in place 5 additional minutes to allow for any pressure to dissipate before removal of the tip. After removal of the tip, the incision was sealed using Vetbond, antibiotic gel was applied to the surgical site, and mice were removed from isoflurane. Mice were monitored daily for 7 days following surgery to ensure normal recovery. Two control mice experienced health issues in this period and were killed.

Perfusion

Three weeks after surgery (P65–P68), mice (16 CSR and 14 controls) were deeply anaesthetized with isoflurane (3% volume) and perfused transcardially with a flush (~30 s) of saline followed by 4% paraformaldehyde (PFA) in phosphate buffer (PB). Mice were then decapitated, and heads were kept in 4% PFA until shipping to the Allen Institute for serial two-photon tomography.

Serial two-photon tomography

Briefly, carefully dissected brains were prepared for serial two-photon (STP) tomography, which integrates optical imaging and vibratome sectioning, by first rinsing with PBS before embedding in an agarose block as previously described in detail (Oh et al., 2014).

Images were acquired on TissueCyte 1000 2-photon systems (TissueVision) coupled with Mai Tai HP DeepSee lasers (Spectra Physics) using 925 nm wavelength light through a Zeiss 20× water immersion objective (NA = 1.0). One optical plane was imaged 75 µm below the cutting surface. After an entire section was imaged at an XY resolution of ~0.35 µm/pixel, a 100 µm section was cut by the vibratome and then the specimen was returned to the objective for imaging of the next plane. Images from 140 coronal sections were collected to cover the full mouse brain. Data from one CSR mouse could not be used due to a problem in image alignment. Another CSR mouse was excluded due to problems during imaging, and thus the final analysis included 14 controls and 14 CSR mice.

Image data processing

The Allen Institute informatics data pipeline managed processing and organization of the images and quantified data for analyses. Algorithms developed for the *Allen Mouse Connectivity Atlas* for signal detection and image registration were used on this dataset (Oh et al., 2014). Detailed descriptions of the neuroinformatics developed for segmentation and registration for this atlas were published recently (Kuan et al., 2015). Briefly, the signal detection algorithm was applied to each image to segment positive fluorescent signals from background. Steps include low-pass filtering to remove noise, followed by adaptive edge/line detection and classification, then integration of the detected results and rejection of artifacts or outliers. For registration, as STP tomography results in inherently aligned section images, we can simply stack the section images together to form a coherent reconstructed 3D volume. Each image stack is first registered to an intermediate "template" brain, created by iteratively averaging across ~1700 brains from the *Allen Mouse Connectivity Atlas*. Registration to this template occurs in two broad steps; global alignment followed by local alignment effected through a coarse-to-fine deformation

registration. The final step is then to align to the 3D Allen Mouse Common Coordinate Framework model.

Project density estimation

After segmentation and registration, signal was quantified for each voxel (10 ×10 × 10 μm) in the reference space and for each structure in the ontology by combining voxels from the same structure in the 3D reference model.

Thresholding

The regions that had mean projection fractions <0.1% were removed from the comparison analysis because the signal was too weak to be reliable across mice. For the ipsilateral side of the injection, 56 regions were removed (237 remained) and 92 regions (201 remained) for the contralateral side.

Injection volume normalization

Due to the experimental difficulties in controlling for the injection volume in every animal, we sought to account for the differences by normalizing by a factor proportional to the injection volume. We observed that a direct division of the projection fractions by injection volumes was not suitable and resulted in a negative correlation between total projection fraction and injection volume (not shown). Thus, we proceeded to normalize the data by fitting a power law:

$$\sum PF = A(InjVol)^n + B$$

Where $\sum PF$ is the sum of all projection fractions for an animal (after thresholding), $InjVol$ is the injection volume, and (A, B, n) are constants. It can be seen that $B = 0$ as there will be no fluorescence signal in the absence of any injection. Taking the logarithm:

$$\log(\sum PF) = n \log(InjVol) + \log A$$

A linear regression fit allowed us to determine that $n = 0.216$ was optimal and hence all the projection fractions were divided by $(InjVol)^n$. Note that once this normalization is done, the projection fraction values are no longer guaranteed to be ≤ 1.

General linear model

A general linear model (GLM) was used to control for differences in the centroids of the injections. This was done on the data after having normalized by the injection volume as described above. For every region, a GLM was fit to see the effect of the group type (CSR or control) on the normalized projection fraction. To allow comparisons between regions, every region was normalized to have unit mean. This was followed by fitting the following GLM:

$$PF_{i,j} = \beta_j + k_{xj}x_i + k_{yj}y_i + k_{zj}z_i + k_{cj}c_i$$

Where $PF_{i,j}$ is the normalized projection fraction for animal i at region j, x_i is the medial-lateral distance of the injection site from the midline for animal i after adjusting for all animals, such that $\overline{x_i} = 0$. y_i corresponds to the anterior-posterior distance (from the anterior commissure) and z_i to depth measurements (from the pia). c_i corresponds to the condition of the animal, where control = 1 and CSR = −1. The terms k_{xj}, k_{yj}, k_{zj}, and k_{cj} are factors that capture the influence of their corresponding variable and are determined by maximum likelihood estimation with the MATLAB 2015b Statistics and Machine Learning Toolbox. β_j is the

intercept term of the GLM for every region j. It should be noted that if k_{cj} is positive, then that indicates that control animals ($c_i = 1$) will have an increased projection fraction due to their condition. The opposite is true if k_{cj} is negative. If $k_{cj} = 0$ then there is no effect due to the condition. Although our analysis shows that individually k_{cj} values are not significant, we observe that all of the k_{cj} values are positively biased with a positive mean (Figure 2C). The mean of all k_{cj} values is called μ_{k_c}. However, the $\mu_{k_c} > 0$ result does not pass a bootstrap significance test as described below.

Bootstrap test

To test the confidence of the positive μ_{k_c} result, we performed a bootstrap test on the data. Each group was separately resampled (with replacement) to create a total of 50 new data sets while maintaining the same size for each group. Thus, any single resampling case may have some animals selected multiple times and others not selected at all. This allowed for 2500 (50 CSR × 50 Control) comparisons where we determined the fraction of times that μ_{k_c} was negative as the p-value. Note that every comparison involved determining a new GLM for every region. With these comparisons, the best *p* value that may be claimed is $1/50^2$ though the attained p-values were significantly larger. For the test where the female mice were investigated separately, μ_{k_c} changed sign ($\mu_{k_c} < 0$) and hence the opposite one-tailed bootstrap was performed (ratio of positive μ_{k_c} to total number of comparisons).

Animal classification

Machine learning techniques were implemented to classify the animals between CSR and control groups. This was done after fitting a modified GLM as described above that did not include a condition parameter. The dependence of the injection centroid for every animal was

then subtracted such that, to the best of our knowledge, only condition was a factor in influencing projection fractions. The algorithms were trained on $n - 1$ animals and classification was tested on the excluded animal. This process was iterated and the classification performance was quantified as the ability to classify all animals in this manner. Using a standard logit-boost decision tree to minimize binomial deviance gave the best classification accuracy at 71% (8 errors). This was due to the large overlap between animal projection values, such that no specific regions were adequate to instantly determine whether there were differences between the two groups. Hence, to improve the performance, a preprocessing step as inspired by role-base similarity was applied (Beguerisse-Díaz et al., 2014). Here, correlations between all regions were calculated to generate a 237 × 237 correlation matrix (ipsilateral hemisphere only considered). The matrix was thresholded at zero to create a positive-only correlation matrix in addition to zeroing the diagonal. Multiscale clustering was achieved using the dynamics-based clustering framework of Markov Stability (Billeh et al., 2014; Delvenne et al., 2010; Schaub et al., 2012). The clustering algorithm used a Markov process to find clusters at different scales (Schaub et al., 2012). Each cluster was then merged by summing each region within it. For instance, if a group of regions were grouped into a cluster, then for each animal the projection fractions were summed up to attain merged projection values for all regions in that cluster. At the different scales found by the Markov stability algorithm, a binary decision tree that minimizes the binomial deviance between a root node and targets was used to classify the compacted data (MATLAB 2015b Statistics and Machine Learning Toolbox). The classification improved to an accuracy of 82% (5 errors).

Anatomical analysis of MOs projections

Overall MOs projection pattern was highly consistent with what reported in the literature (Reep et al., 2008; Stuesse and Newman, 1990). Specifically, starting from the injection site in MOs, strong labeling was seen in fiber tracts extending rostrally and bilaterally into MOs, primary motor cortex, orbital area, and claustrum. Fibers weakly labeled were seen extending into the olfactory tubercle and surrounding olfactory areas bilaterally, including tenia tecta. All these bilateral projections were stronger in the hemisphere ipsilateral to the injection. Weak bilateral labeled fibers were also seen along the midline in the lateral septal nucleus and diagonal band nucleus, with roughly equal strength in both hemispheres. Moving caudally from the site of the injection, projections could be seen bilaterally in MOs, primary motor cortex and claustrum, and ipsilaterally in retrosplenial cortex. Ipsilateral primary and secondary somatosensory cortex was strongly labeled, especially in the deep and superficial layers (a similar pattern was seen in contralateral somatosensory cortex, but fluorescence was much weaker). Weak fluorescence was visible ipsilaterally in auditory and visual cortex and in postsubiculum, mostly in the deep layers, with weaker fluorescence in the same areas on the contralateral side. A reliable signal was visible across all layers in bilateral ectorhinal cortex. Fibers descended ventrally and bilaterally into caudate putamen, nucleus accumbens, and basolateral amygdala, as well as in the dorsal portion of the bed nucleus of the stria terminalis. Fibers also descended within the internal capsule toward the thalamus ipsilateral to the injection. Thalamic projections extended into rostral reticular thalamic nucleus, ventral posteromedial nucleus, ventral medial nucleus, and ventral anterior-lateral nucleus of the thalamus. More caudally, projections were visible bilaterally (but always stronger ipsilaterally) in central medial nucleus, ventral medial nucleus, mediodorsal nucleus, parafascicular nucleus, and rhomboid nucleus, whereas ipsilateral projections were

present in central lateral nucleus and posterior complex. Very faint projections were sometimes visible in the hippocampus, usually along the medial dorsal border of CA1 and dentate gyrus. Further caudally, ipsilateral projections were seen in the zona incerta, subthalamic nucleus, parasubthalamic nucleus, substantia nigra, ventral tegmental area, and extended dorsally into retrorubral area, red nucleus, midbrain reticular nucleus, and superior colliculus. Much weaker projections were visible in the same areas contralaterally. Fibers were also visible in periaqueductal gray and midline nuclei including Edinger–Westphal nucleus and rostral linear nucleus raphe. Midline nuclei showed similar projection strength bilaterally, and projections to periaqueductal gray were visible bilaterally, although they were stronger ipsilaterally. Additionally, strongly labeled fibers were present in the cerebral peduncle along the ventral side of the brain in the ipsilateral hemisphere. Throughout the pons, diffuse projections were visible in roughly equal strength bilaterally, largely in the pontine reticular nucleus. Major projection fibers descended to the medulla via the pyramidal tract resulting in a similar diffuse projection pattern with bilateral weak projections to vestibular nuclei and stronger projections to ventral midline nuclei including raphe magnus, raphe pallidus, magnocellular reticular nucleus, parapyramidal nucleus, and inferior olivary complex. More caudally through the medulla, ipsilateral fibers begin to move contralaterally as the pyramidal tract decussates. To our knowledge, no projections to the hippocampus from MOs have been previously reported in rats or mice. We noted very faint traces of labeled projections in the most medial dorsal portions of the hippocampus along the borders of CA1. Though faint, these projections were visible in all mice. In general, because we expected that thin, distal projections would be more affected by CSR, we aimed at including as MOs targets all regions that showed labeled projections, even if those projections were sparse. To verify that thin projections were not a result of noise or false

positives, and that other sparse projections were not lost to false negatives, we manually inspected positive signal masks generated after signal detection and compared them to fluorescence images in two mice. We found that the detected signal was highly concordant with observed fluorescence of all intensities, with very few false positives or negatives.

Statistics

Values in the text and figures are reported as mean ± SD. Experiments were analyzed using two-tailed t-tests, linear regression, a general linear model (see above), bootstrap test (see above), and computation of binomial cumulative distribution function probabilities. All p-values < 0.05 were considered significant *a priori*. Analysis was performed in MATLAB and all statistical tests are summarized in Table 1.

Results

Mice of the same age from five litters were split into two groups (Figure 1A). One group was subjected to 5 days of CSR in the middle of early adolescence, from P25 to P30, using ecologically relevant stimuli (see Materials and Methods), whereas during the same period control siblings were allowed to sleep *ad libitum*. At the beginning of the experiment, each group included 16 mice, but two animals in each condition were excluded for various technical reasons (see Materials and Methods). The final analysis therefore included 14 controls and 14 CSR mice. Mice were not equipped with EEG electrodes to avoid potential damage to the cortex. However, based on continuous visual monitoring and a previous study with EEG recordings using similar sleep restriction methods (de Vivo et al., 2016), we estimate that overall sleep loss was between 50 and 60% (see Materials and Methods). Approximately 2 weeks later (P44–P47) CSR mice

and controls were injected with recombinant adeno-associated virus (AAV)-expressing enhanced green fluorescent protein (EGFP) in the right MOs, to map its projections. We focused on MOs because it has diffuse projections (Zingg et al., 2014) and is highly plastic (Cao et al., 2015). Exactly 3 weeks after each animal's injection the brains were perfused. Fluorescent signals were then imaged using serial two-photon tomography and informatically reconstructed within the Allen Mouse Common Coordinate Framework, a high-resolution coordinate system that allows the systematic analysis of the entire brain (see Materials and Methods; (Oh et al., 2014)).

As expected, robust anterograde tracing from right MOs was observed throughout the brain (Figure 1B). The overall pattern of projections was consistent across mice and similar to the one previously described for rat supplementary motor cortex, also known as medial agranular cortex (Reep et al., 2008; Stuesse and Newman, 1990). Briefly, strong projections were seen to orbital area, primary motor cortex, primary and secondary somatosensory cortex, claustrum, striatum, many thalamic nuclei, as well as zona incerta, ventral tegmental area, midbrain reticular nucleus, and several midline nuclei in the pons (see Materials and Methods for detailed anatomical description). Projections were always stronger, or only present, on the side of the injection, again consistent with previous studies showing that most MOs projections are ipsilateral (Reep et al., 2008; Stuesse and Newman, 1990). Thus, subsequent analyses primarily focused on the right side.

To identify potential differences in connectivity between CSR mice and controls we examined the projection fraction (also referred to as projection density) values for each brain structure that receives axonal projections from MOs. The projection fraction is defined as the total number of voxels that fluoresce in a target brain structure divided by the total number of voxels in that structure (see Materials and Methods). Hence, projection fraction is positive-only,

has a maximal value of 1, and its use allows to control for differences in volume across anatomically defined regions. Note that the projection fraction includes both passing fibers and axon terminals, because they could not be differentiated informatically. Before direct comparisons between the two groups were made, projection fractions were normalized to control for small differences in injection volume across mice (see Materials and Methods). Moreover, regions with very weak signal were removed (projection fractions < 0.1%; see Materials and Methods). For the ipsilateral hemisphere, this thresholding resulted in dropping 56 regions from a total of 293, leaving 237 regions for analysis (Table 2). To avoid discarding genuine weak projections, we set the threshold for projection fraction fairly low. To ensure that signal within the weakest of the 237 regions was not simply due to false signal detection, detected signal overlays were compared to raw fluorescent images in two mice. Manual inspection in these mice confirmed that there were very few false positives and negatives, meaning that weak detected signals corresponded closely to real fluorescence. Figure 2A visualizes the normalized and thresholded data for the two groups; every row corresponds to a different mouse injection into MOs and every column is a different region. The projection fraction from MOs to that brain region is plotted by color.

A challenge in the outlined experiments is the difficulty in precisely replicating the injection site position. To determine the effect of such variations, plots of the mouse projection correlations relative to the mice with the injections farthest from the anatomical landmark for each axis are shown in Figure 2B. Note the farthest injected mouse, for instance most distant from the midline, has a perfect correlation of 1 as it is compared with itself. As can be seen there is a strong dependence relative to the injected medial-lateral position ($r = 0.954$). Similar patterns could be observed for the other dimensions (Figure 2B). We emphasize that in determining the

correlation for Figure 2B, we normalize by the mean of every region (to have unit mean) to account for differences between injections, which is why we observe negative correlation values. Without this normalization and using solely the heat map in Figure 2A gives a high mean pairwise correlation between all injections (0.903 ± 0.07). The effect also showed site specificity where, for instance, the anterior–posterior axis had a strong relationship in the isocortex (r = 0.602) and a significant influence by the depth axis was seen in the olfactory areas (r = 0.340). To account for this experimental variance, a GLM was fit to the normalized unit-mean projection fraction for every region (see Materials and Methods for more details). In the GLM, the effect of condition (Control or CSR) on a specific region is captured by a parameter k_{cj}, where, by construction, if k_{cj} is positive then the control group has a higher projection fraction to region j relative to the CSR group and vice versa. We found that k_{cj} was not significant on a region level, though the distribution of k_{cj} values did appear more positively biased with a positive mean (Figure 2C, left). However, running a bootstrap to test this effect yielded nonsignificant results ($\mu_{k_c} = 0.026$, $p = 0.252$; see Materials and Methods). Observing the distribution of k_c across the different macro-regions (Figure 2C, right panel) indicates that certain brain regions may be more affected than others by sleep restriction. Once again, however, none of the divisions considered passed the bootstrap significance test. Performing the same analysis on the contralateral side yielded similar results.

To determine whether there were sex-specific differences, we performed the same analysis on the males and female animals separately. This was possible as we had a similar number of males and females (14 males, 8 controls; 15 females, 6 controls). Our results show that the sleep deprivation paradigm did not influence the males' (μ_{k_c} = 0.013, p = 0.491) nor the

females' ($\mu_{k_c} = -0.034$, p = 0.258) mesoscale connectivity. Due to the small number of animals, however, we cannot rule out that subtle effects do exist that we are unable to detect.

We also investigated whether we could use the MOs normalized projection fractions (adjusted for injection positions; see Materials and Methods) to classify animals using machine-learning techniques. We trained classification algorithms on all but one animal, used the algorithm to predict the group of the excluded mouse, and repeated the procedure for all mice. We then evaluated the performance of our algorithm by its ability to classify all 28 mice. The best performance we could attain on the normalized data was 71% (8 errors; see Materials and Methods for details). To see if we could improve classification accuracy, we applied a preprocessing step as inspired by a newly developed graph-theory technique termed role-base similarity ((Beguerisse-Díaz et al., 2014); see Materials and Methods). Briefly, we found the positive correlations between all regions to create a positive-only correlation matrix that was then clustered at different levels of granularity using a Markov stability algorithm (Billeh et al., 2014; Delvenne et al., 2010; Schaub et al., 2012). By considering different levels of granularity and using classification tree algorithms on the compacted data, we reached a classification accuracy of 82% (5 errors; see Materials and Methods). Because the classification problem is binomial in nature, the classification accuracy corresponds to a p-value of 0.0005 (determined from a binomial cumulative distribution function with 5 errors, 28 attempts, at a probability of 0.5). This indicates that although CSR does not affect the brain in a single homogenous direction, it does have an intricate heterogeneous effect that can be captured by machine learning classification. Overall, the variability observed in the decision trees from dropping animals did not show a clear hypothesis for *post hoc* testing. Nonetheless, we conclude that long-term

changes in brain connectivity at the mesoscopic level do occur, and further investigations are required to fully uncover the differences.

Discussion

To our knowledge, this is the first study that tested whether there are structural changes in the adult mammalian brain after sleep was restricted during early adolescence. Brains were collected soon after mice reached adulthood, but younger mice were not tested. Thus, there may have been acute effects of CSR that we missed. Our goal, however, was to search for late, possibly irreversible effects of sleep loss on the adult connectivity. We found some evidence that early adolescence may affect the adult brain connectivity, but the changes were subtle and heterogeneous. This finding may be a true biological result, and/or it may reflect the technical limitations of our approach. The method implemented here was never used before to compare projection strength across animals in response to a behavioral manipulation. Moreover, it is based on a measure of "projection density" that combines both fibers of passage and axonal terminals and thus specific effects on the terminals may have been missed and may be better assessed using array tomography combined with excitatory and inhibitory presynaptic and postsynaptic markers (Wang et al., 2014). We note, however, that the method was sensitive enough to be significantly affected by small changes in the injection site along the medial–lateral or anterior–posterior axes, which led in some cases to noticeable differences in projection fraction profiles across animals. Finally, another limitation of the study is that we targeted a high-order area that is presumably still undergoing synaptic refinement during early adolescence, but only a systematic analysis of many brain regions can assess the full extent of the effects of chronic sleep loss.

Epidemiological studies consistently find that adolescents build a chronic sleep debt during the school days, which they are assumed to "repay" during the weekends by sleeping 1–2 hours longer (Leger et al., 2012; Roenneberg et al., 2007; Wolfson and Carskadon, 1998). Our protocol of chronic sleep restriction was quite severe but relatively short lasting (50–60% sleep loss for 5 days), but whether the milder but repeated pattern of sleep restriction observed in humans impairs the maturation of brain circuits is unknown. The inter-individual variability of the structural effects of chronic sleep loss in adolescents is also unknown, but adults vary in their susceptibility to the cognitive impairment caused by sleep deprivation (Rupp et al., 2012; Van Dongen et al., 2004), and differences in the microstructure of white and grey matter can predict inter-individual differences in the resistance to sleep loss (Bernardi et al., 2016; Cui et al., 2015; Rocklage et al., 2009).

We investigated the effect of gender in our study because sex differences in sleep exist in both humans and rodents (Mong et al., 2011): relative to males, adult female C57BL/6J mice (the strain used in the current study) are awake ∼1.5 hours more per day, recover relatively more sleep after acute sleep deprivation (Paul et al., 2006), and respond to restraint stress with a smaller rebound in REM sleep (Paul et al., 2009). Moreover, CSR mice were kept awake using mild forced locomotion, exposure to novel objects and social enrichment. None of these methods is routinely used in chronic variable stress paradigms. Yet, sleep is tightly homeostatically regulated and sleep pressure becomes irresistible even after just a few hours of extended wake (Borbély et al., 2016). Thus, extending wake beyond its physiological duration is inherently stressful, and chronic sleep loss in male adult rats leads to increased levels of catecholamines, and to a lesser extent, ACTH and glucocorticoids (Rechtschaffen and Bergmann, 2002). The behavioral effects of stress are sexually dimorphic. For instance, C57BL/6J mice that were kept

awake by gentle handling for 3 hours daily from P5 to P42 show changes in sociability and repetitive behavior (but not in anxiety measures) when tested as adults, and these effects differ between males and females (Saré et al., 2016). The structural effects of chronic stress are also sexually dimorphic in rodent prefrontal cortex and hippocampus, with loss of dendritic spines only seen in males but not in females (Leuner and Shors, 2013), although the underlying mechanisms are unclear and may include different sensitivity to glucocorticoids (Gillies and McArthur, 2010; Leuner and Shors, 2013), and/or differences in the response to other hormones and neurotransmitters involved in stress and arousal, including glutamate or noradrenaline (Valentino et al., 2012). Because our two groups of mice included a similar number of males and females (14 males, 8 controls; 14 females, 6 controls) we specifically test for any sex-related difference in our findings, but could not find any. However, we cannot rule out that the number of animals may have been too small to detect subtle differences.

Loss of sleep is associated with cellular stress, impaired protein synthesis, and increased energy demand (Borbély et al., 2016; Mackiewicz et al., 2008; Vecsey et al., 2012; de Vivo et al., 2016), consistent with a general anabolic role for sleep. Although all mice gained weight between P21 (weaning) and P30 (end of CSR), controls did so more than CSR mice (gain weight in grams, C: +44.2 ± 12.2%; CSR: +20.7 ± 9.3%; t-test, $p < 0.001$). Of note, in each group males gained more weight than females, almost twice as much in the CSR group, suggesting that CSR affected body growth more in females than males (Controls/F +34.8 ± 12.7%; Controls/M +51.1 ± 12.2%; t-test, $p = 0.007$; CSR/F +15.8 ± 9.8%; CSR/M +27.9 ± 8.3%; t-test, $p = 0.008$). Independent of the body however, growth and maintenance of neural circuits is energetically expensive and requires continuous protein synthesis (Kleim et al., 2003; Li et al., 2004). Of note, a recent study subjected flies to total sleep deprivation for 36 hours starting soon after eclosion

and tested them as “young adults” (5 days old; (Kayser et al., 2014)). In these male flies, courtship behavior was impaired, and the volume of one specific olfactory glomerulus was reduced (Kayser et al., 2014). Intriguingly, this glomerulus was the one showing the largest growth after eclosion, suggesting that the most rapidly maturing brain regions are uniquely sensitive to sleep deprivation (Kayser et al., 2014). It is possible, therefore, that had we tested younger mice, we would have found more severe permanent structural effects caused by early chronic sleep loss.

Figure 1. Experimental Timeline and MOs Projections. **A**. Experimental timeline. Between P25 and P30, mice were allowed to sleep normally (C) or subjected to CSR. All mice were injected with AAV-GFP between P44 and P47, and each mouse was perfused exactly 3 weeks later. Middle, Right, The location of the viral injections on the skull and in a coronal brain section. A, Anterior; P, posterior; D, dorsal; V ventral; B, bregma. **B**. Example of projections from MOs in two representative mice (C and CSR) 3 weeks after injection of AAV-GFP. Measurements are given in millimeters from bregma. Final analysis included 14 mice in each group.

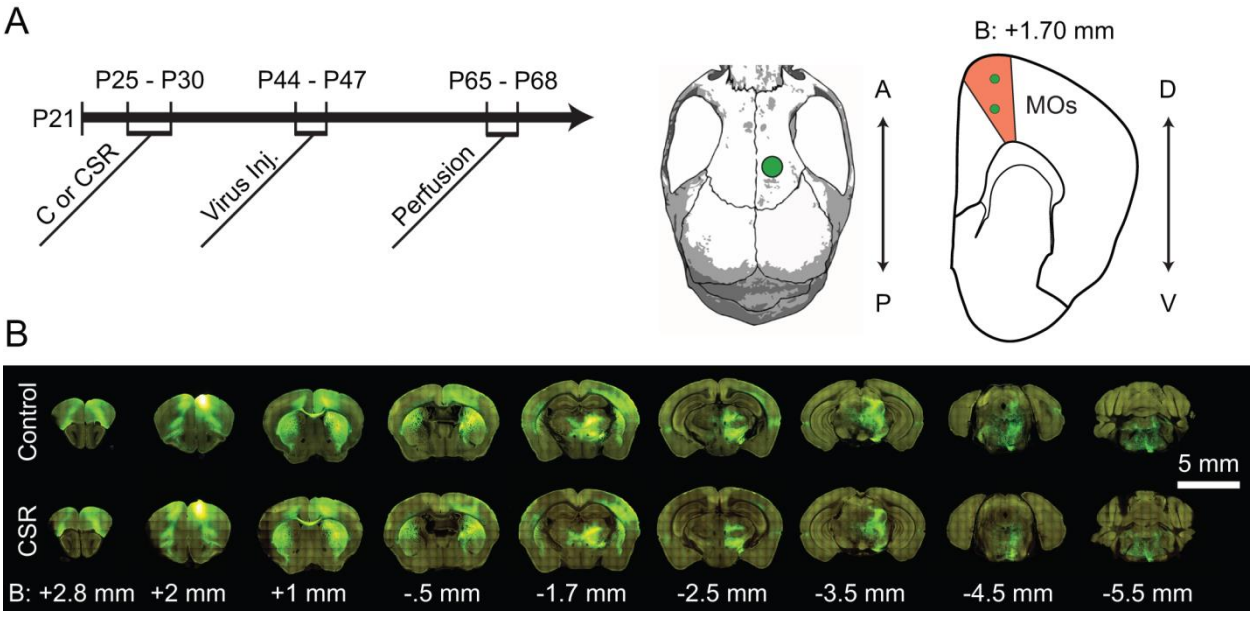

Figure 2. Projection Fractions in Controls and CSR Mice. **A**. A plot of projection fractions (normalized by injection volume) across all mice (*y*-axis) and all regions (*x*-axis). **B**. Correlations of projection fraction patterns in mice with injection site. The mouse with the most extreme distance in injection location is taken as the basis for correlation (and is by definition equal to one). All regions were first normalized to have unit means to account for differences between injections. Without this normalization, the mean pairwise correlation of all animals is 0.903 ± 0.07. Distance in micrometers is measured to the center of the injection site from the midline (826 ± 140, left), the midline merging of the anterior commissure (1771 ± 262, middle) or the pial surface (636± 60, right). Values are given for Pearson's rho. *C*. Left, Box plot of the condition influence, k_{cj} , of the GLM for all regions. A positive k_{cj} indicates that the control group has a higher connectivity than the CSR group (see Results for details). Right, An expanded version that is aligned and color-coded to match the subdivision in major anatomical regions.

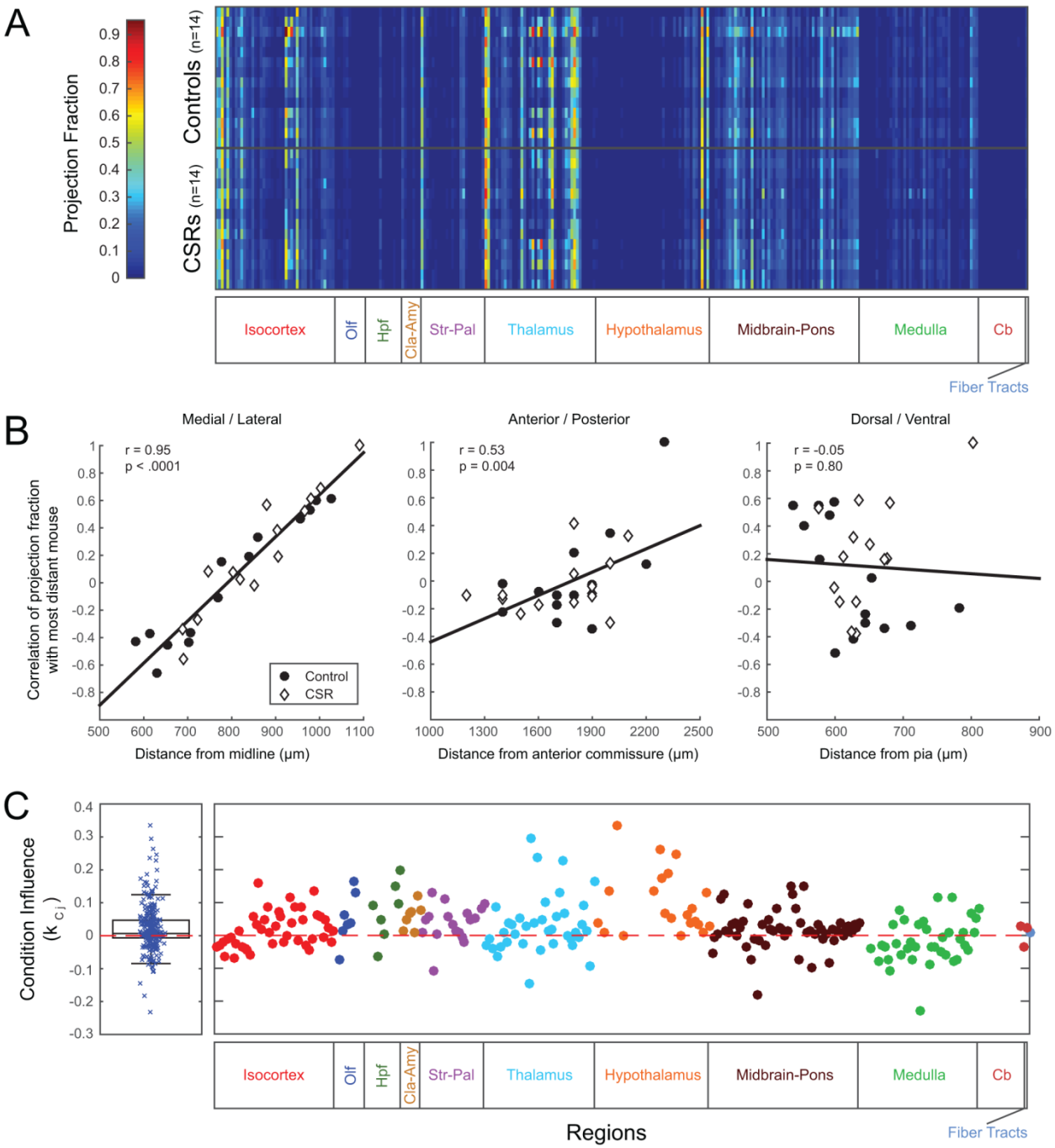
A
Projection Fraction
0.9
0.8
0.7
0.6
0.5
0.4
0.3
0.2
0.1
0
Controls (n=14)
CSRs (n=14)
Isocortex
Olf
Hpf
Cla-Amy
Str-Pal
Thalamus
Hypothalamus
Midbrain-Pons
Medulla
Cb
Fiber Tracts
B
Medial / Lateral
r = 0.95
p < .0001
Correlation of projection fraction with most distant mouse
Control
CSR
Distance from midline (μm)
Anterior / Posterior
r = 0.53
p = 0.004
Distance from anterior commissure (μm)
Dorsal / Ventral
r = -0.05
p = 0.80
Distance from pia (μm)
C
Condition Influence
(k c j)
Isocortex
Olf
Hpf
Cla-Amy
Str-Pal
Thalamus
Hypothalamus
Midbrain-Pons
Medulla
Cb
Regions
Fiber Tracts

Table 1. Statistics

Property	Data Structure	Type of test	p-value
Fig 2B: Medial/lateral effect on injections	Normally distributed	Student's t-test	< 0.0001
Fig 2B: Anterior/posterior effect on injections	Normally distributed	Student's t-test	0.004
Fig 2B: Dorsal/ventral effect on injections	Normally distributed	Student's t-test	0.796
Control/CSR influence on connectivity ($\mu_{k_c} > 0$)	Normality not assumed	One-tailed Bootstrap	0.252
Males: Control/CSR influence on connectivity ($\mu_{k_c} > 0$)	Normality not assumed	One-tailed Bootstrap	0.491
Females: Control/CSR influence on connectivity ($\mu_{k_c} < 0$)	Normality not assumed	One-tailed Bootstrap	0.258
Control/CSR influence on weight (control > CSR)	Normally distributed	Paired t-test	<0.0001
Control: Male/Female weight gain (male > female)	Normally distributed	Paired t-test	0.007
CSR: Male/Female weight gain (male > female)	Normally distributed	Paired t-test	0.008
Accuracy of classification algorithm	Binomial distributed	Binomial cumulative distribution function test	0.0005

Table 2. List of brain regions

Region Number	Region abbreviation	Region Name	Region Category
1	FRP	Frontal pole, cerebral cortex	Isocortex
2	MOp	Primary motor area	Isocortex
3	MOs	Secondary motor area	Isocortex
4	SSp-n	Primary somatosensory area, nose	Isocortex
5	SSp-bfd	Primary somatosensory area, barrel field	Isocortex
6	SSp-ll	Primary somatosensory area, lower limb	Isocortex
7	SSp-m	Primary somatosensory area, mouth	Isocortex
8	SSp-ul	Primary somatosensory area, upper limb	Isocortex
9	SSp-tr	Primary somatosensory area, trunk	Isocortex
10	SSp-un	Primary somatosensory area, unassigned	Isocortex
11	SSs	Supplemental somatosensory area	Isocortex
12	GU	Gustatory areas	Isocortex
13	VISC	Visceral area	Isocortex
14	AUDd	Dorsal auditory area	Isocortex
15	AUDp	Primary auditory area	Isocortex
16	AUDpo	Posterior auditory area	Isocortex
17	AUDv	Ventral auditory area	Isocortex
18	VISal	Anterolateral visual area	Isocortex
19	VISam	Anteromedial visual area	Isocortex
20	VISl	Lateral visual area	Isocortex
21	VISp	Primary visual area	Isocortex
22	VISpl	Posterolateral visual area	Isocortex
23	VISpm	Posteromedial visual area	Isocortex
24	VISli		Isocortex
25	VISpor		Isocortex
26	ACAd	Anterior cingulate area, dorsal part	Isocortex
27	ACAv	Anterior cingulate area, ventral part	Isocortex
28	PL	Prelimbic area	Isocortex
29	ILA	Infralimbic area	Isocortex
30	ORBl	Orbital area, lateral part	Isocortex
31	ORBm	Orbital area, medial part	Isocortex
32	ORBvl	Orbital area, ventrolateral part	Isocortex
33	AId	Agranular insular area, dorsal part	Isocortex
34	AIp	Agranular insular area, posterior part	Isocortex
35	AIv	Agranular insular area, ventral part	Isocortex
36	RSPagl	Retrosplenial area, lateral agranular part	Isocortex
37	RSPd	Retrosplenial area, dorsal part	Isocortex

38	RSPv	Retrosplenial area, ventral part	Isocortex
39	VISa		Isocortex
40	VISrl		Isocortex
41	TEa	Temporal association areas	Isocortex
42	PERI	Perirhinal area	Isocortex
43	ECT	Ectorhinal area	Isocortex
45	AOB	Accessory olfactory bulb	Olfactory Areas
46	AON	Anterior olfactory nucleus	Olfactory Areas
47	TT	Taenia tecta	Olfactory Areas
48	DP	Dorsal peduncular area	Olfactory Areas
49	PIR	Piriform area	Olfactory Areas
50	NLOT	Nucleus of the lateral olfactory tract	Olfactory Areas
51	COAa	Cortical amygdalar area, anterior part	Olfactory Areas
57	CA3	Field CA3	Hippocampal Formation
59	FC	Fasciola cinerea	Hippocampal Formation
60	IG	Induseum griseum	Hippocampal Formation
61	ENTl	Entorhinal area, lateral part	Hippocampal Formation
65	POST	Postsubiculum	Hippocampal Formation
66	PRE	Presubiculum	Hippocampal Formation
67	SUB	Subiculum	Hippocampal Formation
68	CLA	Claustrum	Claustrum + Amygdala
69	EPd	Endopiriform nucleus, dorsal part	Claustrum + Amygdala
70	EPv	Endopiriform nucleus, ventral part	Claustrum + Amygdala
71	LA	Lateral amygdalar nucleus	Claustrum + Amygdala
72	BLA	Basolateral amygdalar nucleus	Claustrum + Amygdala
73	BMA	Basomedial amygdalar nucleus	Claustrum + Amygdala
74	PA	Posterior amygdalar nucleus	Claustrum + Amygdala
75	CP	Caudoputamen	Striatum + Pallidum
76	ACB	Nucleus accumbens	Striatum + Pallidum
77	FS	Fundus of striatum	Striatum + Pallidum
78	OT	Olfactory tubercle	Striatum + Pallidum
79	LSc	Lateral septal nucleus, caudal (caudodorsal) part	Striatum + Pallidum
80	LSr	Lateral septal nucleus, rostral (rostroventral) part	Striatum + Pallidum
83	SH	Septohippocampal nucleus	Striatum + Pallidum
84	AAA	Anterior amygdalar area	Striatum + Pallidum
86	CEA	Central amygdalar nucleus	Striatum + Pallidum
87	IA	Intercalated amygdalar nucleus	Striatum + Pallidum
88	MEA	Medial amygdalar nucleus	Striatum + Pallidum
89	GPe	Globus pallidus, external segment	Striatum + Pallidum
90	GPi	Globus pallidus, internal segment	Striatum + Pallidum

91	SI	Substantia innominata	Striatum + Pallidum
92	MA	Magnocellular nucleus	Striatum + Pallidum
94	NDB	Diagonal band nucleus	Striatum + Pallidum
96	BST	Bed nuclei of the stria terminalis	Striatum + Pallidum
97	BAC	Bed nucleus of the anterior commissure	Striatum + Pallidum
98	VAL	Ventral anterior-lateral complex of the thalamus	Thalamus
99	VM	Ventral medial nucleus of the thalamus	Thalamus
100	VPL	Ventral posterolateral nucleus of the thalamus	Thalamus
101	VPLpc	Ventral posterolateral nucleus of the thalamus, parvicellular part	Thalamus
102	VPM	Ventral posteromedial nucleus of the thalamus	Thalamus
103	VPMpc	Ventral posteromedial nucleus of the thalamus, parvicellular part	Thalamus
104	SPFm	Subparafascicular nucleus, magnocellular part	Thalamus
105	SPFp	Subparafascicular nucleus, parvicellular part	Thalamus
106	SPA	Subparafascicular area	Thalamus
107	PP	Peripeduncular nucleus	Thalamus
108	MG	Medial geniculate complex	Thalamus
110	LP	Lateral posterior nucleus of the thalamus	Thalamus
111	PO	Posterior complex of the thalamus	Thalamus
112	POL	Posterior limiting nucleus of the thalamus	Thalamus
113	SGN	Suprageniculate nucleus	Thalamus
114	AV	Anteroventral nucleus of thalamus	Thalamus
115	AM	Anteromedial nucleus	Thalamus
116	AD	Anterodorsal nucleus	Thalamus
117	IAM	Interanteromedial nucleus of the thalamus	Thalamus
118	IAD	Interanterodorsal nucleus of the thalamus	Thalamus
119	LD	Lateral dorsal nucleus of thalamus	Thalamus
120	IMD	Intermediodorsal nucleus of the thalamus	Thalamus
121	MD	Mediodorsal nucleus of thalamus	Thalamus
122	SMT	Submedial nucleus of the thalamus	Thalamus
123	PR	Perireunensis nucleus	Thalamus
124	PVT	Paraventricular nucleus of the thalamus	Thalamus
125	PT	Parataenial nucleus	Thalamus
126	RE	Nucleus of reunions	Thalamus
127	RH	Rhomboid nucleus	Thalamus
128	CM	Central medial nucleus of the thalamus	Thalamus
129	PCN	Paracentral nucleus	Thalamus
130	CL	Central lateral nucleus of the thalamus	Thalamus

131	PF	Parafascicular nucleus	Thalamus
132	RT	Reticular nucleus of the thalamus	Thalamus
133	IGL	Intergeniculate leaflet of the lateral geniculate complex	Thalamus
134	LGv	Ventral part of the lateral geniculate complex	Thalamus
135	SubG	Subgeniculate nucleus	Thalamus
137	LH	Lateral habenula	Thalamus
138	SO	Supraoptic nucleus	Hypothalamus
140	PVH	Paraventricular hypothalamic nucleus	Hypothalamus
142	PVi	Periventricular hypothalamic nucleus, intermediate part	Hypothalamus
145	AVP	Anteroventral preoptic nucleus	Hypothalamus
147	DMH	Dorsomedial nucleus of the hypothalamus	Hypothalamus
158	VLPO	Ventrolateral preoptic nucleus	Hypothalamus
160	LM	Lateral mammillary nucleus	Hypothalamus
161	MM	Medial mammillary nucleus	Hypothalamus
162	SUM	Supramammillary nucleus	Hypothalamus
163	TMd	Tuberomammillary nucleus, dorsal part	Hypothalamus
164	TMv	Tuberomammillary nucleus, ventral part	Hypothalamus
166	PMd	Dorsal premammillary nucleus	Hypothalamus
168	PVHd	Paraventricular hypothalamic nucleus, descending division	Hypothalamus
170	PH	Posterior hypothalamic nucleus	Hypothalamus
171	LHA	Lateral hypothalamic area	Hypothalamus
172	LPO	Lateral preoptic area	Hypothalamus
173	PST	Preparasubthalamic nucleus	Hypothalamus
174	PSTN	Parasubthalamic nucleus	Hypothalamus
176	STN	Subthalamic nucleus	Hypothalamus
177	TU	Tuberal nucleus	Hypothalamus
178	ZI	Zona incerta	Hypothalamus
179	SCs	Superior colliculus, sensory related	Midbrain + Pons
180	IC	Inferior colliculus	Midbrain + Pons
181	NB	Nucleus of the brachium of the inferior colliculus	Midbrain + Pons
182	SAG	Nucleus sagulum	Midbrain + Pons
183	PBG	Parabigeminal nucleus	Midbrain + Pons
184	MEV	Midbrain trigeminal nucleus	Midbrain + Pons
185	SNr	Substantia nigra, reticular part	Midbrain + Pons
186	VTA	Ventral tegmental area	Midbrain + Pons
187	RR	Midbrain reticular nucleus, retrorubral area	Midbrain + Pons
188	MRN	Midbrain reticular nucleus	Midbrain + Pons
189	SCm	Superior colliculus, motor related	Midbrain + Pons
190	PAG	Periaqueductal gray	Midbrain + Pons

191	APN	Anterior pretectal nucleus	Midbrain + Pons
192	MPT	Medial pretectal area	Midbrain + Pons
193	NOT	Nucleus of the optic tract	Midbrain + Pons
194	NPC	Nucleus of the posterior commissure	Midbrain + Pons
195	OP	Olivary pretectal nucleus	Midbrain + Pons
196	PPT	Posterior pretectal nucleus	Midbrain + Pons
197	CUN	Cuneiform nucleus	Midbrain + Pons
198	RN	Red nucleus	Midbrain + Pons
199	III	Oculomotor nucleus	Midbrain + Pons
200	EW	Edinger-Westphal nucleus	Midbrain + Pons
201	IV	Trochlear nucleus	Midbrain + Pons
202	VTN	Ventral tegmental nucleus	Midbrain + Pons
203	AT	Anterior tegmental nucleus	Midbrain + Pons
204	LT	Lateral terminal nucleus of the accessory optic tract	Midbrain + Pons
205	SNc	Substantia nigra, compact part	Midbrain + Pons
206	PPN	Pedunculopontine nucleus	Midbrain + Pons
207	IF	Interfascicular nucleus raphe	Midbrain + Pons
208	IPN	Interpeduncular nucleus	Midbrain + Pons
209	RL	Rostral linear nucleus raphe	Midbrain + Pons
210	CLI	Central linear nucleus raphe	Midbrain + Pons
211	DR	Dorsal nucleus raphe	Midbrain + Pons
212	NLL	Nucleus of the lateral lemniscus	Midbrain + Pons
213	PSV	Principal sensory nucleus of the trigeminal	Midbrain + Pons
214	PB	Parabrachial nucleus	Midbrain + Pons
215	SOC	Superior olivary complex	Midbrain + Pons
216	B	Barringtons nucleus	Midbrain + Pons
217	DTN	Dorsal tegmental nucleus	Midbrain + Pons
218	PCG	Pontine central gray	Midbrain + Pons
219	PG	Pontine gray	Midbrain + Pons
220	PRNc	Pontine reticular nucleus, caudal part	Midbrain + Pons
221	SG	Supragenual nucleus	Midbrain + Pons
222	SUT	Supratrigeminal nucleus	Midbrain + Pons
223	TRN	Tegmental reticular nucleus	Midbrain + Pons
224	V	Motor nucleus of trigeminal	Midbrain + Pons
225	CS	Superior central nucleus raphe	Midbrain + Pons
226	LC	Locus ceruleus	Midbrain + Pons
227	LDT	Laterodorsal tegmental nucleus	Midbrain + Pons
228	NI	Nucleus incertus	Midbrain + Pons
229	PRNr	Pontine reticular nucleus	Midbrain + Pons
230	RPO	Nucleus raphe pontis	Midbrain + Pons

231	SLC	Subceruleus nucleus	Midbrain + Pons
232	SLD	Sublaterodorsal nucleus	Midbrain + Pons
236	CU	Cuneate nucleus	Medulla
239	NTB	Nucleus of the trapezoid body	Medulla
240	NTS	Nucleus of the solitary tract	Medulla
241	SPVC	Spinal nucleus of the trigeminal, caudal part	Medulla
242	SPVI	Spinal nucleus of the trigeminal, interpolar part	Medulla
243	SPVO	Spinal nucleus of the trigeminal, oral part	Medulla
244	VI	Abducens nucleus	Medulla
245	VII	Facial motor nucleus	Medulla
246	ACVII	Accessory facial motor nucleus	Medulla
247	AMB	Nucleus ambiguus	Medulla
248	DMX	Dorsal motor nucleus of the vagus nerve	Medulla
249	GRN	Gigantocellular reticular nucleus	Medulla
250	ICB	Infracerebellar nucleus	Medulla
251	IO	Inferior olivary complex	Medulla
252	IRN	Intermediate reticular nucleus	Medulla
253	ISN	Inferior salivatory nucleus	Medulla
254	LIN	Linear nucleus of the medulla	Medulla
255	LRN	Lateral reticular nucleus	Medulla
256	MARN	Magnocellular reticular nucleus	Medulla
257	MDRNd	Medullary reticular nucleus, dorsal part	Medulla
258	MDRNv	Medullary reticular nucleus, ventral part	Medulla
259	PARN	Parvicellular reticular nucleus	Medulla
260	PAS	Parasolitary nucleus	Medulla
261	PGRNd	Paragigantocellular reticular nucleus, dorsal part	Medulla
262	PGRNl	Paragigantocellular reticular nucleus, lateral part	Medulla
263	NR	Nucleus of Roller	Medulla
264	PRP	Nucleus prepositus	Medulla
265	PPY	Parapyramidal nucleus	Medulla
266	LAV	Lateral vestibular nucleus	Medulla
267	MV	Medial vestibular nucleus	Medulla
268	SPIV	Spinal vestibular nucleus	Medulla
269	SUV	Superior vestibular nucleus	Medulla
270	x	Nucleus x	Medulla
271	XII	Hypoglossal nucleus	Medulla
272	y	Nucleus y	Medulla
273	RM	Nucleus raphe magnus	Medulla
274	RPA	Nucleus raphe pallidus	Medulla
275	RO	Nucleus raphe obscurus	Medulla

290	FN	Fastigial nucleus	Cerebellum
291	IP	Interposed nucleus	Cerebellum
292	DN	Dentate nucleus	Cerebellum
293	fiber tracts	Fiber tracts	Fiber Tracts

References

Aghajanian, G.K., and Bloom, F.E. (1967). The formation of synaptic junctions in developing rat brain: A quantitative electron microscopic study. Brain Res. *6*, 716–727.

Ashby, M.C., and Isaac, J.T.R. (2011). Maturation of a Recurrent Excitatory Neocortical Circuit by Experience-Dependent Unsilencing of Newly-Formed Dendritic Spines. Neuron *70*, 510–521.

Beguerisse-Díaz, M., Garduño-Hernández, G., Vangelov, B., Yaliraki, S.N., and Barahona, M. (2014). Interest communities and flow roles in directed networks: the Twitter network of the UK riots. J. R. Soc. Interface *11*.

Bernardi, G., Cecchetti, L., Siclari, F., Buchmann, A., Yu, X., Handjaras, G., Bellesi, M., Ricciardi, E., Kecskemeti, S.R., Riedner, B.A., et al. (2016). Sleep reverts changes in human grey and white matter caused by wake-dependent training. NeuroImage *129*, 367–377.

Billeh, Y.N., Schaub, M.T., Anastassiou, C.A., Barahona, M., and Koch, C. (2014). Revealing cell assemblies at multiple levels of granularity. J. Neurosci. Methods *236*, 92–106.

Borbély, A.A., Daan, S., Wirz-Justice, A., and Deboer, T. (2016). The two-process model of sleep regulation: a reappraisal. J. Sleep Res. *25*, 131–143.

Cancedda, L., Putignano, E., Sale, A., Viegi, A., Berardi, N., and Maffei, L. (2004). Acceleration of visual system development by environmental enrichment. J. Neurosci. Off. J. Soc. Neurosci. *24*, 4840–4848.

Cao, V.Y., Ye, Y., Mastwal, S., Ren, M., Coon, M., Liu, Q., Costa, R.M., and Wang, K.H. (2015). Motor Learning Consolidates Arc-expressing Neuronal Ensembles in Secondary Motor Cortex. Neuron *86*, 1385–1392.

Cui, J., Tkachenko, O., Gogel, H., Kipman, M., Preer, L.A., Weber, M., Divatia, S.C., Demers, L.A., Olson, E.A., Buchholz, J.L., et al. (2015). Microstructure of frontoparietal connections predicts individual resistance to sleep deprivation. NeuroImage *106*, 123–133.

De Felipe, J., Marco, P., Fairén, A., and Jones, E.G. (1997). Inhibitory synaptogenesis in mouse somatosensory cortex. Cereb. Cortex N. Y. N 1991 *7*, 619–634.

Delvenne, J.-C., Yaliraki, S.N., and Barahona, M. (2010). Stability of graph communities across time scales. Proc. Natl. Acad. Sci. U. S. A. *107*, 12755–12760.

Frank, M.G. (2011). Sleep and developmental plasticity not just for kids. Prog. Brain Res. *193*, 221–232.

Frank, M.G., and Heller, H.C. (1997). Development of diurnal organization of EEG slow-wave activity and slow-wave sleep in the rat. Am. J. Physiol. *273*, R472-478.

Frank, M.G., Issa, N.P., and Stryker, M.P. (2001). Sleep enhances plasticity in the developing visual cortex. Neuron *30*, 275–287.

Gillies, G.E., and McArthur, S. (2010). Estrogen Actions in the Brain and the Basis for Differential Action in Men and Women: A Case for Sex-Specific Medicines. Pharmacol. Rev. *62*, 155–198.

Gramsbergen, A. (1976). The development of the EEG in the rat. Dev. Psychobiol. *9*, 501–515.

Harris, J.A., Oh, S.W., and Zeng, H. (2012). Adeno-associated viral vectors for anterograde axonal tracing with fluorescent proteins in nontransgenic and cre driver mice. Curr. Protoc. Neurosci. *Chapter 1*, Unit 1.20.1-18.

Innocenti, G.M., and Price, D.J. (2005). Exuberance in the development of cortical networks. Nat. Rev. Neurosci. *6*, 955–965.

Kayser, M.S., Yue, Z., and Sehgal, A. (2014). A Critical Period of Sleep for Development of Courtship Circuitry and Behavior in Drosophila. Science *344*, 269–274.

Kleim, J.A., Bruneau, R., Calder, K., Pocock, D., VandenBerg, P.M., MacDonald, E., Monfils, M.H., Sutherland, R.J., and Nader, K. (2003). Functional organization of adult motor cortex is dependent upon continued protein synthesis. Neuron *40*, 167–176.

Ko, H., Cossell, L., Baragli, C., Antolik, J., Clopath, C., Hofer, S.B., and Mrsic-Flogel, T.D. (2013). The emergence of functional microcircuits in visual cortex. Nature *496*, 96–100.

Koester, S.E., and O'Leary, D.D. (1992). Functional classes of cortical projection neurons develop dendritic distinctions by class-specific sculpting of an early common pattern. J. Neurosci. Off. J. Soc. Neurosci. *12*, 1382–1393.

Kuan, L., Li, Y., Lau, C., Feng, D., Bernard, A., Sunkin, S.M., Zeng, H., Dang, C., Hawrylycz, M., and Ng, L. (2015). Neuroinformatics of the Allen Mouse Brain Connectivity Atlas. Methods San Diego Calif *73*, 4–17.

Leger, D., Beck, F., Richard, J.-B., and Godeau, E. (2012). Total sleep time severely drops during adolescence. PloS One *7*, e45204.

Leuner, B., and Shors, T.J. (2013). Stress, anxiety, and dendritic spines: what are the connections? Neuroscience *251*, 108–119.

Li, Z., Okamoto, K.-I., Hayashi, Y., and Sheng, M. (2004). The importance of dendritic mitochondria in the morphogenesis and plasticity of spines and synapses. Cell *119*, 873–887.

Mackiewicz, M., Naidoo, N., Zimmerman, J.E., and Pack, A.I. (2008). Molecular mechanisms of sleep and wakefulness. Ann. N. Y. Acad. Sci. *1129*, 335–349.

Maravall, M., Koh, I.Y.Y., Lindquist, W.B., and Svoboda, K. (2004). Experience-dependent changes in basal dendritic branching of layer 2/3 pyramidal neurons during a critical period for developmental plasticity in rat barrel cortex. Cereb. Cortex N. Y. N 1991 *14*, 655–664.

Micheva, K.D., and Beaulieu, C. (1996). Quantitative aspects of synaptogenesis in the rat barrel field cortex with special reference to GABA circuitry. J. Comp. Neurol. *373*, 340–354.

Mong, J.A., Baker, F.C., Mahoney, M.M., Paul, K.N., Schwartz, M.D., Semba, K., and Silver, R. (2011). Sleep, rhythms, and the endocrine brain: influence of sex and gonadal hormones. J. Neurosci. Off. J. Soc. Neurosci. *31*, 16107–16116.

Nelson, A.B., Faraguna, U., Zoltan, J.T., Tononi, G., and Cirelli, C. (2013). Sleep patterns and homeostatic mechanisms in adolescent mice. Brain Sci. *3*, 318–343.

Oh, S.W., Harris, J.A., Ng, L., Winslow, B., Cain, N., Mihalas, S., Wang, Q., Lau, C., Kuan, L., Henry, A.M., et al. (2014). A mesoscale connectome of the mouse brain. Nature *508*, 207–214.

Paul, K.N., Dugovic, C., Turek, F.W., and Laposky, A.D. (2006). Diurnal sex differences in the sleep-wake cycle of mice are dependent on gonadal function. Sleep *29*, 1211–1223.

Paul, K.N., Losee-Olson, S., Pinckney, L., and Turek, F.W. (2009). The ability of stress to alter sleep in mice is sensitive to reproductive hormones. Brain Res. *1305*, 74–85.

Paus, T., Keshavan, M., and Giedd, J.N. (2008). Why do many psychiatric disorders emerge during adolescence? Nat. Rev. Neurosci. *9*, 947–957.

Pompeiano, O., Pompeiano, M., and Corvaja, N. (1995). Effects of sleep deprivation on the postnatal development of visual-deprived cells in the cat's lateral geniculate nucleus. Arch. Ital. Biol. *134*, 121–140.

Rechtschaffen, A., and Bergmann, B.M. (2002). Sleep deprivation in the rat: an update of the 1989 paper. Sleep *25*, 18–24.

Reep, R.L., Wu, J.H., Cheatwood, J.L., Corwin, J.V., Kartje, G.L., and Mir, A. (2008). Quantification of synaptic density in corticostriatal projections from rat medial agranular cortex. Brain Res. *1233*, 27–34.

Rocklage, M., Williams, V., Pacheco, J., and Schnyer, D.M. (2009). White matter differences predict cognitive vulnerability to sleep deprivation. Sleep *32*, 1100–1103.

Roenneberg, T., Kuehnle, T., Juda, M., Kantermann, T., Allebrandt, K., Gordijn, M., and Merrow, M. (2007). Epidemiology of the human circadian clock. Sleep Med. Rev. *11*, 429–438.

Roffwarg, H.P., Muzio, J.N., and Dement, W.C. (1966). Ontogenetic development of the human sleep-dream cycle. Science *152*, 604–619.

Romand, S., Wang, Y., Toledo-Rodriguez, M., and Markram, H. (2011). Morphological development of thick-tufted layer v pyramidal cells in the rat somatosensory cortex. Front. Neuroanat. *5*, 5.

Rupp, T.L., Wesensten, N.J., and Balkin, T.J. (2012). Trait-like vulnerability to total and partial sleep loss. Sleep *35*, 1163–1172.

Sanes, J.R., and Yamagata, M. (2009). Many paths to synaptic specificity. Annu. Rev. Cell Dev. Biol. *25*, 161–195.

Saré, R.M., Levine, M., Hildreth, C., Picchioni, D., and Smith, C.B. (2016). Chronic sleep restriction during development can lead to long-lasting behavioral effects. Physiol. Behav. *155*, 208–217.

Schaub, M.T., Delvenne, J.-C., Yaliraki, S.N., and Barahona, M. (2012). Markov dynamics as a zooming lens for multiscale community detection: non clique-like communities and the field-of-view limit. PloS One *7*, e32210.

Seelke, A.M.H., Dooley, J.C., and Krubitzer, L.A. (2012). The emergence of somatotopic maps of the body in S1 in rats: the correspondence between functional and anatomical organization. PloS One *7*, e32322.

Shaffery, J.P., Oksenberg, A., Marks, G.A., Speciale, S.G., Mihailoff, G., and Roffwarg, H.P. (1998). REM sleep deprivation in monocularly occluded kittens reduces the size of cells in LGN monocular segment. Sleep *21*, 837–845.

Shaffery, J.P., Sinton, C.M., Bissette, G., Roffwarg, H.P., and Marks, G.A. (2002). Rapid eye movement sleep deprivation modifies expression of long-term potentiation in visual cortex of immature rats. Neuroscience *110*, 431–443.

Shaffery, J.P., Lopez, J., and Roffwarg, H.P. (2012). Brain-derived neurotrophic factor (BDNF) reverses the effects of rapid eye movement sleep deprivation (REMSD) on developmentally regulated, long-term potentiation (LTP) in visual cortex slices. Neurosci. Lett. *513*, 84–88.

Spear, L.P. (2000). The adolescent brain and age-related behavioral manifestations. Neurosci. Biobehav. Rev. *24*, 417–463.

Stuesse, S.L., and Newman, D.B. (1990). Projections from the medial agranular cortex to brain stem visuomotor centers in rats. Exp. Brain Res. *80*, 532–544.

Tau, G.Z., and Peterson, B.S. (2010). Normal development of brain circuits. Neuropsychopharmacol. Off. Publ. Am. Coll. Neuropsychopharmacol. *35*, 147–168.

Uddin, L.Q., Supekar, K., and Menon, V. (2010). Typical and atypical development of functional human brain networks: insights from resting-state FMRI. Front. Syst. Neurosci. *4*, 21.

Valentino, R.J., Reyes, B., Van Bockstaele, E., and Bangasser, D. (2012). Molecular and cellular sex differences at the intersection of stress and arousal. Neuropharmacology *62*, 13–20.

Van Dongen, H.P.A., Baynard, M.D., Maislin, G., and Dinges, D.F. (2004). Systematic interindividual differences in neurobehavioral impairment from sleep loss: evidence of trait-like differential vulnerability. Sleep *27*, 423–433.

Vecsey, C.G., Peixoto, L., Choi, J.H.K., Wimmer, M., Jaganath, D., Hernandez, P.J., Blackwell, J., Meda, K., Park, A.J., Hannenhalli, S., et al. (2012). Genomic analysis of sleep deprivation reveals translational regulation in the hippocampus. Physiol. Genomics *44*, 981–991.

de Vivo, L., Nelson, A.B., Bellesi, M., Noguti, J., Tononi, G., and Cirelli, C. (2016). Loss of Sleep Affects the Ultrastructure of Pyramidal Neurons in the Adolescent Mouse Frontal Cortex. Sleep *39*, 861–874.

Wang, G.X., Smith, S.J., and Mourrain, P. (2014). Fmr1 KO and fenobam treatment differentially impact distinct synapse populations of mouse neocortex. Neuron *84*, 1273–1286.

Wolfson, A.R., and Carskadon, M.A. (1998). Sleep schedules and daytime functioning in adolescents. Child Dev. *69*, 875–887.

Yang, G., Lai, C.S.W., Cichon, J., Ma, L., Li, W., and Gan, W.-B. (2014). Sleep promotes branch-specific formation of dendritic spines after learning. Science *344*, 1173–1178.

Zhang, L.I., Bao, S., and Merzenich, M.M. (2002). Disruption of primary auditory cortex by synchronous auditory inputs during a critical period. Proc. Natl. Acad. Sci. U. S. A. *99*, 2309–2314.

Zingg, B., Hintiryan, H., Gou, L., Song, M.Y., Bay, M., Bienkowski, M.S., Foster, N.N., Yamashita, S., Bowman, I., Toga, A.W., et al. (2014). Neural networks of the mouse neocortex. Cell *156*, 1096–1111.

Chapter IV:

Effects of Chronic Sleep Restriction during Early Adolescence on Synaptic Density and Size

Alexander V. Rodriguez, Michele Bellesi, Giulio Tononi and Chiara Cirelli

Abstract

In development, the brain grows and changes rapidly, adding new neurons and synaptic connections and refining them with age. Sleep also changes with development, as total sleep duration decreases with increasing age. Sleep disruption has been shown to interfere with neuronal plasticity at early ages, and increasing evidence shows that the function and structure of synapses are altered by sleep and wake. However, few studies have looked at the effects of chronic sleep restriction (CSR) in adolescence on adult synaptic size and density. Here, I subjected mice to a five-day sleep restriction between P25 and P30, allowed 5 weeks for recovery, and then used immunohistochemistry to visualize synaptic puncta labeled using VGlut1 and VGlut2, markers of excitatory glutamatergic synapses, and VGAT, which labels inhibitory GABAergic synapses. Puncta were imaged in various cortical and subcortical regions using confocal microscopy. I found several differences in VGlut1, VGlut2, or VGAT staining between control and CSR mice, resulting from differences in measures of puncta density and/or size in specific cortical areas. However, the changes were not consistent across two independent experiments. It is possible that technical variability in the immunohistochemistry experiments is large enough to mask any consistent, but small, biological result. Another possibility is that P25 may simply be late enough in the developmental process such that even long term sleep restriction will not disrupt normal synaptic development. Finally, it is possible that there were large short term changes in synaptic growth that were able to recover to different extents in different mice as they reached adulthood. Because of the high relevance of sleep restriction studies in adolescents for humans, further experiments at different ages and with different imaging techniques are still required.

Introduction

Neurons and synapses both grow rapidly during early development, with synapses and neural connections overdeveloping and connecting beyond what is optimal for the adult brain (Innocenti and Price, 2005). Adolescence is instead a time for large scale synaptic pruning and refinement of neural circuits (Feinberg and Campbell, 2010; Huttenlocher, 1979).

The expression of sleep changes along with development, as younger animals require much more sleep than their adult counterparts and the proportion of non-rapid-eye-movement (NREM) sleep and rapid eye movement (REM) sleep changes with age (Frank and Heller, 1997). Adolescence in particular is a time for large changes in electrophysiological measures of sleep, including the expression of slow-wave activity (SWA), a measure of low frequency EEG power that is also a reliable marker of sleep need in adults (Borbély et al., 2016). SWA is relatively high in young animals and early adolescents, and declines as animals age (Feinberg and Campbell, 2010; Paus, 2005; de Vivo et al., 2014). SWA in adults is increased following sleep deprivation (Borbély et al., 1981, 2016; Dijk et al., 1987), but this response is blunted in early adolescents and does not appear until late adolescence (Jenni et al., 2005; Nelson et al., 2013). Sleep deprivation studies in adolescent animals have shown that lack of sleep can have broad effects. For example, ocular dominance plasticity in kittens is impaired following sleep deprivation that occurs in the middle of the critical period (Frank et al., 2001). Selective REM sleep deprivation in developing rats extends the period in which LTP can be induced in slices when compared to normally sleeping rats, indicating that sleep disruptions can lead to aberrant plasticity (Shaffery et al., 2002, 2012). Human adolescents as a group may be especially susceptible to sleep restriction given the combination of early school times, often dictated by social/practical reasons, as well as an increased preference for later sleep times, which is strongly

correlated with puberty status, suggesting a biological basis for this sleep timing shift (Carskadon et al., 1993; Wolfson and Carskadon, 1998). Despite the high risk of sleep restriction in adolescent humans, few studies have looked at the potential long term impacts of chronic sleep restriction (CSR) during adolescence.

A previous study performed in cooperation with the Allen Institute for Brain Science found that structural connectivity from secondary motor cortex (MOs) to its various brain targets did not significantly change in adult mice that underwent five days of CSR as adolescents when compared to control animals that were allowed to sleep freely during the same interval (Billeh, Rodriguez et al., 2016). The aims of this study were targeted in scope, looking only at axonal projections from one higher order cortical area, MOs. I found that while no single anatomical region showed significant changes, machine learning classification could still reliably identify animals as either control or CSR, indicating that there are some subtle but consistent differences between groups. That study, however, left open the possibility that looking at smaller scale features would reveal differences unseen by mesoscale connectivity. To this end, I focused on analyzing synaptic puncta as labeled with immunohistochemistry. Synapses are generally classified by the type of neurotransmitter they release. Glutamate is the primary excitatory neurotransmitter in the brain, and its reuptake into synaptic vesicles is mediated by the vesicular glutamate transporter (VGlut), which is found in three varieties: VGlut1, VGlut2, and VGlut3 (El Mestikawy et al., 2011; Fremeau Jr et al., 2004; Vigneault et al., 2015). I focused specifically on VGlut1 and VGlut2. VGlut1 is strongly expressed within the cortex, and primarily found in corticocortical projections (Kaneko and Fujiyama, 2002; Ni et al., 1995). In contrast, VGlut2 mRNA expression is limited to the thalamus and some neurons within layer 4, and indeed VGlut2 in the cortex is primarily found within thalamocortical projections (Herzog et al., 2001;

Kaneko and Fujiyama, 2002). GABA is the primary inhibitory neurotransmitter within the brain, and its corresponding transporter VGAT is found throughout the brain (Chaudhry et al., 1998). These vesicular transporters act as markers of presynaptic sites, and can be used to assess the size and density of synapses (Ngodup et al., 2015). In order to assess whether CSR in adolescence causes synaptic changes in adulthood, I first used immunohistochemistry to label sections from the same mice used in the previous experiment (Billeh, Rodriguez et al., 2016) for VGlut1, VGlut2, and VGAT, and I found some initial differences in VGlut1 synaptic size between groups. To confirm these findings, I studied a second cohort of control and CSR mice and labeled them for VGlut1.

Methods

Animals

Two separate sets of mice were used for this study. The first set consisted of 5 litters of C57BL/6J mice of the same age (n=32; 16 male, 16 female) that were subjected to a long term experiment including 5 days of chronic sleep restriction (CSR) or normal sleep between postnatal day 25 and 30 (P25-P30), surgery for cortical injection of viral tracer (AAV1-hSyn-eGFP-WPRE-bGH; 1.79×10^{13}) at P44-P47, and finally perfusion for brain collection at P65-P68. Two control mice experienced health problems after the injection and were killed. Two CSR brains were excluded because of technical issues after perfusion, leaving a final count of 14 control mice and 14 CSR mice. The second mouse set consisted of 17 male C57BL/6J mice. As in the first set, mice went through CSR or could sleep normally between P25 and P30 and the brains were collected only when they reached adulthood, at P65-P68. All animal procedures

followed the National Institutes of Health Guide for the Care and Use of Laboratory Animals and facilities were reviewed and approved by both the IACUC of the University of Wisconsin-Madison and AAALAC.

Chronic sleep restriction

At P21 mice were weaned, weighed, and housed in groups (3-4 per cage) in environmentally controlled conditions (12h:12h light-dark cycle; lights on at 8 am, room temperature 23± 1 °C). At P24, body weight was re-checked and two groups of 16 animals, weight-balanced and sex balanced were created from the total pool of 32 mice in the first set. The second set of mice was divided into 7 control and 10 CSR animals. At P25, each group was moved into a large cage (60 cm x 60cm x 40 cm) where mice were free to interact. Food and water were provided *ab libitum*. Sleep restriction was enforced using several techniques. From 8 am to 8 pm, an experimenter was present in the room at all times and provided novel objects, running wheels, and gentle handling to ensure that mice did not fall asleep. From 8 pm to 8 am, groups of 5-8 mice each were placed on a conveyer over water (COW), which consisted of a slow moving belt over a shallow pool of water equipped with small ladders to allow mice to climb back to the belt surface. Heating lamps were placed ~2 meters above the COWs to ensure that mice were kept warm. The speed of the belt was adjusted such that mice were allowed ~35 seconds of inactivity before reaching the end of the belt. Mice were kept under constant video or direct visual monitoring and to ensure that they were motivated and able to climb back to the belt surface if they fell in the water (falling occurred no more than 5 times per hour). If a mouse fell often enough that it was not allowed time to dry over an extended period of time, that mouse was put into a separate cage filled with novel objects and allowed to dry completely before being placed back into the COW. If a mouse lost motivation to climb back onto the belt, it was moved

into a separate cage and kept awake with novel objects until it was dry, then placed back onto the COW. After 5 full days of CSR, mice were placed back into normal housing cages in groups of 3 or 4 and left undisturbed except for daily weighing at 8 am. The control group was left mostly undisturbed under video monitoring for the duration of the experiment. To match motor activity between groups as much as possible, between P25 and P30 running wheels were placed in the control mouse cage from 8 pm to 8 am, a time when the mice were naturally awake. Food and water were replaced at 8 am. After 5 days, control mice were moved back into normal housing in groups of 3 or 4 per cage. All mice were switched to single housing after P47 until perfusion at P65-P68 (Figure 1A).

Transcardial perfusion

Between P65-P68, all mice were first deeply anesthetized using 3% isoflurane and then transcardially flushed with 0.9% saline followed by 4% paraformaldehyde (PFA) in 0.1 M phosphate buffer. The first set of mice was then decapitated and heads were kept in PFA for shipment to the Allen Institute for simultaneous slicing and imaging at a thickness of 100 microns per slice as previously described (Billeh, Rodriguez et al., 2016). The brains of the second set were instead immediately dissected and left to postfix in PFA for 24 hours before being sliced in the coronal axis on a vibratome (Leica) at a thickness of 50 microns.

Immunohistochemistry

All sections were first washed 5 times for 5 minutes in 0.05 M phosphate buffered saline (PBS) then blocked in 10% normal goat serum (NGS) in PBS for 1 hour at room temperature prior to incubation with the primary antibody. Slices were placed in one of three different antibody dilutions in PBS: 1:1000 guinea pig anti-VGlut1 (Millipore, AB5905), 1:1000 guinea

pig anti-VGlut2 (Millipore, AB2251), or 1:500 rabbit anti-VGAT (Synaptic Systems, 131002) for 2 hours at room temperature, and then incubated overnight at 4 ºC. After overnight incubation, slices were washed 5 times for 5 minutes in PBS, incubated in 10% NGS for 25 minutes, and then left in one of two different secondary antibody dilutions in PBS: for VGlut1 and VGlut2, 1:1000 goat anti-guinea pig Alexa fluor 568 (Life Technologies, A11075) or, for VGAT, 1:1000 goat anti-rabbit (Life Technologies, A11011) at room temperature for 1 hour. Slices were then washed again 5 times for 5 minutes each in PBS, mounted onto glass slides, allowed to dry, and then covered with Vectashield (Vector Labs, H-1000). Two brain sections were mounted per slide, one belonging to a mouse from the control group and another from the CSR group. In cases where numbers of control and CSR mice were not equal, some slides had two sections from the same group.

Confocal imaging

Sections were imaged using a confocal microscope (Olympus), with control and CSR sections imaged in counterbalanced order. For each region, 3 image series along the z-axis (stacks) per hemisphere were taken for a total of 6 stacks per region. For VGlut1 and VGAT, the 3 stacks were focused on layers 1, 5, and 6. For VGlut2, the 3 stacks were focused on layers 1, 4, and 6 (Figure 1B). Layer 4 can be easily identified by a brighter band in sections with VGlut2 staining. One or two sections were used to calibrate laser power and brightness of the images, and then these same settings were used across all slices for each antibody. The two VGlut1 mouse sets were calibrated separately. Because antibodies generally only stain the surface of slices, image stacks were taken starting above the plane of the slice and proceeding in 0.3 um intervals until visible puncta were no longer in focus. Due to artifacts or complications in the

staining process, some areas received very little or no fluorescence as a result of staining. Stacks that did not provide reliable signal were not used for analysis.

Image Analysis

Images were analyzed using ImageJ software using several different methods. Specifically, I performed region of interest (ROI), single image, max projection, and standard deviation projection analyses. ROIs were selected as follows: first, a single image of best focus was selected from each image stack. Next, six square regions of interest were manually selected within each image selecting from areas that were in focus and representative of the image. Max and standard deviation projections were performed by opening an entire stack and using "Z Project…" with either "Maximum" or "Standard Deviation" as options to collapse the stack into a single image. The images produced from these different methods all used a similar algorithm to remove areas of the image that were puncta free either due to cell bodies or being out of focus. First, the contrast of the image was enhanced to make detectable puncta brighter. Next, the image was thresholded using the default thresholding algorithm in imageJ. The thresholded image was run through a dilation process 5 times to inflate visible puncta and close gaps between them. Next, any gaps that still remained larger than 16.6 μm^2 were detected using "Analyze Particles", highlighted, dilated to compensate for the previous signal dilation, and merged to outline all the empty areas of the image. The inverse of the empty selection was used for analysis and referred to as the 'active area' of the image. All of the images, except for those generated by a standard deviation projection, were run through the "Subtract Background" option. The active area was thresholded using the default algorithm within imageJ, run through a watershed algorithm to separate merged signal, and then subjected to the "Analyze Particles" option to detect puncta. Only puncta between 0.17 – 8.32 μm^2 (10-500 pixels) were kept for further analysis. To measure

synaptic density, I counted the total number of puncta detected and divided that number by the total size of the active area. To get an average puncta size for each image, I took the average puncta size for all detected puncta within the active area.

Statistics

Numbers obtained from image analysis in imageJ were imported into MATLAB (Mathworks) where I used the function 'ttest2' (a two-sample t-test) to compare control and CSR values for synaptic density and size. Each anatomical region was considered separately without correcting for multiple comparisons.

Results

I used 32 mice of the same age from 5 litters split into equal control and CSR groups, of which 14 control (8 male, 6 female) and 14 CSR (6 male, 8 female) mice were used for analysis. The CSR group was subjected to 5 days of sleep restriction between P25 and P30 using ecologically relevant stimuli during the light period and forced locomotion in the dark period (see Methods). Control mice were allowed to sleep freely during the 5 days, and running wheels were introduced during the dark period to control for locomotor activity between groups. Though there was no electrophysiological monitoring of these animals as to avoid damaging brain tissue, previous experiments using this same CSR technique, and in which mice were implanted with EEG electrodes, led to a sleep loss of about 50 – 60% (de Vivo et al., 2016a). Mice were perfused and brains sectioned 5 weeks after the end of sleep restriction at P65-P68 (Figure 1A). Select slices were stained separately for antibodies against vesicular glutamate transporters VGlut1 and VGlut2, as well as the vesicular GABA transporter VGAT and imaged with a

confocal microscope. I focused on taking bilateral images from a variety of brain regions and layers in a systematic manner, based on boundaries set by the Allen Brain Atlas (Figure 1 B).

VGlut1

Within VGlut1 stained slices, I imaged ventral anterior cingulate cortex (ACAv), primary motor cortex (MOp), secondary somatosensory cortex (SSs), piriform cortex (PIR), and caudoputamen (CP) by taking stacks of images from several layers (Figure 1B). VGlut1 showed strong, puncta-shaped expression within cortex, similar to previously published results (Fremeau Jr et al., 2004). To mitigate the possibility of false findings or potential bias from one analysis type, I used four different image processing techniques (see Methods). The results between the four types of analysis were generally in agreement, so I present here only results obtained using the single image of best focus from each stack (Figure 1C).

To begin, I measured average puncta density and size for each image and compared them between control and CSR mice for each anatomical structure separately without correcting for multiple comparisons. Looking at puncta density, I found that there were no significant differences between control and CSR mice in ACAv (n=27 mice, 84 control images, 72 CSR images; two sample t-test, p=0.96) MOp (n=84 control, 75 CSR; p=0.52) , SSs (n=84 control, 78 CSR; p=0.11), PIR (n=84 control, 78 CSR; p=0.72), or CP (n=84 control, 78 CSR; p=0.15). Next, examining puncta size, I found no difference between control and CSR mice in MOp (p=0.10), SSs (p=0.18), PIR (p=0.16), and CP (p=0.76). However, in ACAv, puncta size was significantly larger in control mice over CSR mice (p=0.018).

To verify these findings, I repeated the sleep restriction experiment in a second set of mice. The second sleep restricted set of mice consisted of 17 male C57BL/6J mice that were split

into 7 control and 10 CSR mice. As before, the CSR mice were sleep restricted from P25 to P30 and then allowed to sleep ad libitum until transcardial perfusion between P65 and P68. Because I previously found an effect in ACAv, I specifically looked at puncta density and size there. I found that puncta density was significantly higher in CSR mice (n=42 control images, 60 CSR images; two sample t-test, p=0.022) and that puncta size was also larger in CSR mice (n=42 control, 60 CSR; p=0.0002), in opposition to the results from the first set of mice.

VGAT

Next, to investigate whether there were any changes to inhibitory signaling within the same areas investigated for glutamatergic synapses, I stained slices adjacent to those used for VGlut1 and imaged the same regions (ACAv, MOp, SSs, PIR, and CP). Overall VGAT staining was consistent with previously published observations (Chaudhry et al., 1998). Average puncta density for each image showed no changes between control and CSR mice (n=28 mice; 84 control images, 84 experimental images; two sample t-test; ACAv: p=0.44; MOp: p=0.69; SSs: p=0.995; PIR: p=0.59; CP: p=0.67). Puncta size also showed no change between control and CSR mice (ACAv: p=0.52; MOp: p=0.73; SSs: p=0.19; PIR: p=0.64; CP: p=0.42).

VGlut2

I next focused on cortical synaptic puncta containing VGlut2, which primarily marks thalamocortical axonal projections into cortex (Hur and Zaborszky, 2005; Kaneko and Fujiyama, 2002). Because some of the most prominent thalamocortical projections carry sensory information (Clascá et al., 2012), I investigated VGlut2 puncta within primary areas, including primary motor cortex (MOp), primary somatosensory trunk area (SSptr), and primary somatosensory barrel field area (SSPbfd). VGlut2 sparsely labeled the cortex with an especially

strong band of expression in layers 1 and 4, consistent with previously published works (Kaneko and Fujiyama, 2002). I analyzed the images as before, but found no changes in either puncta density (n=28 mice; 84 control images, 84 experimental images; two sample t-test; MOp: p=0.56; SSptr: p=0.49; SSpbfd: p=0.94) or puncta size (MOp: p=0.79; SSptr: p=0.36; SSpbfd: p=0.80).

Discussion

This study, as an extension to previously published work (Billeh, Rodriguez et al., 2016), is to my knowledge the first that tested whether chronic sleep restriction in adolescence could have an effect on adult synaptic density and size. Previously, I showed that connectivity from secondary motor cortex (MOs) showed some heterogeneous and subtle differences between control and CSR animals (Billeh, Rodriguez et al., 2016). By investigating synaptic changes rather than mesoscale connectivity, I set out to determine if there were more consistent or stronger effects at the synaptic level. However, after looking across a number of different anatomical regions and synaptic types, I was unable to find any reliable differences in puncta density and size when comparing control and CSR mice.

This may be in part due to limitations within the experimental design. For instance, sleep restricting mice at an earlier age may have caused more noticeable changes. Some proteins with effects on synapse formation are known to peak in expression as early as P9 (Gonzalez-Lozano et al., 2016), suggesting that there are other critical development stages that could show greater effects from sleep deprivation. However, long term sleep restriction on mice much younger than P25 is difficult because, due to its intrinsically stressful nature, chronic sleep restriction can often

slow down the weight gain normally seen in developing animals (Billeh, Rodriguez et al., 2016), an effect also observed within the new CSR cohort (data not shown). Mice that are much younger would not be able to tolerate this slower growth, and would be unlikely to survive. Mice do not reach weaning age until around P20, and unless mice are able to reliably feed themselves, there is an additional confound created when trying to sleep restrict mouse pups and simultaneously ensure they are able to nurse.

From a technical perspective, there are other potential methods that I could employ. In the second sleep restriction set, I observed effects opposite to those found in my first experiment. This implies that either there is a variable response to sleep restriction, or perhaps that my methodology has some degree of variability built in. Immunohistochemistry combined with confocal microscopy may simply be too susceptible to technical variability to reliably detect synaptic changes, and more sensitive and more quantitative techniques such as serial block face scanning electron microscopy may be needed (de Vivo et al., 2016a, 2016b). In the future, comparing results across repeated samples of the same areas may provide extra information as to methodological reliability. An alternative approach might involve array tomography (Micheva et al., 2010), which allows for examining not only the synaptic density and size of each marker, but their colocalization as well, although technical variability may still be an issue with this method. It is possible that though the overall density and size of each synapse type do not change, the colocalization and balance of excitatory and inhibitory signals might be altered.

Is has recently been demonstrated that sleep and wake at younger ages can indeed have structural effects on synapses, at least acutely. Following spontaneous or enforced wake for 6 hours in P30 mice, axon-spine interfaces and postsynaptic densities were larger compared to 6 hours of sleep (de Vivo et al., 2016b). However, synapses were examined directly after wake or

sleep, not after days of sleep restriction and recovery. Adolescent mice are known to have a high amount of spine turnover (Maret et al., 2011), and it is possible that this period of high turnover extends past P30, the time where the deprivation ended. If this were the case, spine formation may still be plastic enough to resist any large insults such as chronic sleep restriction. That is, even though the chronic sleep restriction likely modified synapses, the weeks of recovery allowed before the brains were examined were a sufficient amount of time for the brain to return to normal. Many human adolescents experience a shift towards a later preferred sleep time and simultaneously must endure early school times, making sleep restriction a prevalent problem (Carskadon et al., 1993, 1998; Wolfson and Carskadon, 1998). Sleep restriction over a longer period of time is equivalent to shorter periods of total sleep deprivation (Van Dongen et al., 2003), and sleep loss is associated with a number of deficits in attention, working memory, and higher cognitive function (Killgore, 2010; Killgore et al., 2006; Lim and Dinges, 2008). Though I was unable to find any evidence of long term alterations in synaptic density and size, further experiments are needed at different time points in order to understand potential problems that could arise when sleep is restricted in children and adolescents.

Figure 1. Experimental design. **A**. Timeline of control (C) or chronic sleep restriction (CSR) duration and perfusion. **B**. Schematic showing approximate locations of image stacks taken over coronal section outlines from the Allen Brain Atlas. Each red square denotes the location of an acquired image stack, and blue highlights the regions from which stacks were taken, with adjacent labels. ACAv = anterior cingulate area, ventral part; MOp = primary motor area; SSs = supplemental somatosensory area; PIR = piriform area; CP = caudoputamen; SSptr = primary somatosensory area, trunk; SSpbfd = primary somatosensory area, barrel field. **C**. An example of a single image of best focus before processing (left), the same image with the "active area" outlined (middle), and with detected puncta highlighted in black (right). Scale bar = 10 microns.

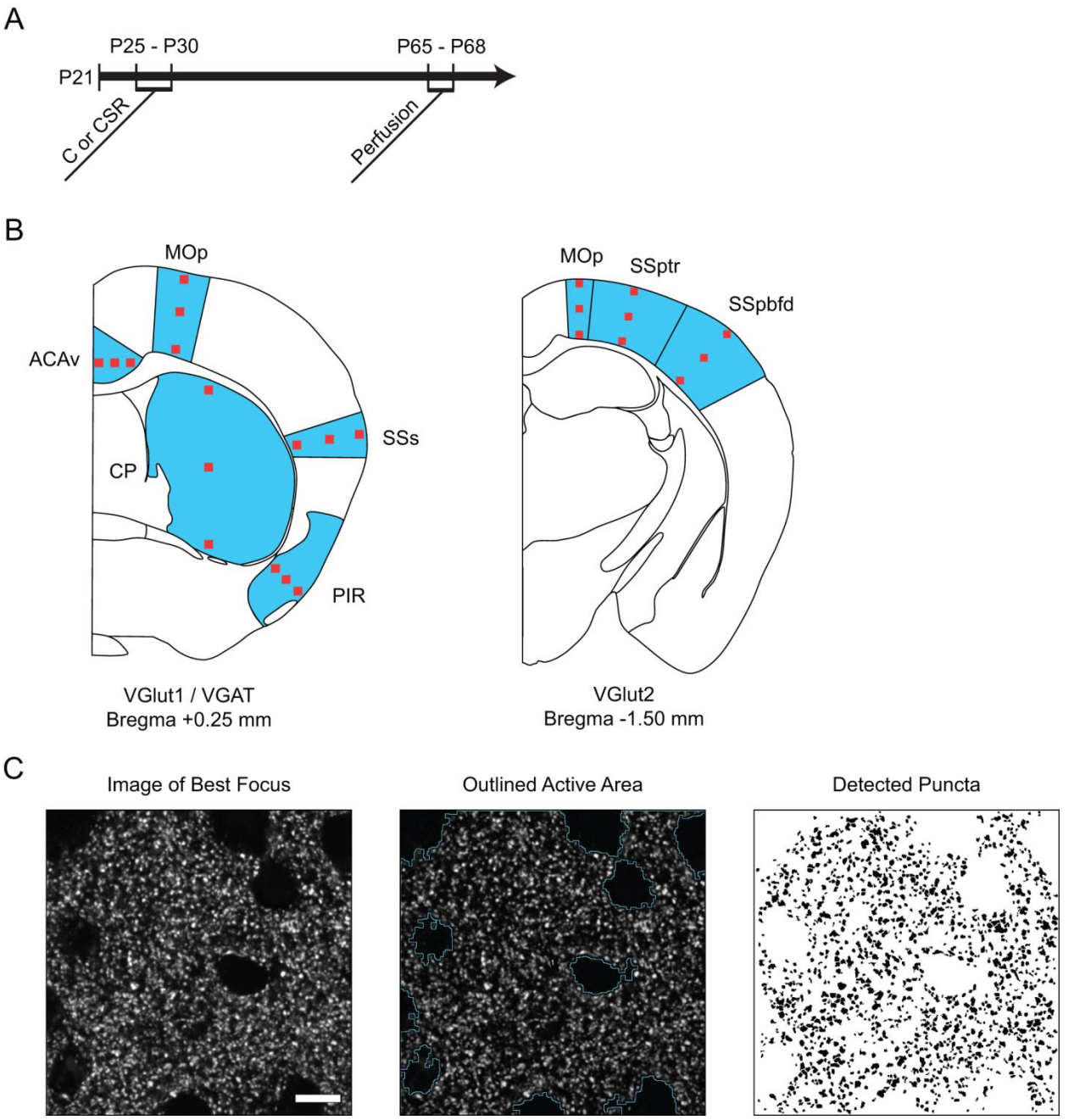
A
P25 - P30
P65 - P68
P21
C or CSR
Perfusion
B
MOp
ACAv
SSs
CP
PIR
VGlut1 / VGAT
Bregma +0.25 mm
MOp
SSptr
SSpbfd
VGlut2
Bregma -1.50 mm
C
Image of Best Focus
Outlined Active Area
Detected Puncta

References

Billeh, Y.N., Rodriguez, A.V., Bellesi, M., Bernard, A., de Vivo, L., Funk, C.M., Harris, J., Honjoh, S., Mihalas, S., Ng, L., et al. (2016). Effects of Chronic Sleep Restriction during Early Adolescence on the Adult Pattern of Connectivity of Mouse Secondary Motor Cortex. eNeuro *3*.

Borbély, A.A., Baumann, F., Brandeis, D., Strauch, I., and Lehmann, D. (1981). Sleep deprivation: effect on sleep stages and EEG power density in man. Electroencephalogr. Clin. Neurophysiol. *51*, 483–495.

Borbély, A.A., Daan, S., Wirz-Justice, A., and Deboer, T. (2016). The two-process model of sleep regulation: a reappraisal. J. Sleep Res. *25*, 131–143.

Carskadon, M.A., Vieira, C., and Acebo, C. (1993). Association between puberty and delayed phase preference. Sleep *16*, 258–262.

Carskadon, M.A., Wolfson, A.R., Acebo, C., Tzischinsky, O., and Seifer, R. (1998). Adolescent sleep patterns, circadian timing, and sleepiness at a transition to early school days. Sleep *21*, 871–881.

Chaudhry, F.A., Reimer, R.J., Bellocchio, E.E., Danbolt, N.C., Osen, K.K., Edwards, R.H., and Storm-Mathisen, J. (1998). The Vesicular GABA Transporter, VGAT, Localizes to Synaptic Vesicles in Sets of Glycinergic as Well as GABAergic Neurons. J. Neurosci. *18*, 9733–9750.

Clascá, F., Rubio-Garrido, P., and Jabaudon, D. (2012). Unveiling the diversity of thalamocortical neuron subtypes. Eur. J. Neurosci. *35*, 1524–1532.

Dijk, D.J., Beersma, D.G.M., and Daan, S. (1987). EEG Power Density during Nap Sleep: Reflection of an Hourglass Measuring the Duration of Prior Wakefulness. J. Biol. Rhythms *2*, 207–219.

El Mestikawy, S., Wallén-Mackenzie, Å., Fortin, G.M., Descarries, L., and Trudeau, L.-E. (2011). From glutamate co-release to vesicular synergy: vesicular glutamate transporters. Nat. Rev. Neurosci. *12*, 204–216.

Feinberg, I., and Campbell, I.G. (2010). Sleep EEG changes during adolescence: An index of a fundamental brain reorganization. Brain Cogn. *72*, 56–65.

Frank, M.G., and Heller, H.C. (1997). Development of REM and slow wave sleep in the rat. Am. J. Physiol. *272*, R1792-1799.

Frank, M.G., Issa, N.P., and Stryker, M.P. (2001). Sleep Enhances Plasticity in the Developing Visual Cortex. Neuron *30*, 275–287.

Fremeau Jr, R.T., Voglmaier, S., Seal, R.P., and Edwards, R.H. (2004). VGLUTs define subsets of excitatory neurons and suggest novel roles for glutamate. Trends Neurosci. *27*, 98–103.

Gonzalez-Lozano, M.A., Klemmer, P., Gebuis, T., Hassan, C., van Nierop, P., van Kesteren, R.E., Smit, A.B., and Li, K.W. (2016). Dynamics of the mouse brain cortical synaptic proteome during postnatal brain development. Sci. Rep. *6*.

Herzog, E., Bellenchi, G.C., Gras, C., Bernard, V., Ravassard, P., Bedet, C., Gasnier, B., Giros, B., and Mestikawy, S.E. (2001). The Existence of a Second Vesicular Glutamate Transporter Specifies Subpopulations of Glutamatergic Neurons. J. Neurosci. *21*, RC181-RC181.

Hur, E.E., and Zaborszky, L. (2005). Vglut2 afferents to the medial prefrontal and primary somatosensory cortices: A combined retrograde tracing in situ hybridization. J. Comp. Neurol. *483*, 351–373.

Huttenlocher, P.R. (1979). Synaptic density in human frontal cortex - developmental changes and effects of aging. Brain Res. *163*, 195–205.

Innocenti, G.M., and Price, D.J. (2005). Exuberance in the development of cortical networks. Nat. Rev. Neurosci. *6*, 955–965.

Jenni, O.G., Achermann, P., and Carskadon, M.A. (2005). Homeostatic sleep regulation in adolescents. Sleep *28*, 1446–1454.

Kaneko, T., and Fujiyama, F. (2002). Complementary distribution of vesicular glutamate transporters in the central nervous system. Neurosci. Res. *42*, 243–250.

Killgore, W.D.S. (2010). Effects of sleep deprivation on cognition. In Progress in Brain Research, G.A.K. and H.P.A. van Dongen, ed. (Elsevier), pp. 105–129.

Killgore, W.D.S., Balkin, T.J., and Wesensten, N.J. (2006). Impaired decision making following 49 h of sleep deprivation. J. Sleep Res. *15*, 7–13.

Lim, J., and Dinges, D.F. (2008). Sleep Deprivation and Vigilant Attention. Ann. N. Y. Acad. Sci. *1129*, 305–322.

Maret, S., Faraguna, U., Nelson, A.B., Cirelli, C., and Tononi, G. (2011). Sleep and waking modulate spine turnover in the adolescent mouse cortex. Nat. Neurosci. *14*, 1418–1420.

Micheva, K.D., O'Rourke, N., Busse, B., and Smith, S.J. (2010). Array tomography: immunostaining and antibody elution. Cold Spring Harb. Protoc. *2010*, pdb.prot5525.

Nelson, A.B., Faraguna, U., Zoltan, J.T., Tononi, G., and Cirelli, C. (2013). Sleep Patterns and Homeostatic Mechanisms in Adolescent Mice. Brain Sci. *3*, 318–343.

Ngodup, T., Goetz, J.A., McGuire, B.C., Sun, W., Lauer, A.M., and Xu-Friedman, M.A. (2015). Activity-dependent, homeostatic regulation of neurotransmitter release from auditory nerve fibers. Proc. Natl. Acad. Sci. U. S. A. *112*, 6479–6484.

Ni, B., Wu, X., Yan, G.M., Wang, J., and Paul, S.M. (1995). Regional expression and cellular localization of the Na(+)-dependent inorganic phosphate cotransporter of rat brain. J. Neurosci. *15*, 5789–5799.

Paus, T. (2005). Mapping brain maturation and cognitive development during adolescence. Trends Cogn. Sci. *9*, 60–68.

Shaffery, J.P., Sinton, C.M., Bissette, G., Roffwarg, H.P., and Marks, G.A. (2002). Rapid eye movement sleep deprivation modifies expression of long-term potentiation in visual cortex of immature rats. Neuroscience *110*, 431–443.

Shaffery, J.P., Lopez, J., and Roffwarg, H.P. (2012). Brain-Derived Neurotrophic Factor (BDNF) Reverses the Effects of Rapid Eye Movement Sleep Deprivation (REMSD) on Developmentally Regulated, Long-Term Potentiation (LTP) in Visual Cortex Slices. Neurosci. Lett. *513*, 84–88.

Van Dongen, H.P.A., Maislin, G., Mullington, J.M., and Dinges, D.F. (2003). The cumulative cost of additional wakefulness: dose-response effects on neurobehavioral functions and sleep physiology from chronic sleep restriction and total sleep deprivation. Sleep *26*, 117–126.

Vigneault, É., Poirel, O., Riad, M., Prud'homme, J., Dumas, S., Turecki, G., Fasano, C., Mechawar, N., and El Mestikawy, S. (2015). Distribution of vesicular glutamate transporters in the human brain. Front. Neuroanat. *9*.

de Vivo, L., Faraguna, U., Nelson, A.B., Pfister-Genskow, M., Klapperich, M.E., Tononi, G., and Cirelli, C. (2014). Developmental patterns of sleep slow wave activity and synaptic density in adolescent mice. Sleep *37*, 689–700, 700A–700B.

de Vivo, L., Nelson, A.B., Bellesi, M., Noguti, J., Tononi, G., and Cirelli, C. (2016a). Loss of Sleep Affects the Ultrastructure of Pyramidal Neurons in the Adolescent Mouse Frontal Cortex. Sleep *39*, 861–874.

de Vivo, L., Bellesi, M., Marshall, W., Bushong, E.A., Ellisman, M.H., Tononi, G., and Cirelli, C. (2016b). Ultrastructural Evidence for Synaptic Scaling Across the Wake/sleep Cycle. Science *In press*.

Wolfson, A.R., and Carskadon, M.A. (1998). Sleep schedules and daytime functioning in adolescents. Child Dev. *69*, 875–887.

Chapter V:

Conclusions

Effects of sustained, wake-like neuronal activity during sleep on subsequent sleep need

Extended wake is associated with an increased need to sleep and greater slow-wave activity (SWA) in non-rapid eye movement (NREM) sleep following wake (Borbély et al., 1981, 2016). However, it is still unclear exactly what aspect of wake drives this increased sleep need. I performed experiments to test the synaptic homeostasis hypothesis (SHY), which states that wake leads to an overall increase in synaptic strength associated with learning, and that sleep is required for the renormalization of synaptic weights (Tononi and Cirelli, 2014). Firing rates in the cerebral cortex and many other brain areas are higher in wake than in NREM sleep (Burns et al., 1979; Hobson and McCarley, 1971; Steriade and Hobson, 1976; Vyazovskiy et al., 2009), and increasing synaptic strength naturally leads to higher firing rates (Malenka and Bear, 2004). As a result, it has been difficult to test whether the increased sleep pressure observed following wake is mainly due, as SHY claims, to increased plasticity in wake that leads to higher synaptic strength and firing rates and greater SWA due to more synchronous neuronal activity in NREM sleep (Tononi and Cirelli, 2014), or whether high firing rates alone are sufficient to fatigue neurons and force them to enter periods of silence more frequently (Vyazovskiy and Harris, 2013), thus leading to higher SWA.

In **Chapter II**, I show that sleep following 6 hours of sleep deprivation (SD) is characterized by increased slow wave activity (SWA) and OFF measures, consistent with many previous reports (Borbély, 1982; Borbély and Achermann, 1999; Vyazovskiy et al., 2009, 2011). However, forcing neurons to fire in NREM sleep at high levels using optogenetics, as high as during 6 hours of SD, does not lead to the same changes in SWA and OFF measures observed after sleep loss. In fact, following optogenetic stimulation, SWA is decreased compared to baseline, OFF measures are unaffected, and OFF synchrony is also decreased compared to sleep

following SD. Although some have suggested that rest from high firing rates is a determinant of sleep (Rechtschaffen, 1998; Vyazovskiy and Harris, 2013), I show evidence to suggest that increased OFF measures and SWA are not direct consequences of increased firing rates alone. Instead, these results are more consistent with the hypothesis that increased SWA and OFF measures are more linked to the net synaptic potentiation caused by wake. Previous studies have shown that SWA increases in a use-dependent manner, not only in rats with vibrissal stimulation (Vyazovskiy et al., 2000) or increased exploration (Huber et al., 2007), but also in humans following a motor learning task or audiobook listening (Hung et al., 2013). Though use-dependent changes can be difficult to attribute to neuronal activity or plasticity alone, a study in rats has specifically linked learning to increased SWA (Hanlon et al., 2009) and a study in humans showed that movement associated with learning increased SWA more than movement alone with no learning (Huber et al., 2004), providing further evidence that SWA is linked to learning and not simply neural activity. The results I present here further contribute to the evidence supporting the claim that neuronal firing or activity alone is insufficient to increase sleep pressure as measured through SWA and OFF measures.

In my experiments, I take advantage of the well-known fact that synaptic potentiation is difficult to induce in NREM sleep (Bramham and Srebro, 1989; Leonard et al., 1987) in order to tease apart the effects of neural activity from those of synaptic plasticity. However, it is yet to be determined if increasing firing rates in wake would further increase synaptic strength or SWA in recovery sleep. I attempted to increase firing rates in wake above baseline levels using sustained optogenetic stimulation for hours, but results were difficult to interpret because high firing rates often caused cortical spreading depressions. An alternative experimental design may be required to answer this question. In flies, thermogenetics are often used in place of optogenetics for neural

control (Owald et al., 2015). As with rodents, flies also show a homeostatic regulation of sleep, an increase in synaptic size and number with wake, and relatively decreased neuronal activity in NREM sleep compared to wake (Bushey et al., 2011, 2015). Pilot experiments in our laboratory suggest that for further experiments modulating firing rates, flies may prove a better model organism.

Effects of chronic sleep restriction in adolescence on the adult brain

Though chronic sleep restriction (CSR) is a persistent problem among adolescents (Carskadon et al., 1998), few studies have looked at potential long term deficits as a result of CSR at a young age, even though the short term effects of extended wake on dendritic spines in young mice have been well described (Maret et al., 2011; de Vivo et al., 2016a, 2016b). Using two approaches, I examined the brains of adult mice that were subjected to a five-day CSR during adolescence. First, in **Chapter III**, I used a viral tracer and serial tomography to quantify projections from secondary motor cortex (MOs) throughout the brain. Although I was unable to find effects specific to any one region or network, machine leaning algorithms were able to reliably classify animals as either belonging to the control or CSR group, indicating that there are subtle but identifiable differences between these groups. A key limitation of this study was the inability to differentiate between passing axons and terminal projections, leaving open the question as to whether axon terminals are specifically affected. In **Chapter IV**, I used immunohistochemistry combined with confocal imaging to look at presynaptic puncta from several brain regions and quantify puncta density and size for VGlut1, VGAT, and VGlut2. I was unable to find any consistent differences between control and CSR animals when comparing synaptic density and size. Conflicting results between two separate groups of mice may indicate true biological variability between sleep restriction experiments, or instead methodological

variability in our immunohistochemistry experiments. Other more sensitive and more quantitative methods, such as serial electron microscopy, may be needed to address this issue.

Changes at the synaptic level due to the sleep/wake cycle have been well described in rodents. Following wake, synaptic puncta grow in number (Maret et al., 2011) and size (de Vivo et al., 2016b). Moreover, cortical pyramidal neurons show mitochondrial changes due to chronic sleep restriction that can persist even after recovery sleep (de Vivo et al., 2016a). I looked for, but failed to find, reliable differences in synaptic size or density in adult mice after sleep restriction in adolescence. One possibility is that there are simply no long-term effects resulting from this sort of sleep restriction. Sleep deprivation and restriction can cause a myriad of short-term behavioral and cognitive deficits, most of which show a return to baseline performance with recovery sleep (Dawson and Reid, 1997; Killgore, 2010; Lim and Dinges, 2008). In contrast to adulthood, critical periods of plasticity are more often seen in development (Berardi et al., 2000; Hensch, 2005; Kayser et al., 2014), and experiments in kittens with total sleep deprivation (Frank et al., 2001) or REM-selective deprivation (Shaffery et al., 1998) have demonstrated that sleep is important for proper plasticity during these critical periods. Furthermore, longer sleep restrictions in mice starting from an earlier age than our experiments have led to behavioral changes that persist into adulthood (Saré et al., 2016), suggesting that sufficiently severe sleep disruptions in adolescence cannot be corrected with recovery sleep. Similar findings have been reported within fruit flies, with long term learning deficits arising as a result of sleep deprivation in very early development (Seugnet et al., 2011).

While synaptic density and various other markers of synaptic growth peak earlier than adolescence (Gonzalez-Lozano et al., 2016; Huttenlocher, 1979; Paus et al., 2008), many psychiatric disorders characterized by aberrant plasticity do not become evident until

adolescence (Paus et al., 2008), and SWA in NREM sleep does not show adult-like increases in response to sleep deprivation until late adolescence after puberty (Jenni et al., 2005), indicating that adolescence is still a time for significant remodeling within the brain. As many human adolescents are subjected to sleep restriction due to conflicting drives between a preference for later sleep times and social/school pressures to wake up earlier (Carskadon et al., 1993, 1998; Minges and Redeker, 2016), the effects of such disruptions in adolescence remains a highly relevant area for further study.

References

Berardi, N., Pizzorusso, T., and Maffei, L. (2000). Critical periods during sensory development. Curr. Opin. Neurobiol. *10*, 138–145.

Borbély, A.A. (1982). A two process model of sleep regulation. Hum. Neurobiol. *1*, 195–204.

Borbély, A.A., and Achermann, P. (1999). Sleep homeostasis and models of sleep regulation. J. Biol. Rhythms *14*, 557–568.

Borbély, A.A., Baumann, F., Brandeis, D., Strauch, I., and Lehmann, D. (1981). Sleep deprivation: effect on sleep stages and EEG power density in man. Electroencephalogr. Clin. Neurophysiol. *51*, 483–495.

Borbély, A.A., Daan, S., Wirz-Justice, A., and Deboer, T. (2016). The two-process model of sleep regulation: a reappraisal. J. Sleep Res. *25*, 131–143.

Bramham, C.R., and Srebro, B. (1989). Synaptic plasticity in the hippocampus is modulated by behavioral state. Brain Res. *493*, 74–86.

Burns, B.D., Stean, J.P., and Webb, A.C. (1979). The effects of sleep on neurons in isolated cerebral cortex. Proc. R. Soc. Lond. B Biol. Sci. *206*, 281–291.

Bushey, D., Tononi, G., and Cirelli, C. (2011). Sleep and Synaptic Homeostasis: Structural Evidence in Drosophila. Science *332*, 1576–1581.

Bushey, D., Tononi, G., and Cirelli, C. (2015). Sleep- and wake-dependent changes in neuronal activity and reactivity demonstrated in fly neurons using in vivo calcium imaging. Proc. Natl. Acad. Sci. U. S. A. *112*, 4785–4790.

Carskadon, M.A., Vieira, C., and Acebo, C. (1993). Association between puberty and delayed phase preference. Sleep *16*, 258–262.

Carskadon, M.A., Wolfson, A.R., Acebo, C., Tzischinsky, O., and Seifer, R. (1998). Adolescent sleep patterns, circadian timing, and sleepiness at a transition to early school days. Sleep *21*, 871–881.

Dawson, D., and Reid, K. (1997). Fatigue, alcohol and performance impairment. Nature *388*, 235–235.

Frank, M.G., Issa, N.P., and Stryker, M.P. (2001). Sleep enhances plasticity in the developing visual cortex. Neuron *30*, 275–287.

Gonzalez-Lozano, M.A., Klemmer, P., Gebuis, T., Hassan, C., van Nierop, P., van Kesteren, R.E., Smit, A.B., and Li, K.W. (2016). Dynamics of the mouse brain cortical synaptic proteome during postnatal brain development. Sci. Rep. *6*.

Hanlon, E.C., Faraguna, U., Vyazovskiy, V.V., Tononi, G., and Cirelli, C. (2009). Effects of Skilled Training on Sleep Slow Wave Activity and Cortical Gene Expression in the Rat. Sleep *32*, 719–729.

Hensch, T.K. (2005). Critical period plasticity in local cortical circuits. Nat. Rev. Neurosci. *6*, 877–888.

Hobson, J.A., and McCarley, R.W. (1971). Cortical unit activity in sleep and waking. Electroencephalogr. Clin. Neurophysiol. *30*, 97–112.

Huber, R., Felice Ghilardi, M., Massimini, M., and Tononi, G. (2004). Local sleep and learning. Nature *430*, 78–81.

Huber, R., Tononi, G., and Cirelli, C. (2007). Exploratory behavior, cortical BDNF expression, and sleep homeostasis. Sleep *30*, 129–139.

Hung, C.-S., Sarasso, S., Ferrarelli, F., Riedner, B., Ghilardi, M.F., Cirelli, C., and Tononi, G. (2013). Local Experience-Dependent Changes in the Wake EEG after Prolonged Wakefulness. Sleep *36*, 59–72.

Huttenlocher, P.R. (1979). Synaptic density in human frontal cortex - developmental changes and effects of aging. Brain Res. *163*, 195–205.

Jenni, O.G., Achermann, P., and Carskadon, M.A. (2005). Homeostatic sleep regulation in adolescents. Sleep *28*, 1446–1454.

Kayser, M.S., Yue, Z., and Sehgal, A. (2014). A Critical Period of Sleep for Development of Courtship Circuitry and Behavior in Drosophila. Science *344*, 269–274.

Killgore, W.D.S. (2010). Effects of sleep deprivation on cognition. In Progress in Brain Research, G.A.K. and H.P.A. van Dongen, ed. (Elsevier), pp. 105–129.

Leonard, B.J., McNaughton, B.L., and Barnes, C.A. (1987). Suppression of hippocampal synaptic plasticity during slow-wave sleep. Brain Res. *425*, 174–177.

Lim, J., and Dinges, D.F. (2008). Sleep Deprivation and Vigilant Attention. Ann. N. Y. Acad. Sci. *1129*, 305–322.

Malenka, R.C., and Bear, M.F. (2004). LTP and LTD: An Embarrassment of Riches. Neuron *44*, 5–21.

Maret, S., Faraguna, U., Nelson, A.B., Cirelli, C., and Tononi, G. (2011). Sleep and waking modulate spine turnover in the adolescent mouse cortex. Nat. Neurosci. *14*, 1418–1420.

Minges, K.E., and Redeker, N.S. (2016). Delayed school start times and adolescent sleep: A systematic review of the experimental evidence. Sleep Med. Rev. *28*, 86–95.

Owald, D., Lin, S., and Waddell, S. (2015). Light, heat, action: neural control of fruit fly behaviour. Philos. Trans. R. Soc. B Biol. Sci. *370*.

Paus, T., Keshavan, M., and Giedd, J.N. (2008). Why do many psychiatric disorders emerge during adolescence? Nat. Rev. Neurosci. *9*, 947–957.

Rechtschaffen, A. (1998). Current perspectives on the function of sleep. Perspect. Biol. Med. *41*, 359–390.

Saré, R.M., Levine, M., Hildreth, C., Picchioni, D., and Smith, C.B. (2016). Chronic sleep restriction during development can lead to long-lasting behavioral effects. Physiol. Behav. *155*, 208–217.

Seugnet, L., Suzuki, Y., Donlea, J.M., Gottschalk, L., and Shaw, P.J. (2011). Sleep Deprivation During Early-Adult Development Results in Long-Lasting Learning Deficits in Adult Drosophila. Sleep *34*, 137–146.

Shaffery, J.P., Oksenberg, A., Marks, G.A., Speciale, S.G., Mihailoff, G., and Roffwarg, H.P. (1998). REM sleep deprivation in monocularly occluded kittens reduces the size of cells in LGN monocular segment. Sleep *21*, 837–845.

Steriade, M., and Hobson, J. (1976). Neuronal activity during the sleep-waking cycle. Prog. Neurobiol. *6*, 155–376.

Tononi, G., and Cirelli, C. (2014). Sleep and the Price of Plasticity: From Synaptic and Cellular Homeostasis to Memory Consolidation and Integration. Neuron *81*, 12–34.

de Vivo, L., Nelson, A.B., Bellesi, M., Noguti, J., Tononi, G., and Cirelli, C. (2016a). Loss of Sleep Affects the Ultrastructure of Pyramidal Neurons in the Adolescent Mouse Frontal Cortex. Sleep *39*, 861–874.

de Vivo, L., Bellesi, M., Marshall, W., Bushong, E.A., Ellisman, M.H., Tononi, G., and Cirelli, C. (2016b). Ultrastructural Evidence for Synaptic Scaling Across the Wake/sleep Cycle. Science *In press*.

Vyazovskiy, V.V., and Harris, K.D. (2013). Sleep and the single neuron: the role of global slow oscillations in individual cell rest. Nat. Rev. Neurosci. *14*, 443–451.

Vyazovskiy, V., Borbély, A.A., and Tobler, I. (2000). Fast track:Unilateral vibrissae stimulation during waking induces interhemispheric EEG asymmetry during subsequent sleep in the rat. J. Sleep Res. *9*, 367–371.

Vyazovskiy, V.V., Olcese, U., Lazimy, Y.M., Faraguna, U., Esser, S.K., Williams, J.C., Cirelli, C., and Tononi, G. (2009). Cortical firing and sleep homeostasis. Neuron *63*, 865–878.

Vyazovskiy, V.V., Olcese, U., Hanlon, E.C., Nir, Y., Cirelli, C., and Tononi, G. (2011). Local sleep in awake rats. Nature *472*, 443–447.